NASA-TP-2519 19860010877

NASA Technical Paper 2519

December 1985

Static Internal Performance of a Single-Engine Nonaxisymmetric-Nozzle Vaned-Thrust-Reverser Design With Thrust Modulation Capabilities

Laurence D. Leavitt
and James R. Burley II

NASA

NASA Technical Paper 2519

1985

Static Internal Performance of a Single-Engine Nonaxisymmetric-Nozzle Vaned-Thrust-Reverser Design With Thrust Modulation Capabilities

Laurence D. Leavitt
and James R. Burley II

Langley Research Center
Hampton, Virginia

National Aeronautics
and Space Administration

**Scientific and Technical
Information Branch**

Summary

An investigation has been conducted at wind-off conditions in the static-test facility of the Langley 16-Foot Transonic Tunnel. The tests were conducted on a single-engine reverser configuration with partial and full reverse-thrust modulation capabilities. The reverser design had four ports with equal areas. The ports were angled outboard 30° from the vertical to impart a splay angle to the reverser exhaust flow. This splaying of reverser flow was intended to prevent impingement of exhaust flow on empennage surfaces and to help avoid inlet reingestion of exhaust gas when the reverser is integrated into an actual airplane configuration. External vane boxes were located directly over each of the four ports to provide variation of reverser efflux angle from 140° to 26° (measured forward from the horizontal reference axis). The reverser model was tested with both a butterfly-type inner door and an internal slider door to provide area control for each individual port. In addition, main nozzle throat area and vector angle were varied to examine various methods of modulating thrust levels. Other model variables included vane box configuration (four or six vanes per box), orientation of external vane boxes with respect to internal port walls (splay angle shims), and vane box sideplates. Nozzle pressure ratio was varied from 2.0 to approximately 7.0.

Results of this investigation indicate that the nozzle/reverser configuration had the capability of generating values of thrust ratio ranging from 0.97 (for the main nozzle only) to −0.70 (for full reverse thrust). This modulation of thrust ratio could be obtained by varying reverser efflux angle, inner door angle, and/or main nozzle throat area. The design splay angle of 30° was not achieved. Both inner door angle and slider door position provided effective modulation of weight flow. Differential variation of reverser efflux angle, inner door angle, and/or slider door position generated significant forces and moments in addition to reverse-thrust modulation capabilities. If properly integrated into an airframe, these forces and moments could augment or possibly replace conventional control surfaces.

Introduction

The design requirements for the next generation of fighter aircraft may include the ability to land on short or bomb-damaged runways. This capability will probably require adding thrust-reversing capability to nozzle designs. The idea of thrust reversing after aircraft touchdown is certainly not new. Commercial aircraft have been using reversers during ground roll for many years. Two European tactical aircraft, the Saab-Scania Viggen and the Panavia Tornado, currently use reversers for reduction in landing ground roll. However, much of the capability of these landing–ground-roll reversers is lost by delays in deployment of the reverser upon touchdown and by the relatively long engine spool-up times required for maximum reverse thrust (i.e., maximum dry power) once aircraft touchdown has occurred. (See refs. 1 and 2.)

To eliminate the spool-up time and thus make maximum use of thrust reversing, the engine must be at a high power setting during the approach prior to touchdown. However, the power required for flight at approach conditions is low, and a method must be developed to spoil the excess thrust generated at high power settings. Several nozzle concepts use partial thrust reversing (along with thrust vectoring) to achieve trim and proper approach lift-drag ratios. Once the aircraft has touched down, the partially deployed reverser can be fully deployed in about 1 second to provide maximum reverse thrust nearly at touchdown.

Many studies on the concept of in-flight thrust reversing have been conducted in recent years. (See refs. 1 to 40.) Flight and wind-tunnel test programs on the F-94C (ref. 3), the F-100F (ref. 4), and the F-11A airplanes (refs. 5 and 7 to 11) were conducted between 1956 and 1975. These early programs demonstrated that thrust reversers integrated into single-engine axisymmetric exhaust nozzles provided many benefits, including improved flight-path control and reduced landing ground roll. However, in all studies, problems were found in the handling qualities of the aircraft when the reversers were deployed at landing-approach (low-speed) conditions.

Several research programs have addressed the central problems associated with the use of thrust reversers at landing-approach conditions (refs. 19 to 21, 26, 32, 33, 35 to 37, and 39). In general, thrust-reverser effects on airplane stability and control are somewhat configuration dependent but may often be attributed to specific occurrences such as reverser flow blockage of the free-stream flow over tail surfaces, impingement of reverser flow on empennage surfaces, and entrainment of the free-stream flow by reverser exhaust flow.

In addition to the stability and control problems mentioned above, consideration must be given to the possible reingestion of hot exhaust gases into the engine inlet(s). (See ref. 34.) Reingested gases can generate temperature and pressure distortion levels at the compressor face which could stall the compressor and cause possible engine damage. Susceptibility to reingestion of reverser exhaust flow is a function of such parameters as aircraft forward airspeed, height

above the ground, inlet suction characteristics (hence local aerodynamic characteristics adjacent to the inlet), proximity of reverser port to the inlet engine weight flow, and of course, reverser efflux angle (angle of the projection of reverser exhaust flow in the normal-force/axial-force plane). The aircraft velocity at which the reingestion of reverser exhaust flow occurs dictates the amount of useful reverse thrust available for the reduction of landing ground roll. Obviously, the longer full reverse thrust can be maintained during the ground roll phase, the shorter the landing–ground-roll distance.

One method which has been shown to be very effective in reducing the velocity at which ingestion of reverser exhaust occurs (for a given efflux angle) is to splay (or cant) the reverser flow. In fact, without the ability to splay reverser flow, ingestion speeds can be on the order of touchdown speeds for some configurations, as reported in reference 34. Benefits of splaying reverser flow partially result from increased lateral separation of the reverser jets. This increased lateral separation tends to eliminate the "fountain" effect found for many configurations with splay angles of 0° once the reverser flow impinges upon the ground.

Reduced ground roll upon landing and improved flight-path control have long been recognized as significant advantages of thrust reversing. The problems of stability and control and engine ingestion of exhaust gases are being addressed, but because of the complex nature of the nozzle requirements, a reassessment of current thrust-reversing technology was warranted. This reassessment indicated that the ability to vary reverser efflux angle to modulate thrust by a combination of main nozzle and reverser port area control and to splay the reverser flow will, if properly integrated with flight and propulsion control systems, provide significant reductions in landing-field length. In addition, individual or differential variation of the nozzle variable-geometry features (such as efflux angle and port area) could be especially useful in solving the stability and control problems normally associated with thrust-reverser operation at approach and landing speeds. In addition, since tail surfaces are generally sized by the low-speed control requirements of the aircraft, the use of propulsive controls may lead to a reduction in the size (weight and drag) of tail surfaces or their elimination from the airframe altogether.

To date, few (if any) internal performance data are available on reverser configurations with these capabilities. As a result, an investigation was conducted at wind-off conditions in the static-test facility of the Langley 16-Foot Transonic Tunnel. The tests were conducted on a single-engine reverser configuration with thrust modulation (partial and full reverse-thrust) capabilities. The reverser design had four ports with equal areas. The ports were angled outboard 30° from the vertical to impart a splay angle to the reverser exhaust flow. External vane boxes were located directly over each of the four ports to provide a variation of reverser efflux angle from 140° to 26° measured forward from the horizontal reference axis. The reverser model was tested with both a butterfly-type inner door and an internal slider door to provide area control for each individual port. In addition, main nozzle throat area and vector angle were varied to examine various methods of modulating thrust. Other model variables included vane box configuration (four or six vanes per box), orientation of external vane boxes with respect to internal port walls (splay angle shims), and vane box sideplates. Nozzle pressure ratio was varied from 2.0 to approximately 7.0.

Symbols

All forces (with the exception of resultant gross thrust) and angles are referred to the model centerline (body axis). A detailed discussion of the data-reduction and calibration procedures as well as definitions of forces, angles, and propulsion relationships used herein can be found in reference 4.

$A_{t,\text{main}}$ main exhaust nozzle throat area, (see fig. 2(f)), in^2

F measured thrust along body axis, lbf

F_i ideal isentropic gross thrust, $w_p\sqrt{\frac{RT_{t,j}}{g^2}\frac{2\gamma}{\gamma-1}\left[1-\left(\frac{p_a}{p_{t,j}}\right)^{\frac{\gamma-1}{\gamma}}\right]}$, lbf

F_N measured normal force, lbf

F_r resultant gross thrust, $\sqrt{F^2+F_N^2+F_Y^2}$, positive for thrust vectored aft of vertical plane and negative for thrust vectored forward of vertical plane, lbf

$F_{r,\text{tot}}$ individual resultant gross thrust measured for top left-hand reverser port only (eq. (1)), lbf

F_Y measured side force, lbf

g gravitational constant 32.174 ft/sec^2

l_r reference length, 1.0 in.

M_{int} local Mach number inside nozzle

M_Z measured yawing moment, in-lbf

NPR nozzle pressure ratio, $p_{t,j}/p_a$

p	local static pressure, psi
p_a	ambient pressure, psi
$p_{t,j}$	jet total pressure, psi
R	gas constant for air, 1716 $ft^2/sec^2-°R$
$T_{t,j}$	total temperature, °R
w_i	ideal weight-flow rate based on nominal throat area of 4.0 in^2, lbf/sec
w_p	measured weight-flow rate, lbf/sec
γ	ratio of specific heats, 1.3997 for air
δ_v	geometric thrust pitch vector angle measured from horizontal reference line, positive in downward direction (see fig. 2(f)), deg
θ	measured reverser efflux angle, $-\tan^{-1}(F_N/F)$ for thrust directed aft of vertical plane and $180 - \tan^{-1}(F_N/F)$ for thrust directed forward of vertical plane, deg
θ_t, θ_b	geometric reverser efflux angle on top and bottom reverser ports, respectively, measured from horizontal reference line; positive in counterclockwise direction on top reverser ports and in clockwise direction on bottom reverser ports (see fig. 2(g)), deg
ϕ	resultant reverser splay angle measured from vertical reference line, $\tan^{-1}(F_Y/F_N)$, deg
ψ	geometric inner door angle measured from horizontal reference line, positive in counterclockwise direction on top port and in clockwise direction on bottom port (see fig. 2(a)), deg

Subscripts:

b	bottom
l	left
r	right
t	top

Abbreviations:

C-D	convergent-divergent
conf	configuration
dim	dimension
rad.	radius
sta.	model station, in.
typ.	typical
2-D	two-dimensional

Apparatus and Methods

Static-Test Facility

This investigation was conducted in the static-test facility of the Langley 16-Foot Transonic Tunnel. Testing was conducted in a room with a high ceiling where the jet exhausts to atmosphere through a large open doorway. The control room was remotely located from the test area, and a closed-circuit television camera was used to observe the model. This facility utilized the same clean dry-air supply as that used in the 16-Foot Transonic Tunnel and a similar air-control system including valving, filters, and a heat exchanger to operate the jet flow at constant stagnation temperature.

Single-Engine Propulsion Simulation System

A sketch of the single-engine air-powered nacelle model on which various nozzles were mounted is presented in figure 1 with a typical nozzle configuration attached. The body shell forward of station 20.50 was removed for this investigation.

An external high-pressure air system provided a continuous flow of clean, dry air at a controlled temperature of about 540°R and was varied up to approximately 105 psi at the nozzle. This high-pressure air was brought through the dolly-mounted support strut by six tubes, which connect to a high-pressure plenum chamber. As shown in figure 1, the air was then discharged perpendicularly into the model low-pressure plenum through eight multiholed sonic nozzles equally spaced around the high-pressure plenum. This method was designed to minimize any forces imposed by the transfer of axial momentum as the air passed from the nonmetric high-pressure plenum to the metric (mounted to the force balance) low-pressure plenum. Two flexible metal bellows were used as seals and served to compensate for axial forces caused by pressurization. The air was then passed from the model low-pressure plenum (circular in cross section) through a transition section, choke plate, and instrumentation section. The transition section provided a smooth flow path for the airflow from the round low-pressure plenum to the rectangular choke plate and instrumentation section. The instrumentation section had a flow path width-height ratio of 1.437 and was identical in geometry to the nozzle airflow entrance. The nozzles were attached to the instrumentation section at model station 41.13.

Model Description

Nozzle geometry. The nozzle hardware downstream of station 41.13 represented a single-engine nonaxisymmetric convergent-divergent exhaust system with partial and full reverse-thrust capabilities. Sketches of the hardware tested are shown in figure 2, and photographs of full reverse-thrust configurations are presented in figure 3. The reverser design consisted of four ports with equal areas. The ports were angled outboard 30° from the vertical to impart a desired exhaust flow splay angle. (See fig. 2(a).) Exhaust flow splay would direct exhaust flow away from a single vertical-tail surface and help avoid inlet ingestion of exhaust flow by minimizing the fountain effect on the aircraft lower surface. As seen in figure 2(a), the upstream and downstream port walls were parallel and were aligned 78° from the aft horizontal. External cascade vane boxes were located directly over each of the four ports to allow variation of reverser geometric efflux angle from 140° to 26°. It should be noted that when the vane boxes were located on each port (Splay angle = 30°), the cascade vane box sidewalls were perpendicular to the nozzle external surface and as a result were splayed outward only 7.6°. (See section A-A on fig. 2(a).) Because it was suspected that the orientation of these external vane boxes might reduce the resultant splay angle of the individual ports, a set of splay angle shims (fig. 2(e)) were constructed to allow the vane box sidewalls to be mounted parallel to the reverser port walls (splayed 30°). Note that these shims did result in longer port passages.

Two schemes for modulating port area were investigated: varying the inner door angle and varying the slider door position. As shown in figure 2(a), the inner doors pivot about a longitudinal axis which is parallel to the nozzle centerline. Values of inner door angle ranged from 60° (fully open as shown in fig. 2(a)) to 0° (fully closed for no flow through the reverser port). The other method of modulating port area was to vary the position of the internal slider. (See fig. 2(b).) Four slider door positions ranging from a fully open position to a closed position (reverser port area reduced by approximately 50 percent) were investigated. The intermediate positions, 1/3 and 2/3, reduced the area of each individual port by approximately 17 and 33 percent, respectively. Note that the inner door remained in the fully open position ($\psi = 60°$) when slider door positions were varied.

Other reverser geometry variables were vane configuration (number of vanes), vane box sideplates, and reverser port tab. Two vane box configurations were tested to determine if reverser performance was a function of the number of vanes. Four- and six-vane configurations were tested. (See fig. 2(c).) The cascade vane box sideplates (fig. 2(d)) were designed to prevent exhaust flow leakage through a slot formed between the structural support for the vanes and the nozzle external surface. Use of the sideplates would in effect direct all the reverser port flow through the vanes. The reverser port tab (figs. 2(a) and 2(d)) represented a fairing that provided complete port closure when vanes were in a stowed position on full-scale hardware designs. Because a region of separated flow was expected on the upstream port wall (because of the large turning angle and sharp corner), the upstream vane was placed slightly aft of the upstream port wall in an effort to locate the vane in a region of relatively "clean" flow. The reverser port tab allows no flow to reach the upstream side of the upstream vane, and it virtually guarantees a region of separation between the corner and port tab.

In order to evaluate partial thrust-reversing performance, as would be required at landing-approach conditions, combinations of inner door angle were investigated at a constant geometric efflux angle condition ($\theta_t/\theta_b = 130°/130°$) with the main (normal forward-thrusting) exhaust nozzle flowing. Two main exhaust nozzle throat areas, nominally 0.5 in^2 and 2.0 in^2, and two nozzle vector angles, $\delta_v = 0°$ and 20°, were examined. Sketches of the main exhaust nozzles tested are shown in figure 2(f).

Splitter plate design. To determine the performance of an individual reverser port/vane combination, both force balance and weight flow measurements must be isolated from the whole reverser system. Because of model symmetry in two planes, it was believed that individual port characteristics could be obtained by making one run with both bottom ports closed (to determine normal-force/axial-force characteristics) and one run with both right-hand reverser ports closed (to determine side-force/axial-force characteristics). By proper data-reduction techniques, isolated performance for the top left-hand port can be calculated. It was recognized that the flow characteristics into a pair of reverser ports (for example, the top two ports) might be considerably different if two of the four ports were closed than if all ports were operating. A splitter plate was utilized to alleviate this problem. Sketches of the horizontal and vertical splitter plate designs used during this investigation are shown in figure 4. The specific designs of these splitter plate concepts were refined on the basis of water table tests conducted at the University of Cincinnati, and they feature a corner radius on the upstream end of the splitter plate. This corner radius acts as a bellmouth and

provides the two open reverser ports with what appeared in the water table tests to be flow characteristics which most nearly duplicated the flow characteristics for the reverser configuration with all ports open.

Instrumentation

A six-component strain-gauge balance was used to measure the forces and moments on the model downstream of station 20.50. (See fig. 1.) Jet total pressure was measured at a fixed station in the instrumentation section (see fig. 1) by means of a four-probe rake through the upper surface, a three-probe rake through the side, and a three-probe rake through the corner. A thermocouple, also located in the instrumentation section, was used to measure jet total temperature. Flow rate of the high-pressure air supplied to the nozzle was measured by a pair of critical flow venturis. Internal static-pressure orifices were located on the nozzle upper flap upstream of the reverser ports, in the top left-hand reverser port, and on the nozzle upper and lower flaps. Results from these static-pressure orifices (because of the limited number) were used primarily as a diagnostic tool and as supporting information to the balance force and moment measurements; hence, exact orifice locations are not defined herein. However, whenever static-pressure data are plotted, the figures contain sketches showing relative orifice locations.

Data Reduction

All data were recorded simultaneously on magnetic tape. Approximately 50 frames of data, taken at a rate of 10 frames per second, were used for each data point; average values were used in computations. With the exception of resultant gross thrust F_r, all force data in this report are referenced to the body axis.

The basic performance parameters used for the presentation of results were F/F_i, F_r/F_i, F_N/F_i, F_Y/F_i, $M_Z/F_i l_r$, and w_p/w_i. The internal thrust ratio F/F_i is the ratio of actual nozzle thrust (along the body axis) to ideal nozzle thrust, where ideal nozzle thrust is based on measured weight-flow rate and total temperature and pressure conditions in the nozzle throat as defined in the symbols. The balance axial-force measurement, from which actual nozzle thrust is subsequently obtained, is initially corrected for model weight tares and balance interactions. Although the bellows arrangement was designed to eliminate pressure and momentum interactions with the balance, small bellows tares on all balance components still exist. These tares result from a small pressure difference between the ends of the bellows when internal velocities are high and also small differences in the forward and aft bellows spring constants when the bellows are pressurized. As discussed in reference 14, these bellows tares were determined by running calibration nozzles with known performance over a range of expected normal and side forces and yawing and pitching moments. The balance data were then corrected in a manner similar to that discussed in reference 14 to obtain final forces and moments. The resultant gross thrust F_r, used in the resultant thrust ratio F_r/F_i, was then determined from these corrected balance data as were the individual force and moment ratios F_N/F_i, F_Y/F_i, and $M_Z/F_i l_r$. Significant differences between F_r/F_i and F/F_i occur when jet-exhaust flow is directed away from the axial direction. The individual force ratios are presented to allow a direct comparison of normal- and side-force magnitudes relative to axial-force (thrust ratio) values.

Nozzle discharge coefficient w_p/w_i is the ratio of measured weight-flow rate to ideal weight-flow rate, where ideal weight-flow rate is based on jet total pressure $p_{t,j}$, jet total temperature $T_{t,j}$, and a nominal throat area of 4.0 in^2. Since a nominal throat area (representing a scaled throat area for an intermediate-power main nozzle) was used in the computation of the discharge coefficient instead of actual values of throat area, variations in w_p/w_i occurring as a result of configuration changes reflect not only changes in the ability of the nozzle to pass weight flow but also differences in throat area.

Data from three separate runs were used to calculate the performance characteristics for a single port (top left-hand port). Data from complete configuration runs (all ports open) combined with data from the horizontal (only top left and top right ports open) and vertical (only left-side top and bottom ports open) splitter plate runs were used to determine the performance for the top left-hand reverser port alone. Basic to the following analysis technique is the assumption that each individual reverser port had identical performance to the other three ports. Based on reverser geometry symmetry as shown in figure 2, this assumption should be valid.

As a result of the above assumption, the thrust ratio F/F_i (or the axial-force component) generated by a single reverser port should be similar to the thrust ratio measured for either the complete configuration or for any combination of reverser ports open or closed. In reality, however, small differences in individual port geometry (port throat area, for example) resulted in values of thrust ratio for the splitter plate runs which were not identical to those measured for the complete configuration. These differences in

F/F_i were generally small (within 0.02). It was believed that averaging thrust ratios (at a given NPR) for all three combinations of reverser ports tested would provide a thrust ratio more representative of the individual port. Ratios of normal-force and side-force components to ideal thrust were obtained directly from the horizontal and vertical splitter plate data, respectively. The total resultant thrust ratio was then defined to be

$$\frac{F_{r,\mathrm{tot}}}{F_i} = \sqrt{\left(\frac{F}{F_i}\right)_{t,l}^2 + \left(\frac{F_N}{F_i}\right)_{t,l}^2 + \left(\frac{F_Y}{F_i}\right)_{t,l}^2} \quad (1)$$

where

$$\left(\frac{F}{F_i}\right)_{t,l} = \frac{(F/F_i) + (F/F_i)_t + (F/F_i)_l}{3} \quad (2)$$

in which $(F/F_i)_{t,l}$ represents the average of the thrust ratios obtained from runs without a splitter plate, with a horizontal splitter plate, and with a vertical splitter plate;

$$\left(\frac{F_N}{F_i}\right)_{t,l} = \left(\frac{F_N}{F_i}\right)_t \quad (3)$$

which is obtained from the horizontal splitter plate run; and

$$\left(\frac{F_Y}{F_i}\right)_{t,l} = \left(\frac{F_Y}{F_i}\right)_l \quad (4)$$

which is obtained from the vertical splitter plate run. Note that the above definitions require the assumption, as discussed previously, that weight flow and flow conditions in each port are identical.

The resultant thrust of a single reverser port $F_{r,\mathrm{tot}}$ was computed to present a more complete picture of actual flow conditions in the reverser ports. This was necessitated by the fact that resultant thrust, whether computed for the complete reverser or for splitter plate runs where two ports were closed, always had a net normal-force and/or side-force balance component equal to zero. Thus, some of the force and flow direction information was lost. For example, consider the complete configuration operating with all ports open and all port variables equal. Because of the symmetry of the reverser port arrangement, both the net normal- and side-force components measured by the balance are approximately zero. The upward normal force generated by the lower ports is cancelled by the downward normal force generated by the upper ports. Likewise, the symmetry in splaying the exhaust flow outboard results in zero net side force. The resultant thrust ratio for this configuration is, therefore, equal to the thrust ratio (axial-force component) even though all the flow has been turned from the axial direction. On the other hand, resultant thrust of a single port, which is computed by isolating the normal-, axial-, and side-force components, is a measure of the true efficiency of the reverser ports and is useful for assessing the nozzle system performance losses associated with reversing the exhaust flow.

The individual force components for the single port were then used to compute reverser splay angle ϕ from the equation

$$\phi = \tan^{-1}\left|\frac{F_Y}{F_N}\right| \quad (5)$$

The absolute value of F_Y/F_N was used because the sign of the splay angle (determined by which port is open) was not deemed important; only the magnitude was important. The reverser efflux angle θ was determined from the following two equations. For configurations with exhaust directed aft of the vertical plane,

$$\theta = -\tan^{-1}\frac{F_N}{F} \quad (6)$$

For configurations with exhaust directed forward of the vertical plane,

$$\theta = 180 - \tan^{-1}\frac{F_N}{F} \quad (7)$$

Presentation of Results

The basic performance data for the current investigation are plotted in figure 5. An index to these basic data and sketches of model geometry can be found in table I and figure 2, respectively.

Performance comparisons and summary figures are presented as follows:

Results and Discussion

Basic Data

Basic data for all reverser configurations tested are presented in figure 5. Nozzle internal thrust ratio F/F_i and discharge coefficient w_p/w_i are presented as a function of NPR for each configuration. Resultant thrust ratio F_r/F_i is generally shown for those configurations in which values of F_r/F_i differed from values of F/F_i (at a constant NPR) by 0.005 or more. When F_r/F_i is presented, the ratios of normal force F_N and side force F_Y to ideal thrust F_i are usually provided to allow the reader to determine the reason F_r/F_i differs from F/F_i. The above condition generally resulted for configurations in which two of the reverser ports were closed (splitter plate runs); for configurations in which model variables such as geometric efflux angle, inner door angle, or slider door position were differentially configured; and for approach configurations in which the main exhaust nozzle was pitch vectored. It should be noted that F_r/F_i is not provided for the splitter plate configurations with $\theta_t/\theta_b = 90°/90°$ (figs. 5(g) and 5(h)) because a large change in the vertical scale would have been required to present both F_r/F_i and F/F_i on the same figure. In each case, however, the resultant thrust ratio is almost identical (within 0.005) to measured values of F_Y/F_i and F_N/F_i for the vertical and horizontal splitter plate configurations, respectively.

Configuration 2 was tested at periodic intervals during the test program, and these data are presented in figure 5(b) as a data band to indicate data repeatability. As seen in figure 5(b), the data are scattered over a band of approximately 1 percent. An average of these data was used for the comparisons presented later in the paper.

The internal performance data shown in figure 5 exhibit characteristics typical of other convergent-divergent nozzles (ref. 14), in that performance increases up to a maximum (usually occurring at the NPR for fully expanded flow) and thereafter decreases throughout the NPR range. It should be noted that a decrease in reverser performance (configurations in which exhaust is directed forward) is distinguished by an increase in thrust ratio. Remember that large negative values of F/F_i indicate good thrust-reverser performance.

There appear to be two exceptions to the above trends. For example, consider configuration 11 (fig. 5(r)) in which the inner door angle is 10°. Performance of this reverse-thrust configuration generally increased (became more negative) throughout the range of NPR. As will be shown later, the physical throat moved upstream from the vane boxes to the inner door. This movement of the throat resulted in a large decrease in actual port area and large changes in the expansion ratio (ratio of exit area to throat area) and in the design NPR. Apparently the expansion ratio change was large enough so that design NPR was above 7 and was never reached.

The approach configurations in which $A_{t,\text{main}} = 2.0$ (see figs. 5(nn) to 5(pp)) indicate trends which also appear to be different from the general case. These data show that the general character (shape of curve, NPR at which maximum and minimum performance occurs, etc.) of each performance curve is a function of inner door angle; however, the absolute level of each curve is dependent upon the percentage of the total weight flow being passed through the main exhaust nozzle. For example, consider configuration 33 (fig. 5(nn)) with $\theta_t/\theta_b = 130°/130°$, $\psi_t/\psi_b = 60°/60°$, and $A_{t,\text{main}} = 2.0$ in^2. When compared with configuration 2 (same reverser vane angles and inner door angles, $A_{t,\text{main}} = 0.0$ in^2), it can be seen that the performance curves are very

similar in shape. The absolute levels of thrust ratio indicate a considerable amount of forward thrust (positive F/F_i) is being generated by the main exhaust nozzle (configuration 33). In fact, at NPR = 3.75 the forward thrust generated by the main nozzle exactly cancels the reverse thrust generated by the reverser ports; hence, $F/F_i = 0$.

Values of nozzle discharge coefficient presented in figure 5 range from 0.20 to approximately 1.37. Again, recall that the ideal weight flow w_i is based on a constant throat area of 4.0 in^2. Hence, variations in nozzle discharge coefficient between configurations can reflect physical throat area changes as well as changes in the ability of the throat to pass weight flow.

Attention should also be given to configurations in which F/F_i (hence measured axial force) is nearly equal to zero, such as for $\theta_t/\theta_b = 90°/90°$ (fig. 5(f)). The variation in F_r/F_i (dashed line) occurring for NPR > 5 is misleading and is a result of the change in sign convention for F_r/F_i when the sign of F/F_i changes as noted in the symbols section. As shown in figure 5(f), neither normal-force nor side-force ratio would indicate such a large change in the magnitude of the resultant thrust ratio.

The splitter plate configurations were tested to isolate the internal performance characteristics of the top left-hand port. This information provides hardware designers with more information on loads and load directions than would otherwise be obtained by testing only the complete configuration. Splitter plate data were obtained only for selected configurations as indicated in table I.

As discussed previously, much of the analysis of the splitter plate data was based on the fact that the reverser configurations have geometric symmetry about the centerline vertical and horizontal planes. Because of this symmetry, normal-force and side-force values equal to zero were expected from vertical and horizontal splitter plate runs, respectively. As shown in figures 5(c) and 5(d), this was generally not the case. It is believed that the nonzero values of normal force (vertical splitter plate, fig. 5(c)) and side force (horizontal splitter plate, fig. 5(d)) are the result of small differences in port geometry.

The measured internal performance characteristics of various reverser port configurations determined by the splitter plate technique are intended to be more qualitative in nature than quantitative.

Performance Comparisons

Unless otherwise noted, all configurations have the four-vane external cascade boxes, port tabs installed, no cascade vane box sideplates, and no splay angle shims installed.

Reverser geometric efflux angle. The effects of reverser geometric efflux angle on thrust ratio and on internal static-pressure ratio are presented in figures 6 to 8. Thrust ratio data are presented for configurations in which reverser geometric efflux angle was the same for all reverser ports (symmetrical efflux angles) and for configurations in which reverser geometric efflux angle was set asymmetrically to generate a particular force or moment (differential efflux angles).

Data for the configurations with symmetrical efflux angles are presented in figure 6. For the configuration with no splay angle shims, values of F/F_i range from −0.70 to 0.73 and depend, of course, on values of geometric efflux angle θ_t/θ_b. As can be seen, variation of reverser efflux angle is a very powerful thrust modulator. Thrust ratio F/F_i for cascade vanes removed (configuration 13) fell between performance levels for $\theta_t/\theta_b = 90°/90°$ and $\theta_t/\theta_b = 66°/66°$. This result was expected, since the upstream and downstream walls of the reverser port were aligned 78° from the horizontal, as noted in figure 2(a). Peak reverser performance, whether for spoiled ($\theta < 90°$) or reverse ($\theta > 90°$) thrust, generally occurred near NPR = 3 and decreased as NPR increased.

The exceptions to this were for $\theta_t/\theta_b = 90°/90°$ and 66°/66°. For $\theta_t/\theta_b = 90°/90°$, thrust along the body axis F is equal to zero, and thus the variation in F/F_i is very small. For the configuration with $\theta_t/\theta_b = 66°/66°$, thrust ratio tended to increase slightly (approximately 3 percent of F_i) with increasing NPR until a performance peak occurred at an NPR of about 5.0. It should be noted that these two configurations ($\theta_t/\theta_b = 90°/90°$ and 66°/66°) require less flow turning from the cascade vanes than the other geometric reverser efflux angles tested. This result is supported by the relative level of the data obtained for configurations with the cascade vanes removed.

Characteristic of all the efflux angle variations except $\theta_t/\theta_b = 90°/90°$ and 66°/66°, discussed previously, is the relatively large impact of NPR on measured thrust ratios. As shown in figure 6, this variation in thrust ratio tended to increase as geometric efflux angle increased or decreased from 90°/90° and 66°/66°. Examination of figures 2(c) and 2(d) will lend some insight as to why these trends occur. Each passage between the turning vanes forms a discrete single-expansion-ramp nozzle (one solid jet boundary and one free jet boundary downstream of exhaust exit). As noted in reference 23, nozzle configurations with an external expansion surface generally have a tendency to vector or turn the exhaust flow. The direction of the resultant vector is a function of the

NPR and the orientation of the external expansion surface with respect to the model. At values of NPR greater than required for fully expanded flow (underexpanded nozzle), the exhaust tends to be vectored away from the external expansion surface. For $\theta_t/\theta_b > 90°/90°$, a loss in reverse-thrust performance would be expected at underexpanded flow conditions (NPR > 3.0) because the aft-facing expansion surface would tend to vector exhaust flow back toward the vertical. When efflux angle is such that the external expansion surface is forward facing, $\theta_t/\theta_b < 90°/90°$, losses in forward thrust would be expected at underexpanded flow conditions. These trends can be seen in figure 6. As geometric efflux angle increases from 26° to 90° or decreases from 140° to 90°, the exposed length of the external expansion surface decreases, and the performance losses resulting from flow turning as discussed above would be expected to decrease. This trend is also exhibited by the data in figure 6.

Addition of the splay angle shims (for shim geometry, see fig. 2(e)) reduced levels of both reverse thrust ($\theta_t/\theta_b > 90°/90°$) and spoiled thrust ($\theta_t/\theta_b < 90°/90°$) and had little effect on thrust ratio for $\theta_t/\theta_b = 90°/90°$, as shown in figure 6. Flow visualization observations indicated that the splay angle shims significantly increased the outward cant of exhaust flow from each port and correspondingly decreased the efflux angle θ as the thrust ratio data indicate. This observation indicates that part of the axial-force component is being traded for an increase in the side-force component. The overall character of the curves with respect to NPR remains nearly the same, as discussed previously for the configurations with no splay angle shims.

Internal static-pressure ratios from orifices located in the reverser port and in the nozzle upstream of the reverser port are presented for symmetrical geometric efflux angle configurations without splay angle shims in figures 7(a) and 7(b). Pressure data are presented at NPR = 3.0 only. The data indicate that values of static-pressure ratio decreased and internal Mach number increased as θ approached a value of 78°, which corresponds to the physical reverser port wall angle as shown in figure 2(a). Examination of nozzle discharge coefficient data w_p/w_i presented in figure 5 indicates that this increase in internal Mach number in the nozzle and reverser port was accompanied by an increase in nozzle discharge coefficient. As geometric efflux angle diverged from 78°, discharge coefficient decreased.

Individual pressure taps located in the nozzle upstream of the reverser ports (fig. 7(a)) indicated that flow was being accelerated to higher speeds and, hence, lower static-pressure ratios as it approached the port opening, regardless of geometric efflux angle.

Port orifice locations, represented by circle and square symbols in figure 7(b), appear to have lower pressure ratios on the upstream reverser port wall than on the downstream wall. These lower pressure ratios indicate that the reverser flow is being accelerated around the upstream port corner. As indicated by the decreasing pressure ratios, the reverser exhaust flow is continuously accelerating through the port. However, the fact that the exhaust flow velocity is not sonic ($p/p_{t,j} \leq 0.528$) at the last pressure orifice indicates that the port physical throat probably forms in the cascade vane box located on top of each port.

The effect of splay angle shims on reverser port static-pressure ratios is presented in figure 7(c). As shown, static-pressure ratio decreased with the installation of splay angle shims. Again, an increase in discharge coefficient (see fig. 5) accompanied this decrease in static-pressure ratio in the ports.

In an effort to assess the usefulness of this reverser configuration for providing forces and moments for control, differential geometric efflux angle settings for generating both normal force and yawing moment were investigated. Normal force was generated by setting geometric efflux angles to $\theta_t/\theta_b = 90°/130°$. (See fig. 8(a).) A resulting downward normal force was generated. As expected, levels of reverse-thrust ratio obtained with this differential efflux angle configuration were approximately an average of the thrust ratios obtained for symmetrical efflux angle configurations $\theta_t/\theta_b = 90°/90°$ and $\theta_t/theat_b = 130°/130°$. The normal-force contribution to the resultant thrust ratio was equal to or greater than the axial-force contribution throughout the NPR range tested.

The configuration tested to provide a yawing moment consisted of differential efflux angle settings of 130° on the left-hand ports and 26° on the right-hand ports ($\theta_l/\theta_r = 130°/26°$). Thrust and yawing-moment ratio results in figure 8(b) show that sizable yawing moments can be generated by differential left-hand and right-hand geometric efflux angles. The basic data for this differential efflux angle configuration (fig. 5(rr)) also show that this yawing moment was generated with no side force. These differential efflux angle configurations demonstrate that a reverser which has the capability of independent control of efflux angle and port area can provide control forces to augment or replace conventional tail surfaces or canards.

Inner door angle. The effects of inner door angle on thrust ratio, nozzle discharge coefficient, and internal static-pressure ratio are presented in figures 9 to 12. Data are shown at values of

$A_{t,\text{main}} = 0.0$ in^2 (full reverse) and 2.0 in^2 (landing approach).

As discussed previously, inner door angle was intended to provide weight flow (or area) control of the individual reverser ports. As noted in figure 9, however, inner door angle also had a large impact on thrust ratio (especially for NPR < 5). Thrust ratio increased (hence reverser performance decreased) as the inner door angle was changed from the open position (60°) to the most closed position (10°). Insight into the reasons for these losses in peak reverse-thrust ratio can be gained by examination of the port static-pressure ratios presented in figure 12(b). The decreased static pressures for $\psi < 40°$ (NPR = 3.0) indicate increased velocities in the port. These increased velocities in the port, of course, mean increased velocities entering the cascade vane box. Vane turning losses resulting from separation on the leeward side of each vane would be expected to increase as velocities in the port increased. (Individual vanes are at a high angle of attack with respect to the port flow.)

The performance data for the inner door angles of 10° and 20° (fig. 9) have, in general, different characteristics than the performance data for the larger inner door angles, $\psi > 20°$. Examination of port static pressures (fig. 12(b)) indicates supersonic flow ($p/p_{t,j} \leq 0.528$) in the ports for these two inner door angle configurations. The thrust-reverser throat ($M_{\text{int}} = 1.0$) is apparently formed between the inner door and the port passage walls when the inner doors are nearly closed ($\psi = 10°$ or 20°); hence, large vane-turning losses would be expected in the presence of this supersonic flow.

The effect of inner door angle on thrust ratio for the reverser in an approach configuration ($A_{t,\text{main}} =$ 2.0 in^2) is shown in figure 10. Inner door angle variations resulted in large changes in thrust for both 0° and 20° vectoring configurations. The inner doors are obviously very effective in modulating weight flow between the main nozzle and reverser ports.

Internal port static-pressure ratios for the approach configuration at $\delta_v = 0°$ are shown in figure 12(c) and indicate, as discussed previously for $A_{t,\text{main}} = 0.0$ in^2, that port static pressures decreased as inner door angle decreased. Port pressures for the approach configurations were essentially the same on the downstream wall and slightly lower on the upstream wall for $\psi > 20°$ than for the full reverse configuration, $A_{t,\text{main}} = 0.0$ in^2 (fig. 12(b)). Port pressures for those configurations in which inner door angle was $\leq 20°$ did not generally change, probably because flow is becoming supersonic upstream of the pressure measurements, as discussed previously. Exhaust flow passing through the main exhaust nozzle did result in acceleration of the flow in the nozzle upstream of the ports, as shown in figure 12(a). This acceleration would be expected based solely on the increase in total throat area resulting from the addition of the main exhaust nozzle.

Another area of concern to nozzle designers would be whether or not inner door angle variations have any effect on pressure distributions within the main nozzle passage. As shown in figure 12(d), inner door angle (hence the modulation of weight flow) had no effect on internal static-pressure ratio on the nozzle flap centerline. Unfortunately, no pressures were measured at locations other than the nozzle flap centerline (directly behind the port, for example).

A summary of the effect of inner door angle on nozzle discharge coefficient is presented in figure 11. The modulation of weight flow was the primary function for the variable-angle inner door and, as shown in figure 11, a smooth and effective modulation of weight flow results from varying inner door angle. In combination with the variation of main nozzle throat area, inner door angle was shown to be capable of providing a wide range in values of nozzle discharge coefficient. It should again be stressed that ideal weight flow rate w_i is based on a nominal constant throat area of 4.0 in^2.

Slider door position. The slider door shown in figure 2(b) provides an alternative method of port area control to the inner door. As shown in figure 13, slider door position did not have as large an effect on thrust ratio as inner door angle had for $\theta_t/\theta_b = 130°/130°$. (See fig. 10.) An even smaller effect on thrust ratio can be noted for the reverser configuration with $\theta_t/\theta_b = 90°/90°$. A summary of slider door position effects on thrust ratio and nozzle discharge coefficient is presented in figure 14. In general, reverser performance tended to decrease (become less negative) as the slider door was closed. The closed-slider-door position resulted in a 50-percent reduction in port area. As seen, discharge coefficient for the slider door in the closed position was approximately one-half that for the slider door in the open position.

Reverser upper flap and port static pressures are presented in figure 15. As was the case any time throat area was reduced, static pressures on the nozzle flap upstream of the port increased, and the corresponding internal Mach number decreased. Pressure ratio trends in the port (fig. 15(b)) were, however, dependent upon orifice location. The orifices located directly upstream of the slider door (circle symbols) show increased pressure ratios as the slider door is closed. In fact, in the closed position, the

orifices represented by circle symbols indicate that total pressure is being measured. The only other general trend that can be noted is that when the slider door is closed and the exhaust flow passes between the outboard wall of the reverser port and the inner door, pressures measured by the remaining orifices were generally lower than for any other slider door position. It is obvious that the flow is being accelerated in the outboard portion of the reverser port because the inboard passage is blocked.

Because the slider door method of weight-flow control affected thrust ratio much less than did inner door angle for a similar variation in discharge coefficient, it in all probability would be considered a more desirable method of reverser port area control.

Asymmetric port area modulation. As discussed previously, asymmetric efflux angle configurations were capable of generating substantial normal-force and yawing-moment components. Two methods of modulating the magnitudes of these forces and moments are (1) the use of differential inner door angle and (2) the use of differential slider door position. The effects of differential inner door angle and slider door position on thrust and normal-force ratios for an asymmetric geometric efflux angle configuration ($\theta_t/\theta_b = 90°/130°$) are presented in figure 16. Both methods of port area modulation provided large increases in normal-force ratio (increases on the order of 70 to 115 percent) over the symmetrical inner door/slider door configuration (data represented by circles). Values of normal force were approximately 3 to 4 times larger than the axial-force component (F/F_i).

It appears that by independent actuation of geometric efflux angle, inner door angle, and/or slider door position, the potential for tailoring individual forces and moments generated by the propulsion system would be nearly limitless. Such a capability could be used for low-speed control augmentation during landing approach.

Cascade vane box configuration. The effect of cascade vane box configuration on thrust ratio for the reverser configuration with $\theta_t/\theta_b = 130°/130°$ is presented in figure 17. As shown, the six-vane configuration provided higher levels of reverse thrust than the four-vane configuration throughout the NPR range tested. The improvement in reverse-thrust performance is believed to be a direct result of decreasing the spacing between the vanes. Decreasing vane spacing reduces the length of the external expansion surface available for the exhaust flow to act upon and thus reduces the adverse effect on reverser performance discussed previously.

Port tab. The effect of the port tab (see fig. 2(d)) on thrust ratio and reverser static pressures is presented in figures 18 and 19, respectively. As seen in figure 18, removal of the reverser port tab had little or no effect on thrust ratio for values of NPR ≤ 3.0. However, for NPR > 3.0, reverse-thrust performance was significantly higher (more negative) for the configuration with the port tab removed.

Reasons for this higher performance can best be explained by referring to the sketch of the vane box and port tab in figure 2(d). With the port tab installed, the vanes form three distinct nozzle passages. As discussed previously, all three passages have an aft-facing external expansion surface which is somewhat larger for the efflux angle of 130° than for any other efflux angles except 140° and 26°. As noted in reference 23, nozzle configurations with an external expansion surface generally have a tendency to vector exhaust flow away from the external expansion surface once the NPR is above that required for fully expanded flow on the expansion surface. Reverse-thrust losses (exhaust flow turned more aft) would, therefore, be expected for the configurations with the geometric efflux angles of 130° at the higher NPR values, for which exhaust flow is underexpanded.

With the port tab removed, an additional nozzle passage is created. This passage would exhibit external expansion surface flow characteristics similar to those discussed above, except that the most upstream vane provides an external expansion surface which is forward facing. The external expansion surface for this passage should help turn the exhaust flow upstream (in the reverse-thrust direction) at the higher NPR values. The result is a net decrease in the underexpanded flow turning associated with the aft-facing expansion surfaces of the aft three passages (and a net increase in reverse-thrust performance, as shown in fig. 18).

The static pressures on the flap upstream of the reverser ports and in the reverser ports (fig. 19) were reduced when the port tab was removed. These reductions in static pressure are indicative of an increase in throat area. Examination of discharge coefficients presented in figures 5(b) and 5(hh) confirms this.

Cascade vane box sideplates. The effect of cascade vane box sideplates on thrust ratio is presented in figure 20. The reverser configuration with the vane box sideplates installed provided higher levels of reverse thrust than those for the same configuration without sideplates. The need for the sideplate was identified by means of flow visualization techniques. It was noted during the test that high-energy flow was leaking out of the slot formed between the noz-

zle boattail surface and the structural support for the vanes. (See fig. 2(d).) This leakage did not contribute to the reverse-thrust component because it was directed to the side. When the sideplates were added, all the exhaust flow was then directed through the vanes and therefore contributed to the reverse-thrust component.

Examination of nozzle discharge coefficient data for these two configurations (figs. 5(b) and 5(ii)) shows that there is a 3- to 4-percent reduction in discharge coefficient resulting from the addition of sideplates. This observation lends further credibility to the hypothesis that the physical throat of many of these reverser configurations (especially when the inner doors are fully open) is located in the vane box.

Main exhaust nozzle throat area. Under actual operating conditions, modulation of thrust ratio will in all probability be accompanied by simultaneous variation of reverser port area and main exhaust nozzle area. Port area will open as main nozzle area is closed. Thus, effective throat area will be held constant to prevent disruptions in engine operation resulting in stall or overspeed.

The effect of varying main exhaust nozzle throat area on thrust ratio is presented in figure 21. For all configurations in which the reverser ports were open, geometric efflux angle was held constant at $\theta_t/\theta_b = 130°/130°$ and the inner door and slider doors were fully open.

As shown in figure 21, values of thrust ratio ranged from 0.97 for the main nozzle only to −0.55 for the reversers only. Depending on main nozzle throat area, thrust ratio varied from 0.07 to −0.55 with reversers operating. As certainly would be expected, decreasing the main nozzle throat area resulted in a greater percentage of the exhaust flow being directed to the reverser ports and, hence, an increase in reverser performance (larger negative values of F/F_i).

Main nozzle pitch vector angle. The effect of main nozzle pitch vector angle on thrust ratio is presented in figure 22 for forward-thrust-mode (reverser-ports-closed) and approach (combined main nozzle/reverser) configurations. Data are presented for several values of inner door angle. With the main exhaust nozzle alone (reverser ports closed), significant differences between thrust ratio and resultant thrust ratio, shown by the dashed line, occur for the configuration with $\delta_v = 20°$. These differences are a function of the resultant thrust-vector angle and occur because jet exhaust flow is directed away from the axial direction. For the forward-thrust-mode configuration at $\delta_v = 0°$; F/F_i is equal to F_r/F_i. Differences between F/F_i for the configuration with $\delta_v = 0°$ and F_r/F_i for the configuration with $\delta_v = 20°$ are a measure of the internal performance losses associated with turning (pitch thrust vectoring) the exhaust flow. As can be seen, these losses were less than 1 percent for the forward-thrust-mode (reverser-ports-closed) configuration (fig. 22(a)).

Increases in inner door angle resulted in decreases in thrust ratio (as well as resultant thrust ratio), as noted previously, since a larger percentage of the exhaust flow is being directed out of the reverser ports.

Splay angle. One of the primary objectives of the present reverser design was to provide some outboard cant (splay) of exhaust flow. A splay angle of 30° was originally desired to help prevent hot gas impingement on tail surfaces and reingestion of exhaust flow by the inlet on a fighter configuration. A component breakdown of the various forces measured and the relationships used to compute reverser splay angle are illustrated in figure 23 for configuration 2 ($\theta_t/\theta_b = 130°/130°, \psi_t/\psi_b = 60°/60°$, slider door open). Data are presented at an NPR of 3.0. Note that the signs of all forces presented were reversed in an effort to provide graphical representation of the reverser flow direction instead of the reaction thrust vectors. As discussed in the "Data Reduction" section, this analysis was based on measurements made during splitter plate runs as well as complete configuration runs. Splay angle was computed to be 10.8°, a value considerably below the desired splay angle of 30°. The measured efflux angle of 135.5° indicates that reverser flow for the configuration with a geometric efflux angle of 130° was slightly overturned. This overturning of the exhaust flow may be the result of the external-expansion-ramp characteristic of each individual nozzle passage operating at overexpanded flow conditions. External-expansion-ramp nozzles operating at values of NPR below those for fully expanded flow on the external surface often tend to vector exhaust flow toward the external expansion surface (ref. 23). Hence for the reverser configuration tested, the flow is turned even more than the geometric efflux angle.

The splitter plate data technique was used to determine the effects of geometric efflux angle and inner door angle on reverser splay angle, and the results are presented in figure 24. In all cases, splay angle was less than the desired value of 30°. In fact, the reverser with a geometric efflux angle of 130° provided splay angles less than 12° throughout the NPR range. One reason the desired splay angles were not attained is believed to be the vane box orientation (in the splay direction) with respect to the reverser port wall angle

as shown in figure 2(a). The port walls were aligned at 30° from the vertical; however, the cascade vane box sidewalls were only canted 7.6°. Flow is being directed back toward the vertical by the vane box sidewalls. Had the sidewalls been aligned parallel to the port walls, larger splay angles would probably have resulted. This hypothesis is supported by the data shown in figure 24 for the configuration with $\theta_t/\theta_b = 130°/130°$ and cascade vane box sideplates installed and is discussed later. With no cascade vane box sideplates, splay angle increased as geometric efflux angle decreased from 130° to 26°. Comparison of the individual normal- and side-force components for the efflux angle of 130° (figs. 5(c) and 5(d)) and the efflux angle of 26° (figs. 5(l) and 5(m)) points out the interdependency of splay angle on efflux angle. The side-force components for both configurations were nearly equal (figs. 5(c) and 5(l)), but since the geometric efflux angle of 26° turned flow back toward the horizontal more than the 130° angle, normal-force component for the efflux angle of 26° was considerably smaller (figs. 5(d) and 5(m)); hence, the resultant splay angle was significantly larger.

With cascade vane box sideplates installed on the reverser configuration with an efflux angle of 130°, a further reduction in splay angle was measured, as can be seen in figure 24. As discussed previously, cascade vane box sideplates reduce lateral leakage and direct more flow over the vanes. Both normal force and axial force increase relative to side force for the sideplates-installed configuration (compare figs. 5(c) and 5(d) with 5(jj) and 5(kk)); hence, the reverser configuration with sideplates produces a smaller splay angle than the reverser configuration without sideplates.

Variation of inner door angle for the reverser with $\theta_t/\theta_b = 130°/130°$ and had little or no effect on splay angle for the inner door angles presented. (See fig. 24.)

Results of the splay angle analysis highlight the interrelationship between efflux angle and splay angle. In order to meet both a splay angle and an efflux angle requirement simultaneously, exhaust flow must be overturned more than the desired angles in both directions.

Summary Figures

A summary plot of geometric efflux angle and main nozzle throat area effects on thrust ratio for an inner door angle setting of 60°/60° is presented in figure 25 at NPR = 3.0. Combined use of efflux angle and main nozzle throat area provides very effective modulation of thrust ratio. Values of F/F_i ranged from 0.97 to approximately −0.70. Note that $\theta_t/\theta_b = 0°/0°$ represents the reverser-ports-closed (or forward-thrust) configuration. The effects of main nozzle throat area on F/F_i were large for an efflux angle of 130° and, as indicated by the dashed lines, would be expected to decrease as efflux angle decreased. This decrease is expected, since a decrease in efflux angle results in reverser flow being directed more toward the aft direction coincident with the main exhaust nozzle flow.

A summary of inner door angle and main nozzle throat area effects on thrust ratio for $\theta_t/\theta_b = 130°/130°$ is shown in figure 26 at NPR = 3.0. Again a very large variation in thrust ratio can be generated by combined use of inner door angle and main nozzle throat area. Thrust ratios ranging from 0.58 to −0.55 were generated at a fixed geometric efflux angle. The effect of nozzle throat area on F/F_i increased as inner door angle decreased. This result would be expected on the basis of the relatively large impact of inner door angle (for $\psi \leq 20°$) on thrust ratio, as noted previously. (See fig. 9.)

Summary figures 25 and 26 indicate that the nozzle reverser design of the present investigation has the capability of generating any required value of thrust ratio from 0.97 (for main nozzles only) to almost −0.70 (for full reverse). This variation of thrust ratio can be obtained by various combinations of geometric efflux angle, inner door angle, and main nozzle throat area.

Conclusions

An investigation has been conducted at wind-off conditions in the static-test facility of the Langley 16-Foot Transonic Tunnel. The tests were conducted on a single-engine reverser configuration with partial (thrust modulation) and full reverse-thrust capabilities. The reverser design had four ports with equal areas. The ports were angled outboard 30° from the vertical to impart a splay angle to the reverser exhaust flow. This splay angle was intended to prevent impingement of exhaust flow on empennage surfaces and to help avoid inlet reingestion of exhaust gas when the reverser is integrated into an actual airplane configuration. External vane boxes were located directly over each of the four ports to provide variation of reverser efflux angle from 26° to 140° (measured forward from the horizontal reference axis). The reverser model was tested with both a butterfly-type inner door and an internal slider door to provide area control for each individual port. In addition, main nozzle throat area and vector angle were varied to examine various methods of modulating thrust levels. Other model variables included vane box configuration (four or six vanes per box),

orientation of external vane boxes with respect to internal port walls (splay angle shims), and vane box sideplates. Nozzle pressure ratio was varied from 2.0 to approximately 7.0. Results of this study indicate the following conclusions:

1. For a nonaxisymmetric nozzle with an integrated thrust reverser, use of reverser efflux angle, inner door angle, and main nozzle throat area provides effective control of thrust ratio (magnitude of forward or reverse thrust). For the configuration tested, values of thrust ratio ranged from 0.97 for the main nozzle only to almost -0.70 for full reverse thrust at a typical operating nozzle pressure ratio of 3.0.

2. Orientation of cascade vane box with respect to reverser port walls appears to have a large effect on reverser exhaust splay angle. For the configuration tested, splay angle values less than 12° were measured for the full reverse-thrust configurations. The goal of a splay angle of 30° for each port was not met, partially, because the vane box sidewalls redirected reverser exhaust flow (exiting the reverser ports at a splay angle of approximately 30°) back toward the vertical.

3. Flow visualization observations and measured performance data indicated that addition of the splay angle shims to align cascade vane boxes with reverser port walls significantly increased the reverser flow splay angle for each port but correspondingly decreased the efflux angle.

4. The interrelationship between reverser exhaust efflux angle and splay angle dictates that reverser exhaust flow must be overturned in both the efflux and splay angle directions in order to meet the efflux and splay angle goals simultaneously.

5. Variable inner doors provide a smooth and effective modulation of weight flow on both landing (full reverse-thrust) and approach (combined reverser/main nozzle) configurations. In addition, they had a large impact on thrust ratio. As inner doors were moved from the fully open to the most closed position, losses in reverse thrust performance occurred.

6. Inner door angle (hence variation of weight flow passing through reverser ports) had no effect on static pressures measured along the main nozzle flap centerline.

7. A variable internal slider door is probably a more desirable device for port area control than a variable inner door because varying slider door position had a much smaller impact on thrust ratio for a given change in nozzle discharge coefficient.

8. Differential variation of geometric efflux angle, inner door angle, and/or slider door position generated significant forces and moments which could be used to augment or possibly replace conventional control surfaces.

9. The six-vane reverser configuration provided higher levels of reverse thrust than the four-vane configuration.

NASA Langley Research Center
Hampton, VA 23665-5225
September 10, 1985

References

1. Lorincz, Dale J.; Chiarelli, Charles; and Hunt, Brian L.: Effect of In-Flight Thrust Reverser Deployment on Tactical Aircraft Stability and Control. AIAA Paper No. 81-1446, July 1981.
2. Blackman, J. P.; and Eigenmann, M. F.: Axisymmetric Approach and Landing Thrust Reversers. AIAA Paper No. 81-1650, Aug. 1981.
3. Anderson, Seth B.; Cooper, George E.; and Faye, Alan E., Jr.: *Flight Measurements of the Effect of a Controllable Thrust Reverser on the Flight Characteristics of a Single-Engine Jet Airplane.* NASA MEMO 4- 26-59A, 1959.
4. Kelly, Mark W.; Greif, Richard K.; and Tolhurst, William H., Jr.: *Full-Scale Wind-Tunnel Tests of a Swept-Wing Airplane With a Cascade-Type Thrust Reverser.* NASA TN D-311, 1960.
5. Simpson, W. R.; Covey, M. W.; Palmer, D. F.; and Hewett, M. D.: *Navy Evaluation of F-11A In-Flight Thrust Control System.* SA-75R-75, U.S. Naval Air Test Center, Dec. 15, 1975. (Available from DTIC as AD A019 954.)
6. Steffen, Fred W.; and McArdle, Jack G.: *Performance Characteristics of Cylindrical Target-Type Thrust Reversers.* NACA RM E55I29, 1956.
7. Swihart, John M.: *Effect of Target-Type Thrust Reverser on Transonic Aerodynamic Characteristics of a Single-Engine Fighter Model.* NACA RM L57J16, 1958.
8. Weiss, D. C.; and McGuigan, W. M.: Inflight Thrust Control for Fighter Aircraft. AIAA Paper No. 70-513, Mar. 1970.
9. Linderman, D. L.; and Mount, J. S.: Development of an In-Flight Thrust Reverser for Tactical/Attack Aircraft. AIAA Paper No. 70-699, June 1970.
10. Maiden, Donald L.; and Mercer, Charles E.: *Performance Characteristics of a Single-Engine Fighter Model Fitted With an In-Flight Thrust Reverser.* NASA TN D-6460, 1971.
11. Mercer, Charles E.; and Maiden, Donald L.: *Effects of an In-Flight Thrust Reverser on the Stability and Control Characteristics of a Single-Engine Fighter Airplane Model.* NASA TN D-6886, 1972.
12. Goetz, Gerald F.; Young, John H.; and Palcza, J. Lawrence: A Two-Dimensional Airframe Integrated Nozzle Design with Inflight Thrust Vectoring and Re-

versing Capabilities for Advanced Fighter Aircraft. AIAA Paper No. 76-626, July 1976.
13. Willard, C. M.; Capone, F. J.; Konarski, M.; and Stevens, H. L.: Static Performance of Vectoring/ Reversing Non-Axisymmetric Nozzles. AIAA Paper No. 77-840, July 1977.
14. Capone, Francis J.: *Static Performance of Five Twin-Engine Nonaxisymmetric Nozzles With Vectoring and Reversing Capability.* NASA TP-1224, 1978.
15. Hiley, P. E.; Kitzmiller, D. E.; and Willard, C. M.: Installed Performance of Vectoring/Reversing Nonaxisymmetric Nozzles. *J. Aircr.*, vol. 16, no. 8, Aug. 1979, pp. 532–538.
16. Capone, Francis J.; Gowadia, Nashir S.; and Wooten, W. H.: Performance Characteristics of Nonaxisymmetric Nozzles Installed on the F-18 Aircraft. AIAA Paper No. 79-0101, Jan. 1979.
17. Petit, John E.; and Capone, Francis J.: Performance Characteristics of a Wedge Nozzle Installed on an F-18 Propulsion Wind Tunnel Model. AIAA Paper No. 79-1164, June 1979.
18. Laughrey, J. A.; Drape, D. J.; and Hiley, P. E.: Performance Evaluation of an Air Vehicle Utilizing Nonaxisymmetric Nozzles. AIAA Paper No. 79-1811, Aug. 1979.
19. Capone, Francis J.; and Berrier, Bobby L.: *Investigation of Axisymmetric and Nonaxisymmetric Nozzles Installed on a 0.10-Scale F-18 Prototype Airplane Model.* NASA TP-1638, 1980.
20. Bare, E. Ann; Berrier, Bobby L.; and Capone, Francis J.: *Effects of Simulated In-Flight Thrust Reversing on Vertical-Tail Loads of F-18 and F-15 Airplane Models.* NASA TP-1890, 1981.
21. Capone, Francis J.; Re, Richard J.; and Bare, E. Ann: Thrust Reversing Effects on Twin-Engine Aircraft Having Nonaxisymmetric Nozzles. AIAA Paper No. 81-2639, Dec. 1981.
22. Banks, D. W.; Quinto, P. F.; and Paulson, J. W., Jr.: Thrust-Induced Effects on Low-Speed Aerodynamics of Fighter Aircraft. AIAA Paper No. 81-2612, Dec. 1981.
23. Re, Richard J.; and Berrier, Bobby L.: *Static Internal Performance of Single Expansion-Ramp Nozzles With Thrust Vectoring and Reversing.* NASA TP-1962, 1982.
24. Hiley, P. E.; and Bowers, D. L.: Advanced Nozzle Integration for Supersonic Strike Fighter Application. AIAA Paper No. 81-1441, July 1981.
25. Re, Richard J.; and Leavitt, Laurence D.: *Static Internal Performance Including Thrust Vectoring and Reversing of Two-Dimensional Convergent-Divergent Nozzles.* NASA TP-2253, 1984.
26. Carson, George T., Jr.; Capone, Francis J.; and Mason, Mary L.: *Aeropropulsive Characteristics of Nonaxisymmetric-Nozzle Thrust Reversers at Mach Numbers From 0 to 1.20.* NASA TP-2306, 1984.
27. Leavitt, Laurence D.; and Re, Richard J.: *Static Internal Performance Characteristics of Two Thrust-Reverser*
28. Rowe, R. Kevin; Dusa, D. J.; and Leavitt, Laurence D.: Static Internal Performance Evaluation of Several Thrust Reversing Concepts for 2D-CD Nozzles. AIAA Paper No. 84-1174, June 1984.
29. Obye, R. C.; and Hakim, A. D.: Axisymmetric Approach and Landing Thrust Reverser Concepts: Hot Flow Test Results. AIAA Paper No. 84-1176, June 1984.
30. McLafferty, George H.; and Peterson, Jeffrey L.: Results of Tests of a Rectangular Vectoring/Reversing Nozzle on an F100 Engine. AIAA Paper No. 83-1285, June 1983.
31. Nelson, B. D.; and Nicolai, L. M.: Application of Multi-Function Nozzles to Advanced Fighters. AIAA Paper No. 81-2618, Dec. 1981.
32. Banks, Daniel W.; and Paulson, John W., Jr.: *Aerodynamic Characteristics and Predicted Landing Performance of an F-15 Fighter With Two Thrust-Reverser Configurations.* NASA TP-2466, 1985.
33. Glezer, A.; Hughes, R. V.; and Hunt, B. L.: Thrust Reverser Effects on the Tail Surface Aerodynamics of an F-18 Type Configuration. AIAA Paper No. 83-1860, July 1983.
34. Amin, N. F.; and Richards, C. J.: Thrust Reverser Exhaust Plume Reingestion Tests for a STOL Fighter Model. AIAA Paper No. 83-1229, June 1983.
35. Chiarelli, Charles; Lorincz, Dale; and Hunt, Brian: Thrust Reverser Induced Flow Interference on Tactical Aircraft Stability and Control. AIAA Paper No. 82-1133, June 1982.
36. Chiarelli, Charles; and Compton, Michael: Wind Tunnel Evaluation of Tactical Aircraft Stability and Control as Affected by Nozzle Thrust Reverser Parameter Variations. AIAA Paper No. 83-1228, June 1983.
37. Burger, Karl Heinz: In-Flight Short Field Landing Investigations on a Combat Aircraft With Thrust Reverser. AIAA Paper No. 83-2693, Nov. 1983.
38. Miller, E. H.: Performance of a Forward Swept Wing Fighter Utilizing Thrust Vectoring. AIAA Paper No. 83-2482, Oct. 1983.
39. Eigenmann, M. F.; Kitzmiller, D. E.; and Hakim, A. D.: Axisymmetric Approach and Landing Thrust Reverser Concepts: In-Ground Effects Wind Tunnel Test Results. AIAA Paper No. 84-1215, June 1984.
40. Bittrick, W. C.: Axisymmetric Approach and Landing Thrust Reversers for Single Engine Fighters. AIAA Paper No. 84-1214, June 1984.

TABLE I. INDEX TO BASIC DATA

Conf	Geometric efflux angle, θ_t/θ_b, deg	Inner door angle, ψ_t/ψ_b, deg	Slider door position	Vane box configuration	Port tab	Vane box sideplates	Splay angle shims	$A_{t,\text{main}}$, in^2	δ_v, deg	Basic data figure for configuration with–		
										No splitter	Vertical splitter	Horizontal splitter
1	140/140	60/60	Open	Four vanes	On	Off	Off	0.0	N/A	5(a)		
2	130/130	↓	↓	↓	↓	↓	↓	↓	↓	5(b)	5(c)	5(d)
3	110/110	↓	↓	↓	↓	↓	↓	↓	↓	5(e)		
4	90/90	↓	↓	↓	↓	↓	↓	↓	↓	5(f)	5(g)	5(h)
5	66/66	↓	↓	↓	↓	↓	↓	↓	↓	5(i)		
6	46/46	↓	↓	↓	↓	↓	↓	↓	↓	5(j)		
7	26/26	↓	↓	↓	↓	↓	↓	↓	↓	5(k)	5(l)	5(m)
8	130/130	40/40	↓	↓	↓	↓	↓	↓	↓	5(n)		
9	↓	30/30	↓	↓	↓	↓	↓	↓	↓	5(n)		
10	↓	20/20	↓	↓	↓	↓	↓	↓	↓	5(o)	5(p)	5(q)
11	↓	10/10	↓	↓	↓	↓	↓	↓	↓	5(r)		
12	↓	Off/Off	↓	↓	↓	↓	↓	↓	↓	5(s)	5(t)	5(u)
13	Off/Off	60/60	↓	↓	↓	↓	↓	↓	↓	5(v)	5(w)	
14	130/130	↓	Closed	↓	↓	↓	↓	↓	↓	5(x)	5(y)	5(z)
15	130/130	↓	2/3	↓	↓	↓	↓	↓	↓	5(aa)		
16	130/130	↓	1/3	↓	↓	↓	↓	↓	↓	5(aa)		
17	90/90	↓	Closed	↓	↓	↓	↓	↓	↓	5(bb)		5(cc)
18	90/130	60/10	Open	↓	↓	↓	↓	↓	↓	5(dd)		
19	90/130	60/60	Open	↓	↓	↓	↓	↓	↓	5(ee)		
20	90/130	↓	Open/Closed	↓	↓	↓	↓	↓	↓	5(ff)		
21	130/130	↓	Open	Six vanes	↓	↓	↓	↓	↓	5(gg)		
22	130/130	↓	Open	Four vanes	Off	↓	↓	↓	↓	5(hh)		

TABLE I. Concluded

Conf	Geometric efflux angle, θ_t/θ_b, deg	Inner door angle, ψ_t/ψ_b, deg	Slider door position	Vane box configuration	Port tab	Vane box sideplates	Splay angle shims	$A_{t,\text{main}}$, in^2	δ_v, deg	Basic data figure for configuration with–		
										No splitter	Vertical splitter	Horizontal splitter
23	130/130	60/60	Open	Four vanes	On	On	Off	0.0	N/A	5(ii)	5(jj)	5(kk)
24	130/130	↓	↓	↓	↓	Off	On	↓	↓	5(b)		
25	110/110	↓	↓	↓	↓	↓	↓	↓	↓	5(e)		
26	90/90	↓	↓	↓	↓	↓	↓	↓	↓	5(ll)		
27	66/66	↓	↓	↓	↓	↓	↓	↓	↓	5(i)		
28	46/46	↓	↓	↓	↓	↓	↓	↓	↓	5(j)		
29	26/26	↓	↓	↓	↓	↓	↓	↓	↓	5(k)		
30	130/130	60/60	↓	↓	↓	↓	Off	.5	0	5(mm)		
31	↓	20/20	↓	↓	↓	↓	↓	.5	↓	5(mm)		
32	↓	60/20	↓	↓	↓	↓	↓	.5	↓	5(mm)		
33	↓	60/60	↓	↓	↓	↓	↓	2.0	↓	5(nn)		
34	↓	30/30	↓	↓	↓	↓	↓	↓	↓	5(nn)		
35	↓	20/20	↓	↓	↓	↓	↓	↓	↓	5(oo)		
36	↓	10/10	↓	↓	↓	↓	↓	↓	↓	5(oo)		
37	↓	20/10	↓	↓	↓	↓	↓	↓	↓	5(oo)		
38	↓	30/30	↓	↓	↓	↓	↓	↓	20	5(pp)		
39	↓	20/20	↓	↓	↓	↓	↓	↓	20	5(pp)		
40	↓	10/10	↓	↓	↓	↓	↓	↓	20	5(pp)		
41	*Blank/Blank	Closed	N/A	N/A	N/A	N/A	N/A	2.0	0	5(qq)		
42	*Blank/Blank	Closed	N/A	N/A	N/A	N/A	N/A	2.0	20	5(qq)		
43	†130/126	60/60	Open	Four vanes	On	Off	Off	.0	N/A	5(rr)		

* Reverser ports closed.

† Geometric efflux angle on left and right sides of model instead of top and bottom.

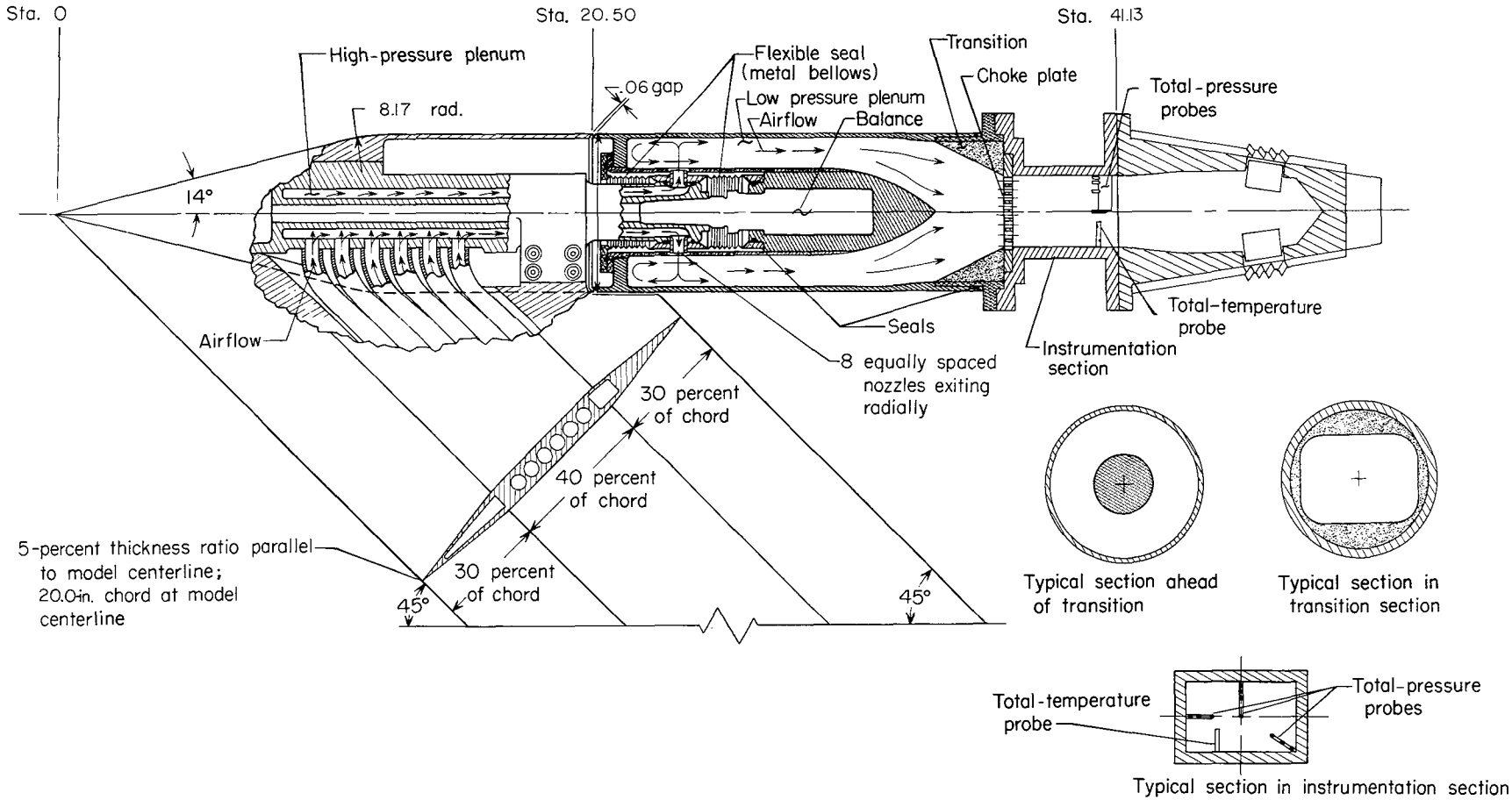

Figure 1. Sketch of air-powered nacelle model with typical reverser configuration installed. All dimensions are in inches unless otherwise noted.

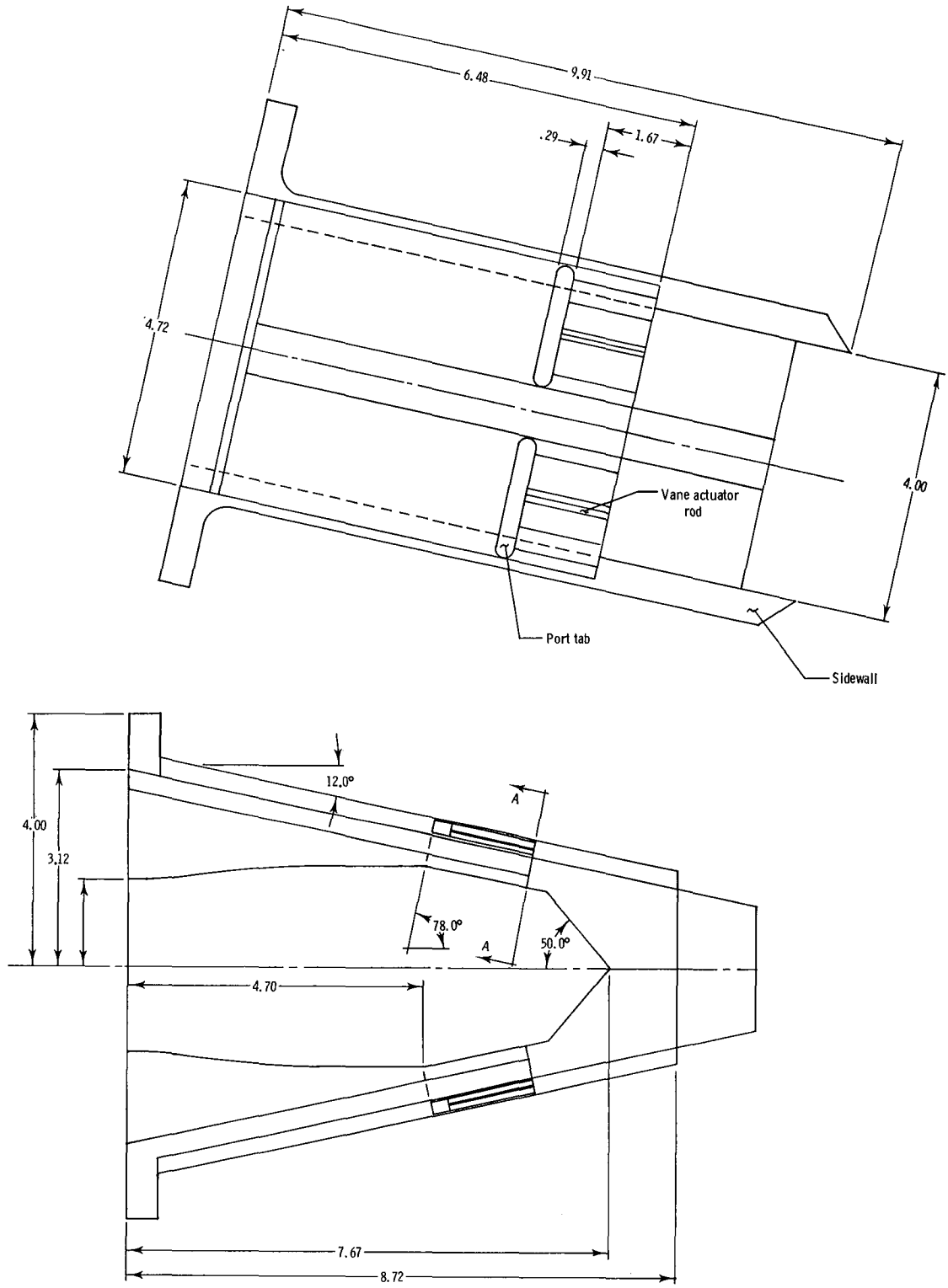

(a) Details of model geometry.

Figure 2. Model sketches of single-engine reverser. All dimensions in inches unless otherwise noted.

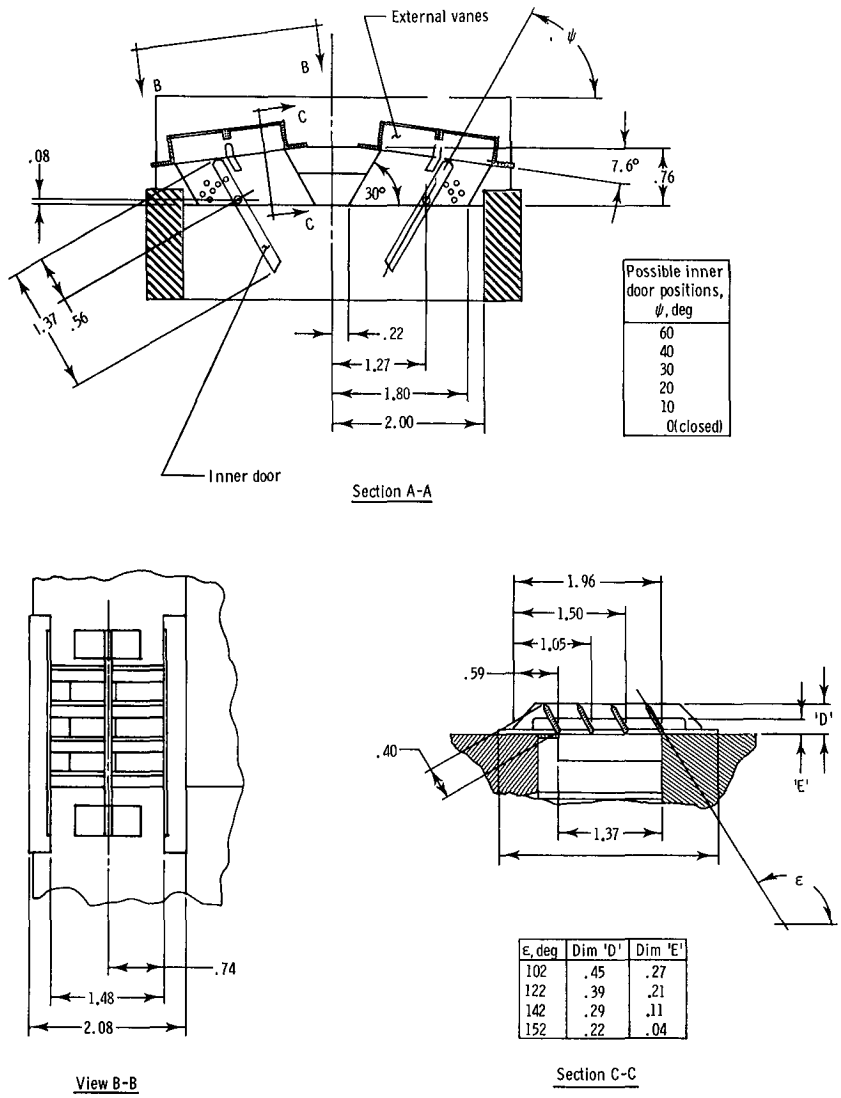

(a) Concluded.

Figure 2. Continued.

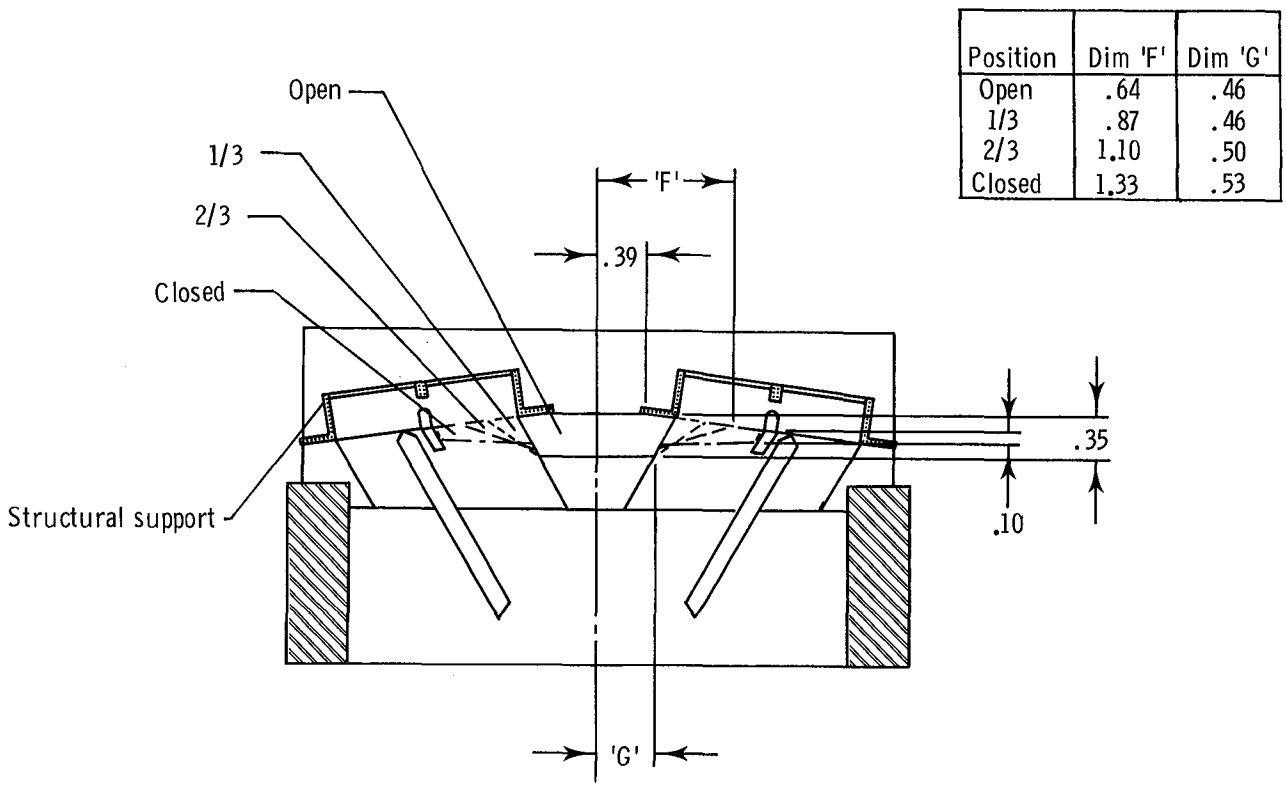

Position	Dim 'F'	Dim 'G'
Open	.64	.46
1/3	.87	.46
2/3	1.10	.50
Closed	1.33	.53

(b) Slider door positions.

Figure 2. Continued.

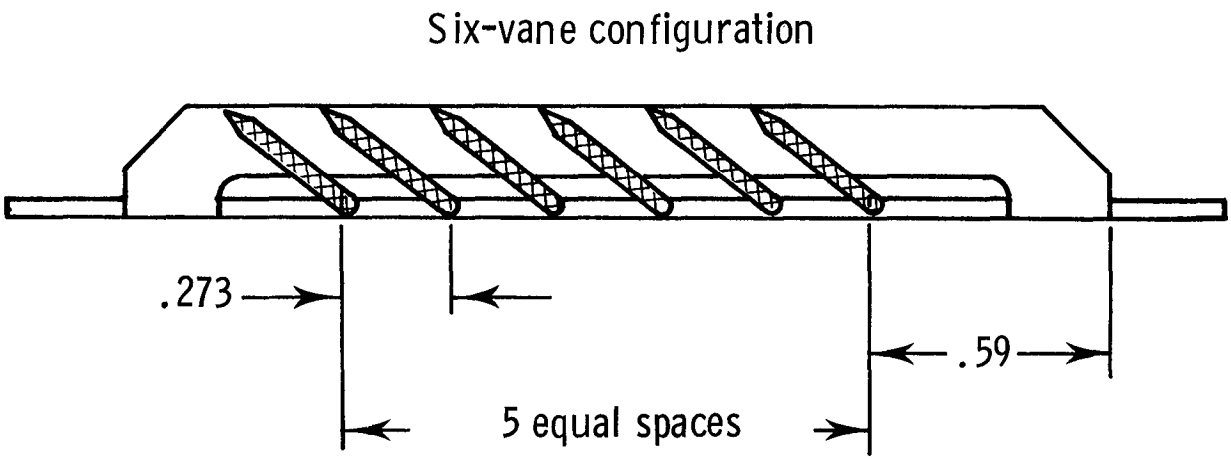

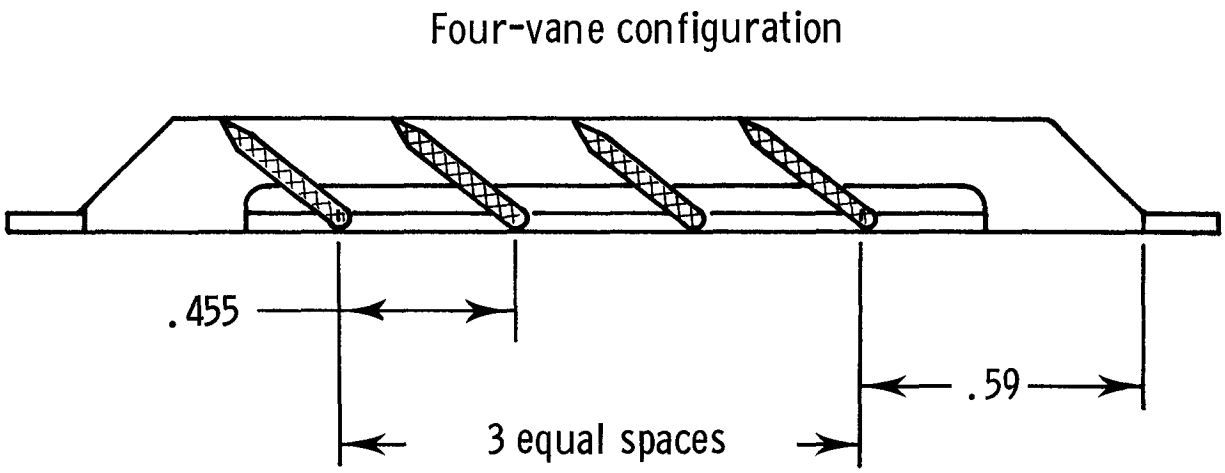

(c) Vane box configurations.

Figure 2. Continued.

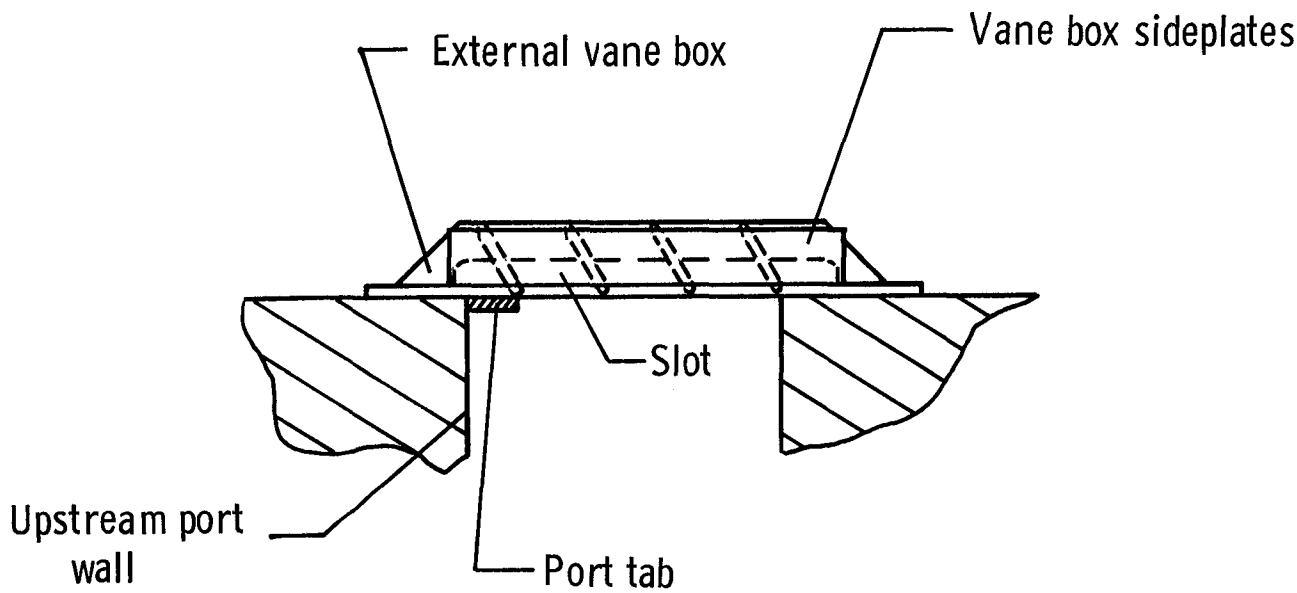

(d) Port tab and vane box sideplates.

Figure 2. Continued.

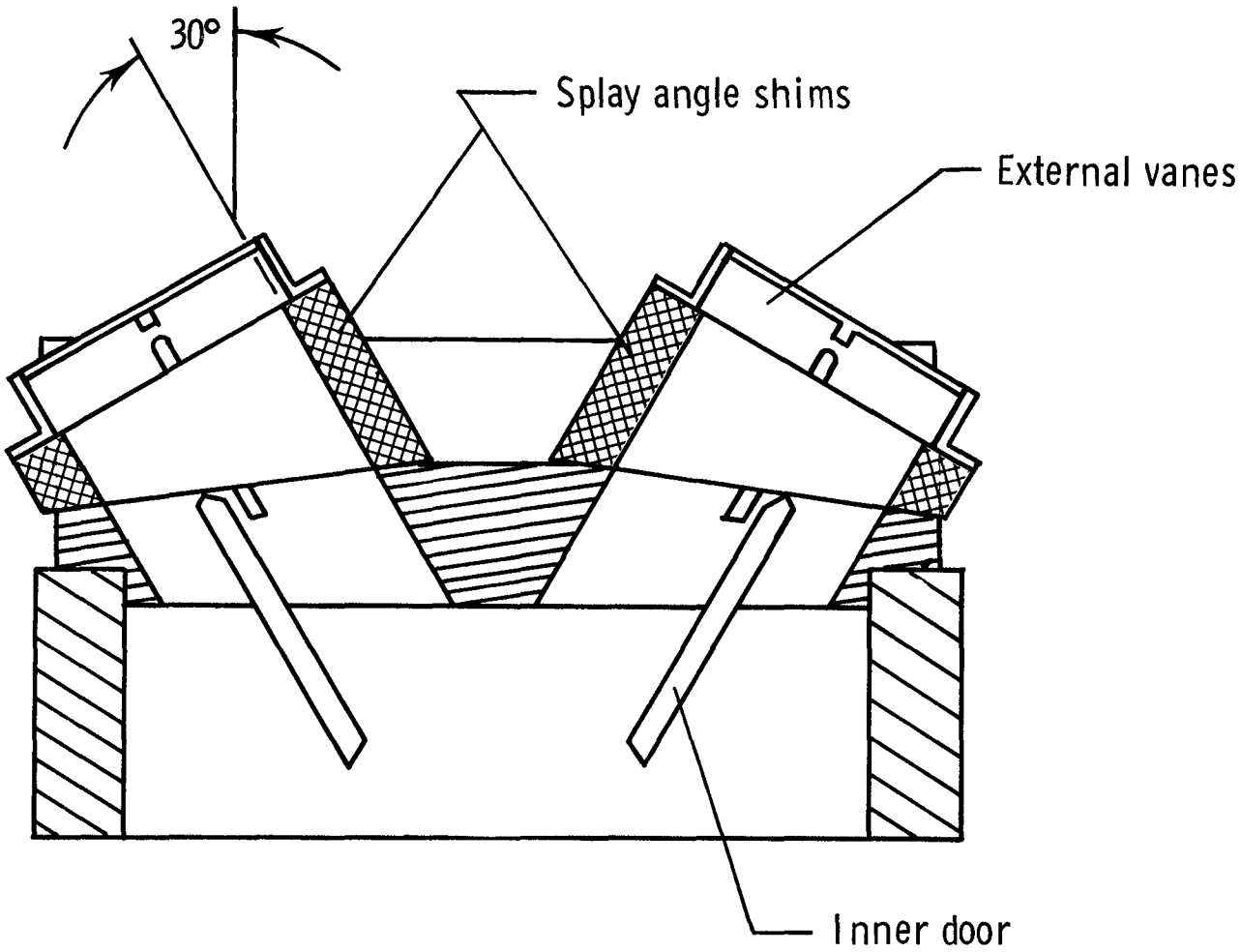

(e) Splay angle shims.

Figure 2. Continued.

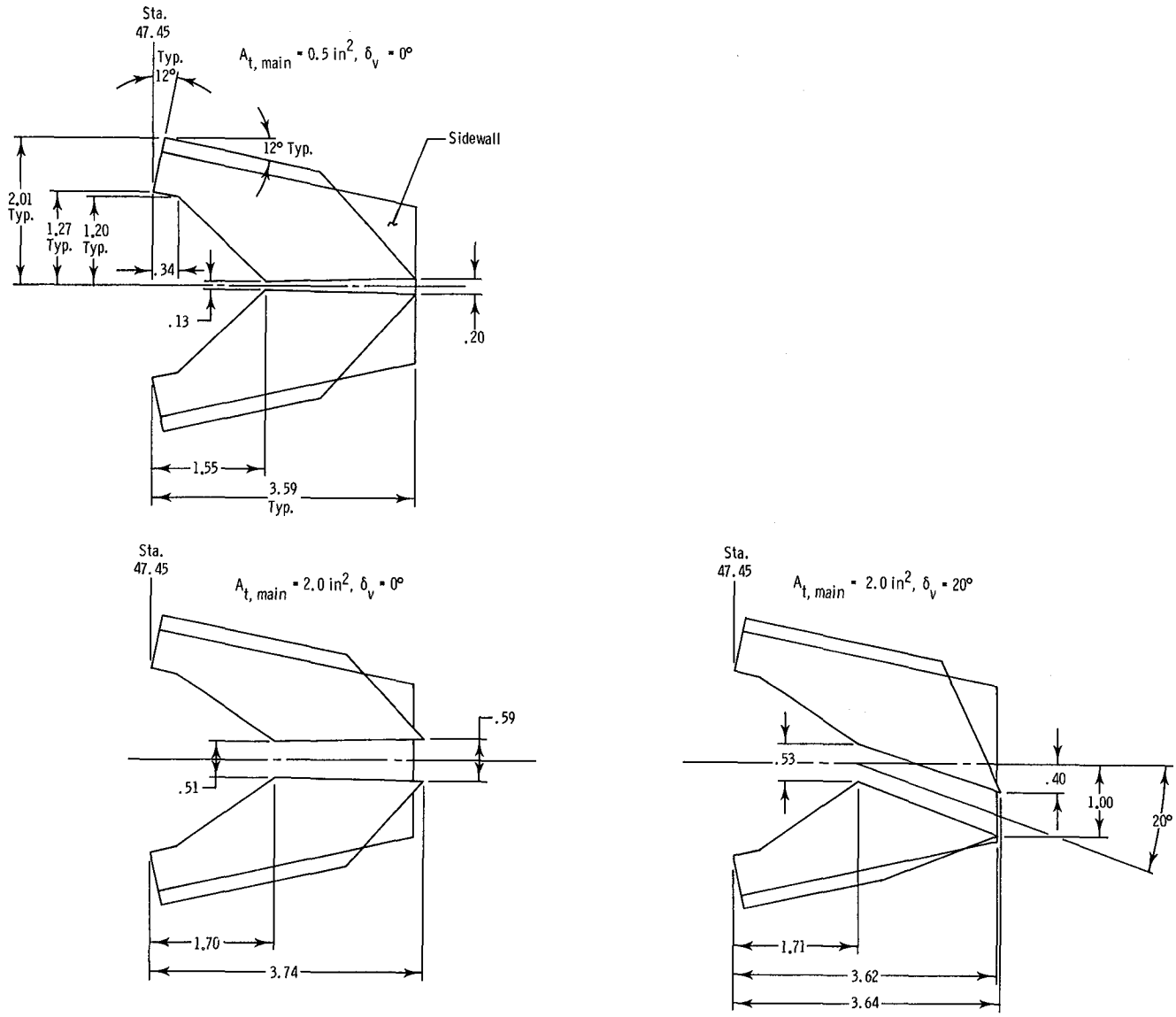

(f) 2-D C-D main exhaust nozzle geometry.

Figure 2. Continued.

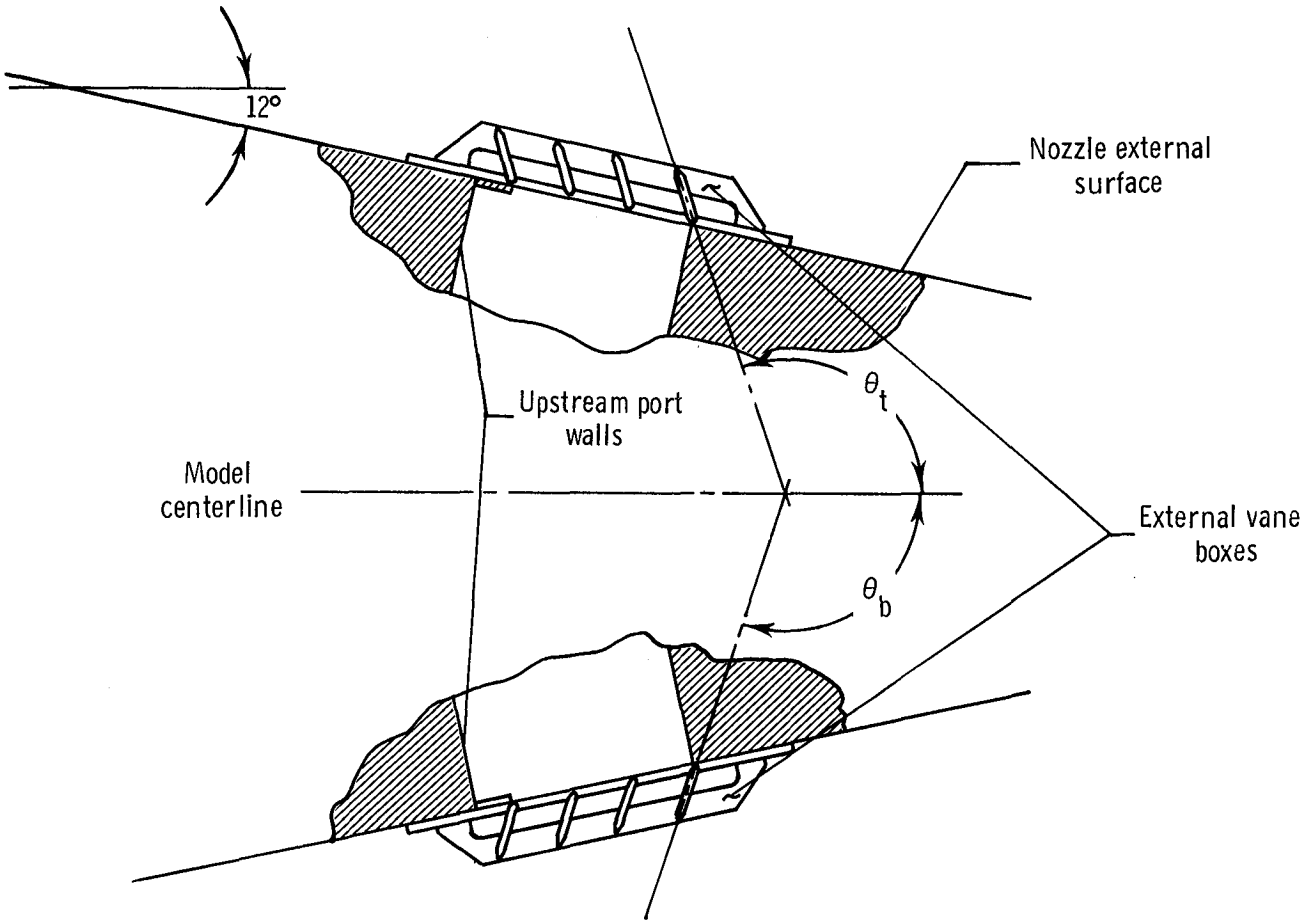

(g) Definition of top and bottom efflux angles.

Figure 2. Concluded.

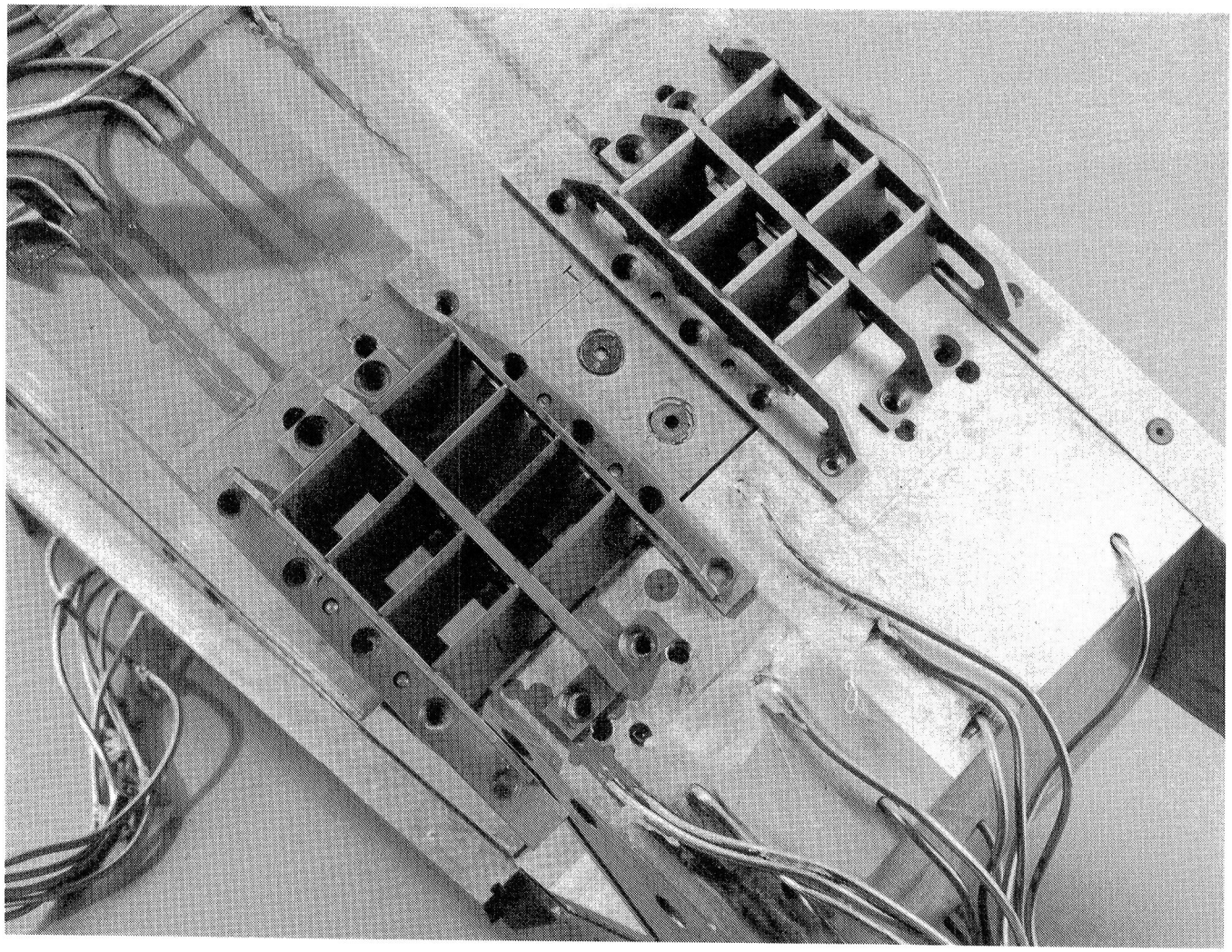

L-85-144

(a) Four-vane cascade box.

Figure 3. Reverser configurations.

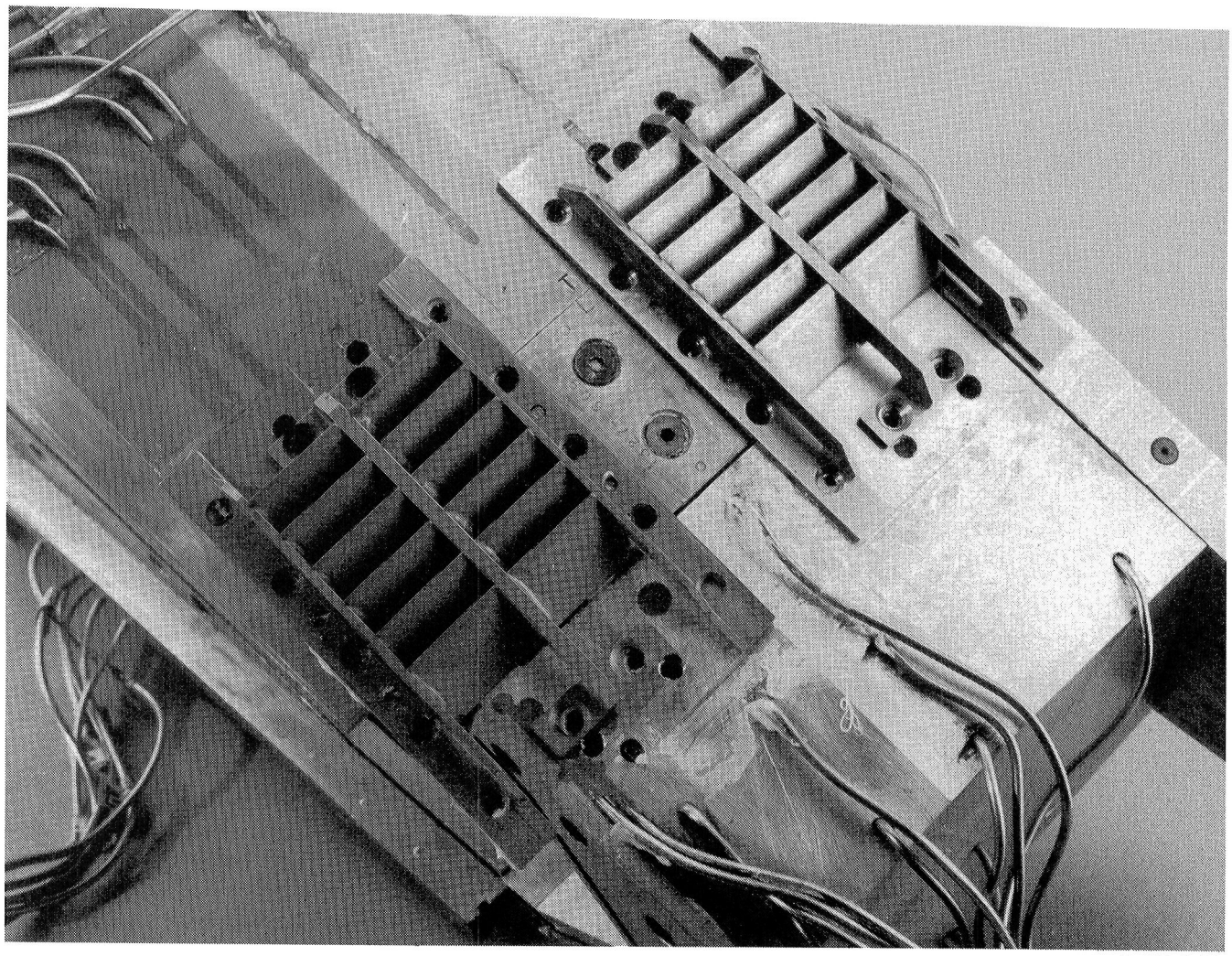

L-85-145

(b) Six-vane cascade box.

Figure 3. Continued.

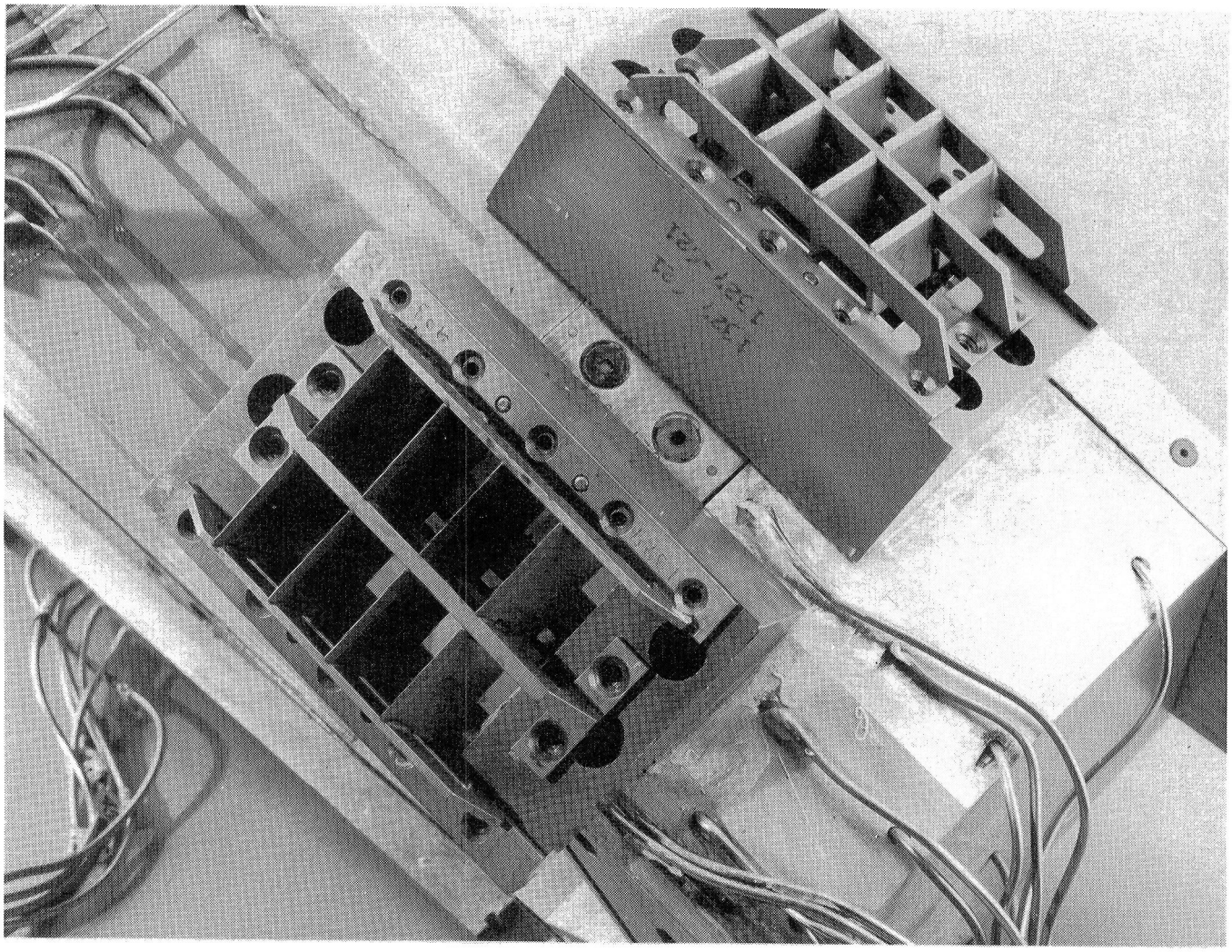

L-85-146

(c) Splay angle shims installed.

Figure 3. Continued.

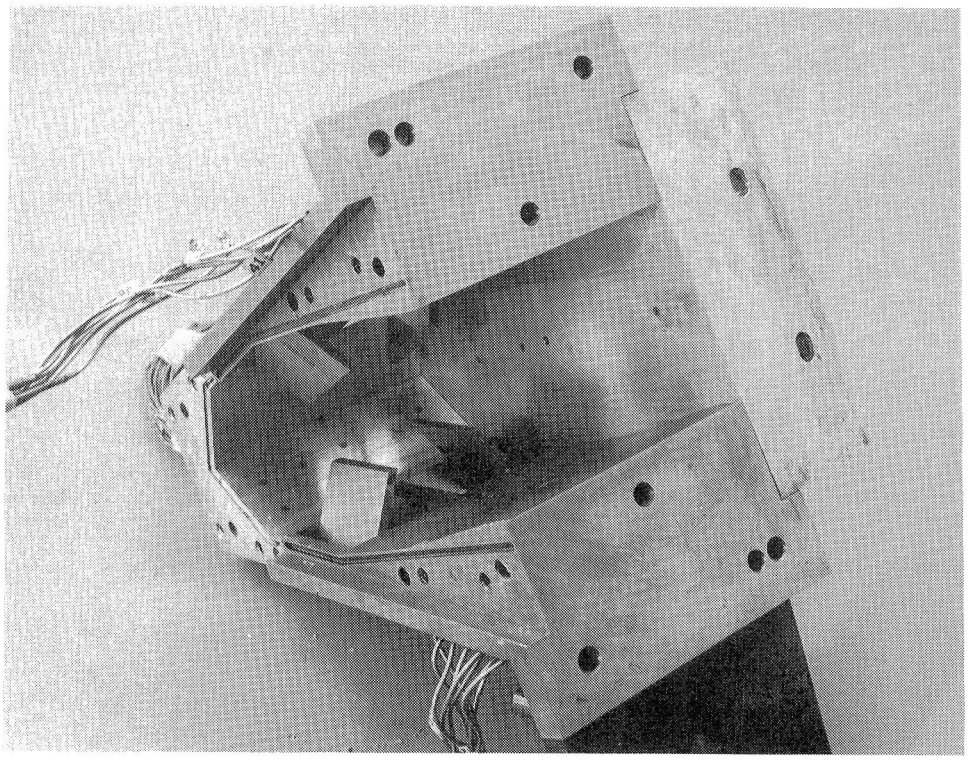

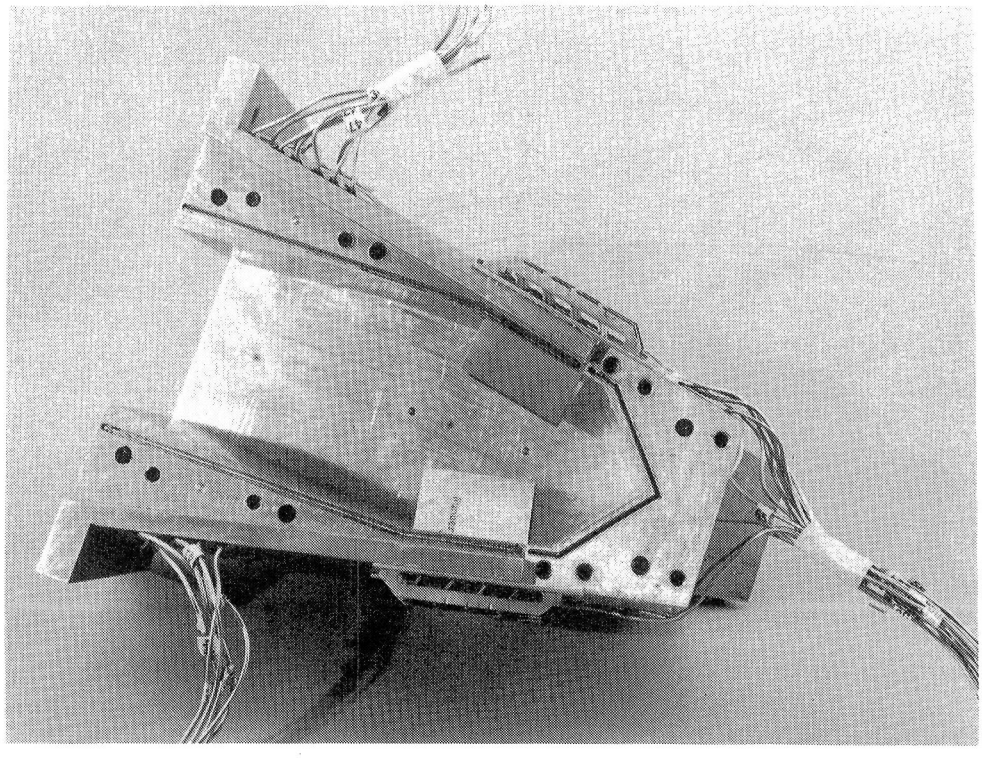

(d) Inner doors.

Figure 3. Concluded.

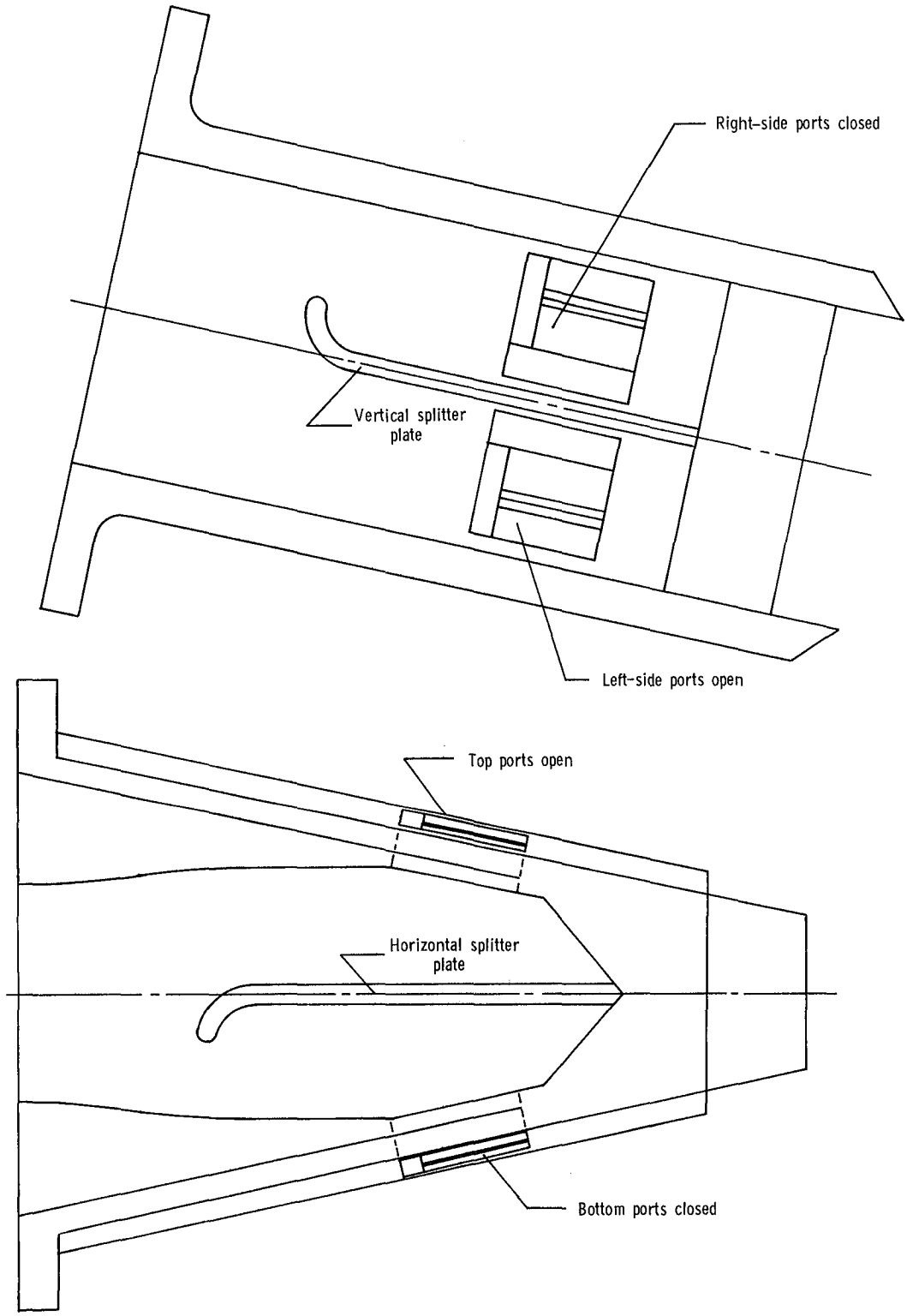

Figure 4. Orientation of horizontal and vertical splitter plates.

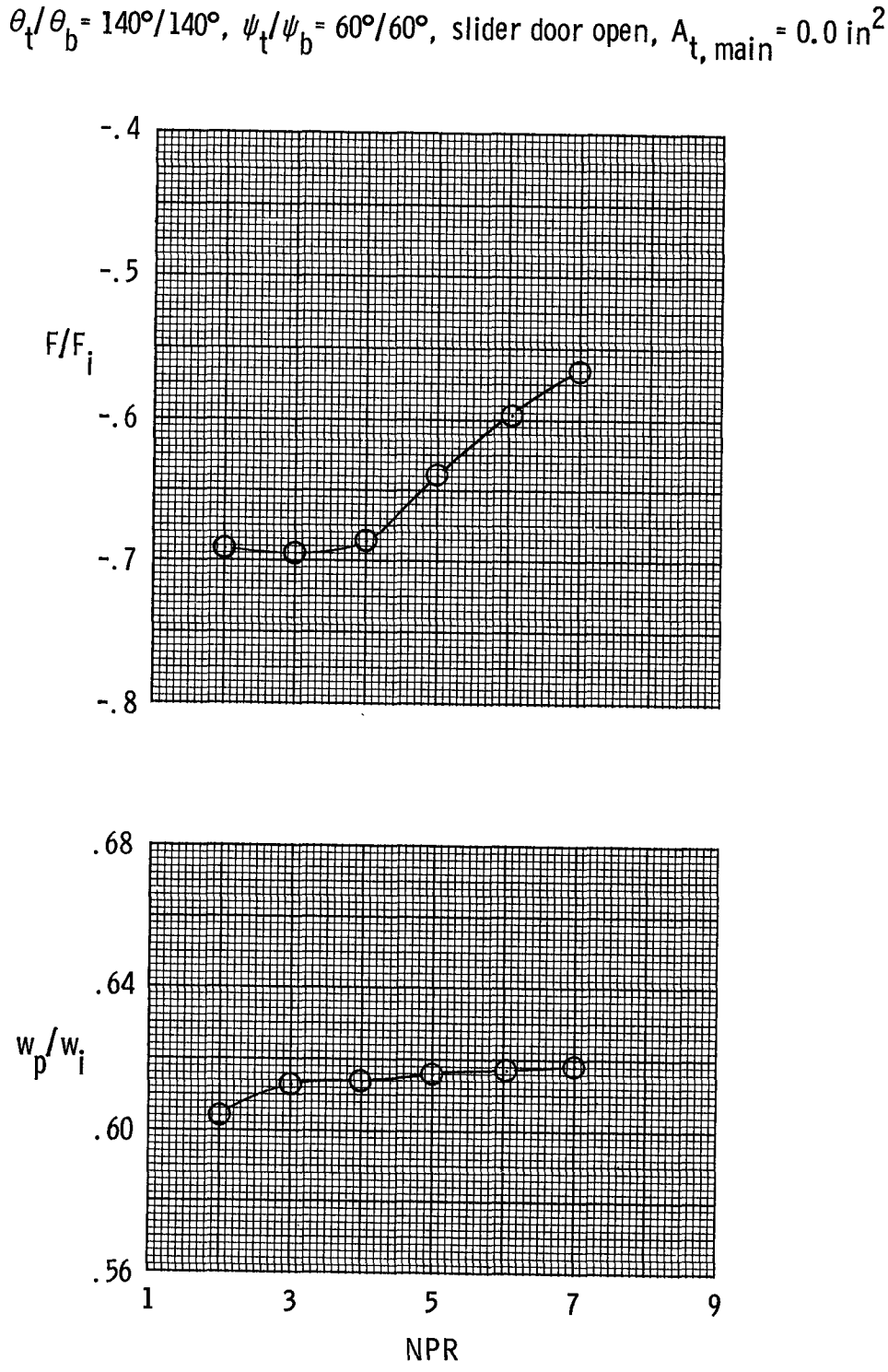

(a) Configuration 1; no splitter plate.

Figure 5. Variation of static internal performance characteristics with nozzle pressure ratio. Lines with no symbols indicate resultant thrust ratio F_r/F_i. Unless otherwise noted, all configurations have four-vane external cascade boxes, port tabs installed, no vane box sideplates, and no splay angle shims.

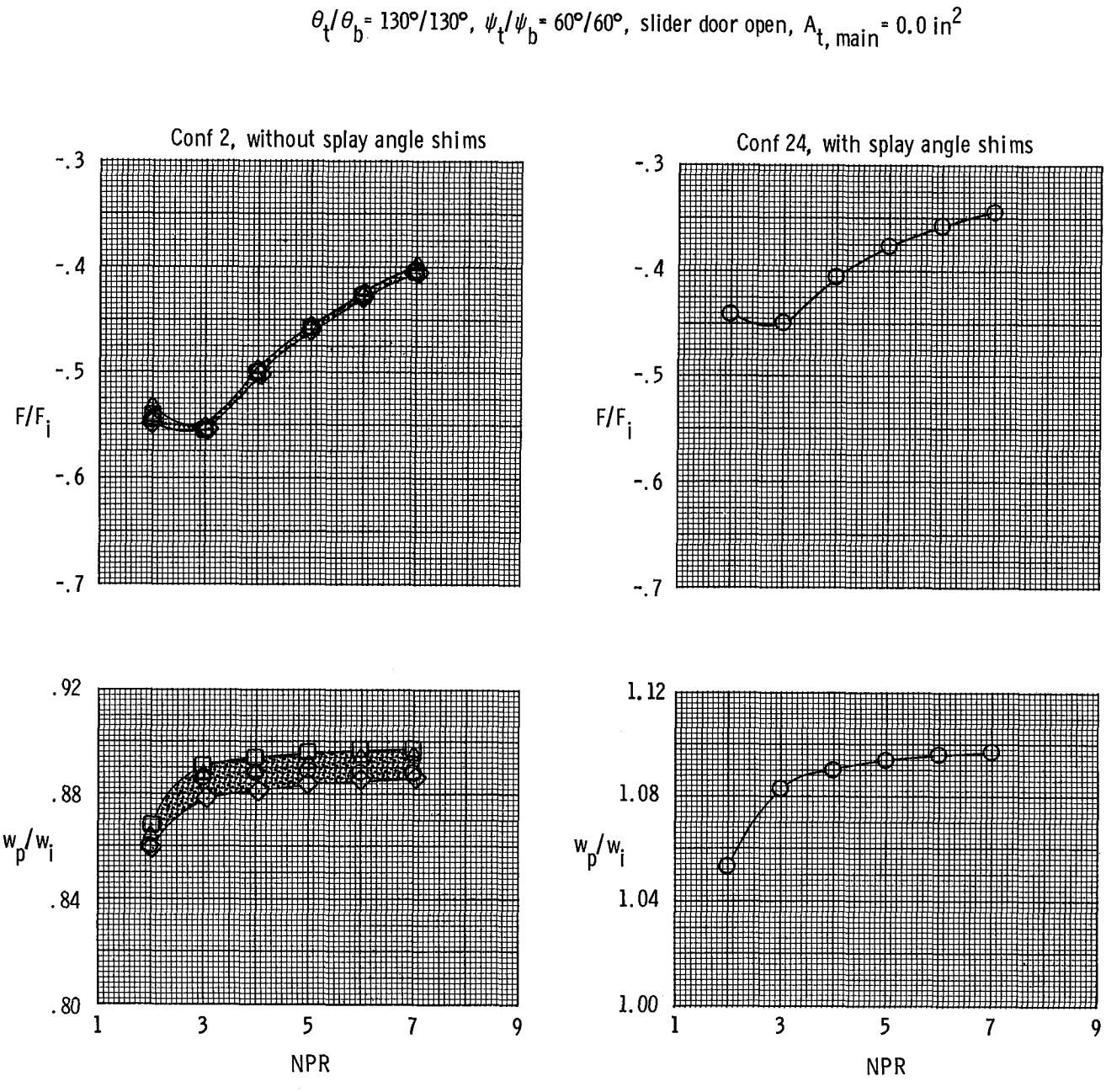

(b) Configurations 2 and 24; no splitter plate.

Figure 5. Continued.

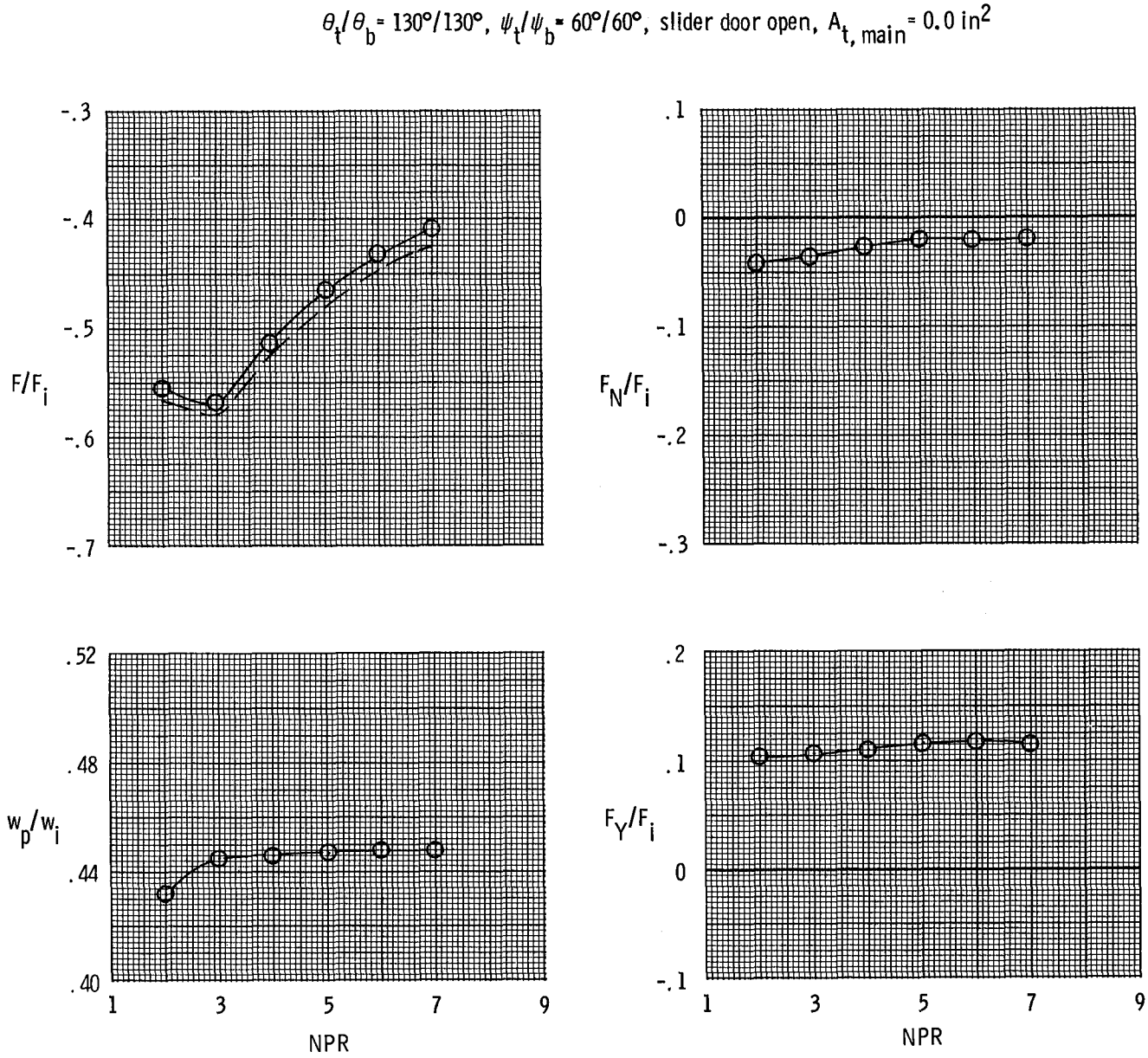

(c) Configuration 2; vertical splitter plate.

Figure 5. Continued.

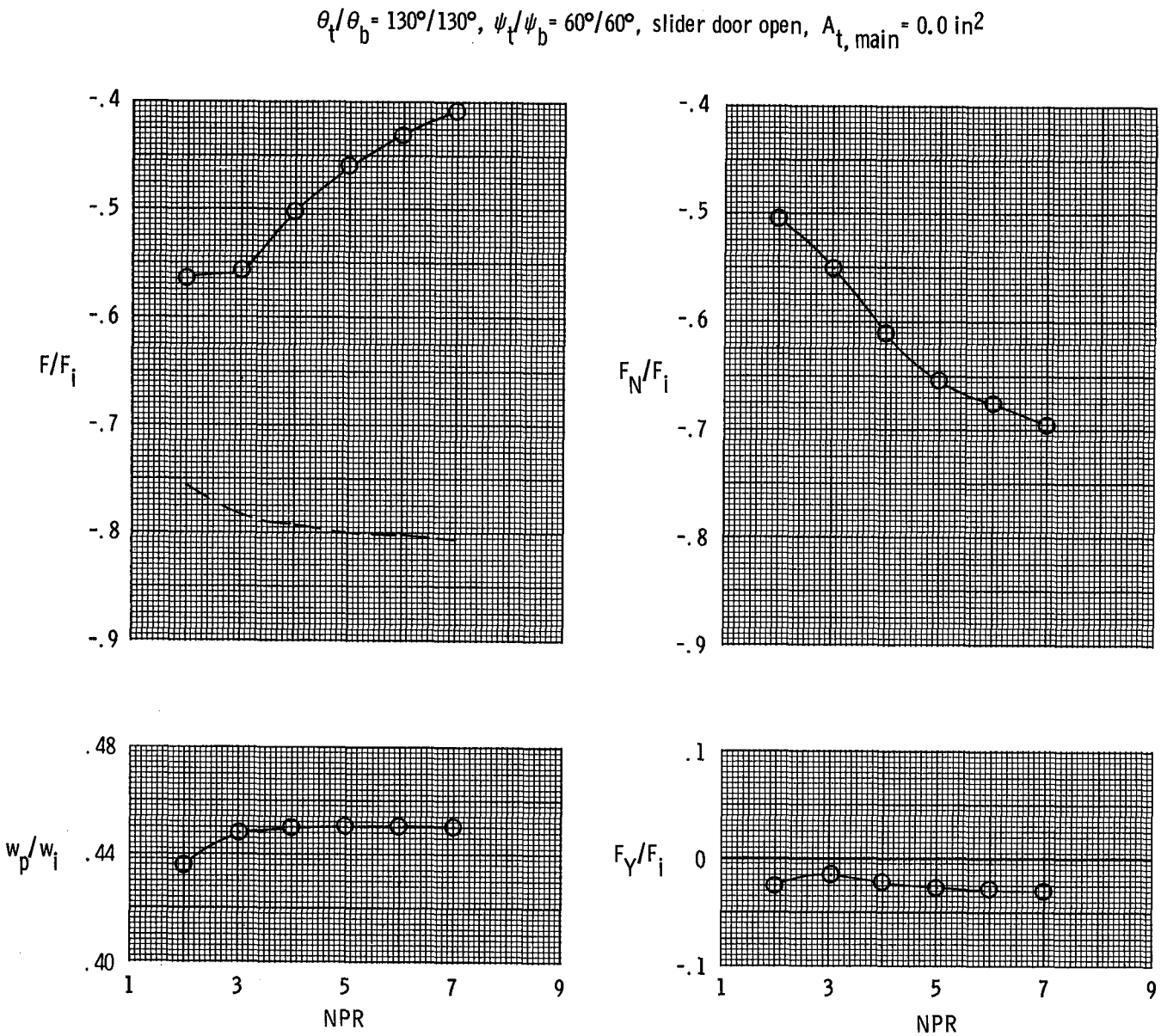

(d) Configuration 2; horizontal splitter plate.

Figure 5. Continued.

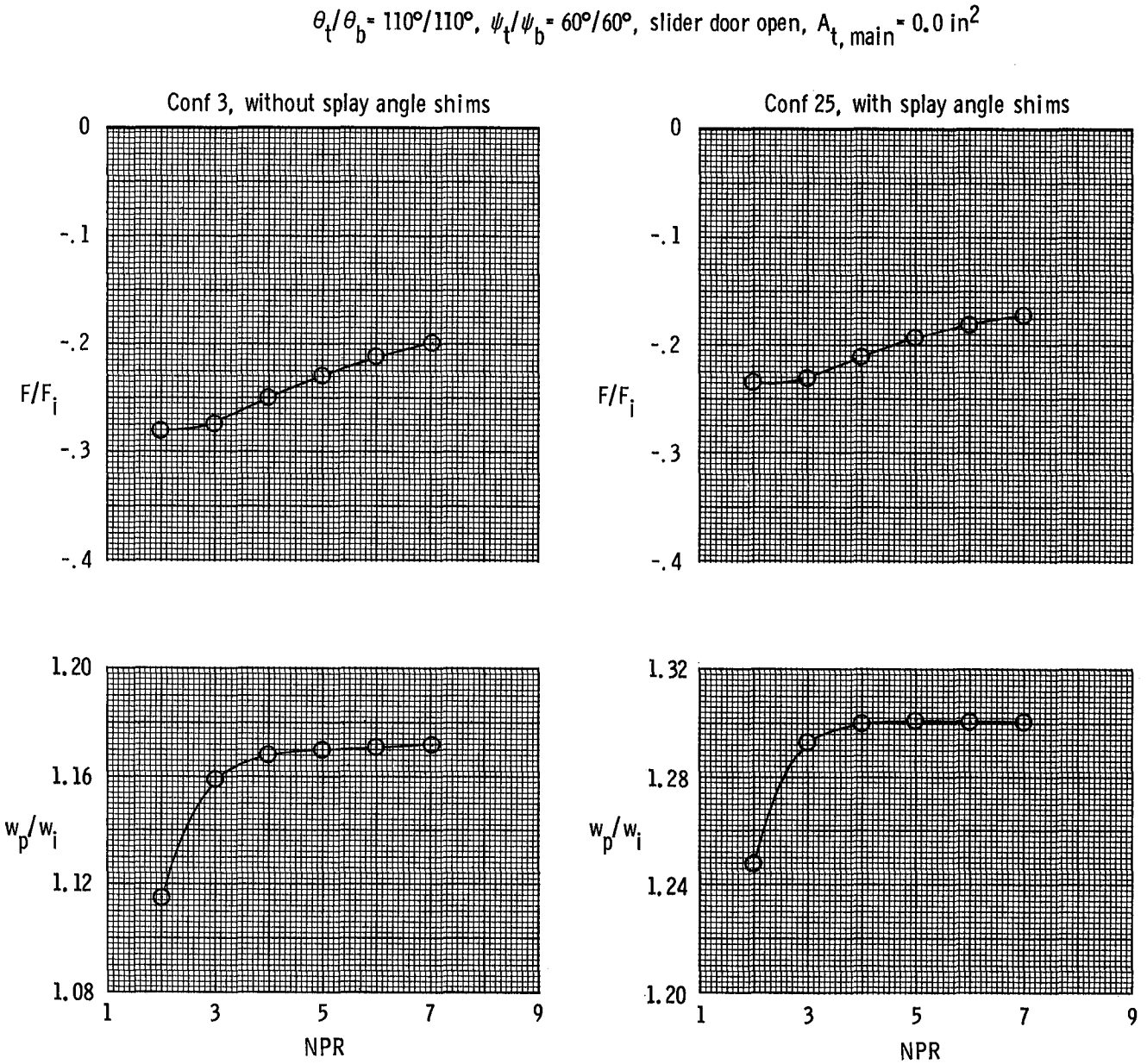

(e) Configurations 3 and 25; no splitter plate.

Figure 5. Continued.

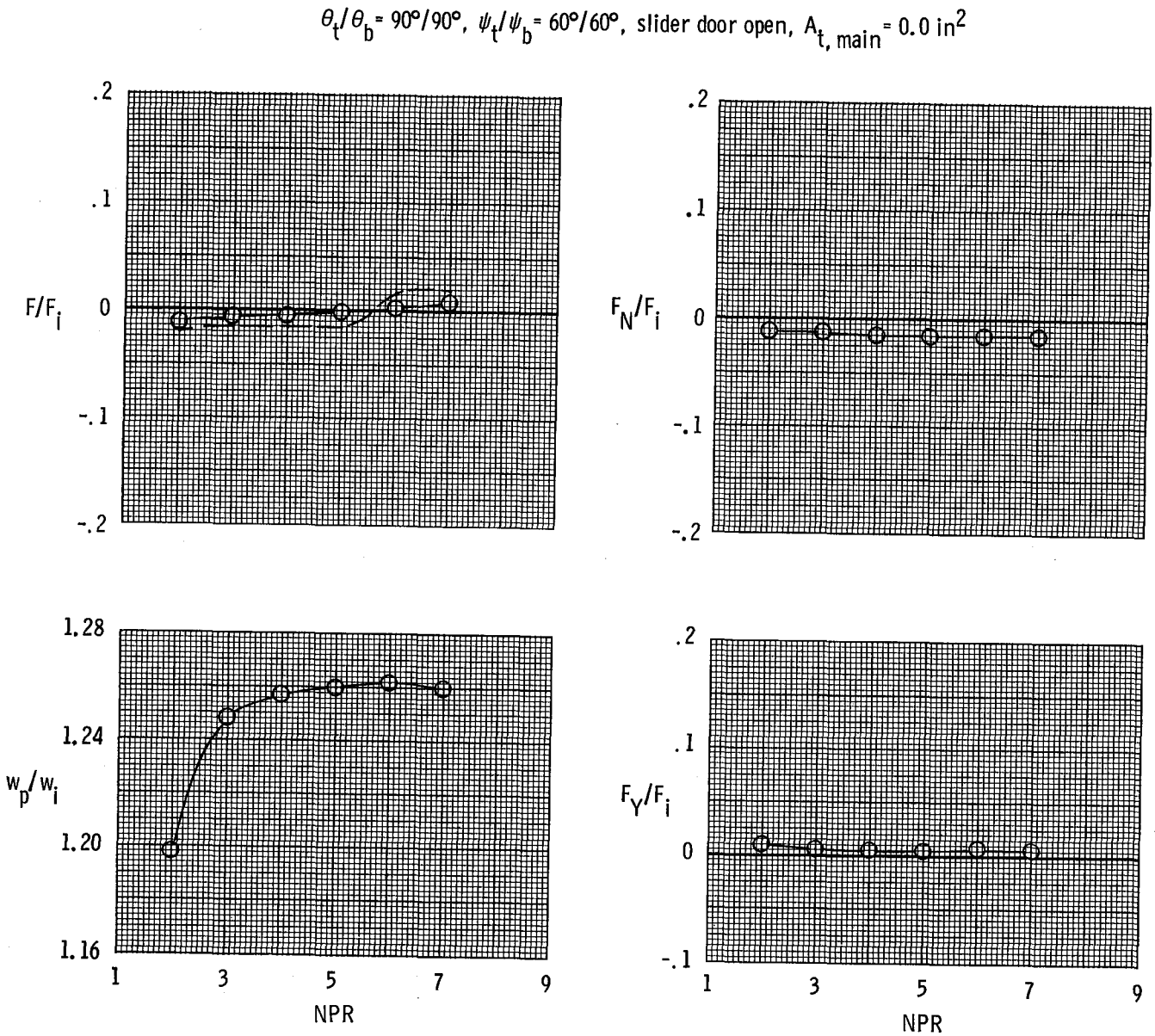

(f) Configuration 4; no splitter plate.

Figure 5. Continued.

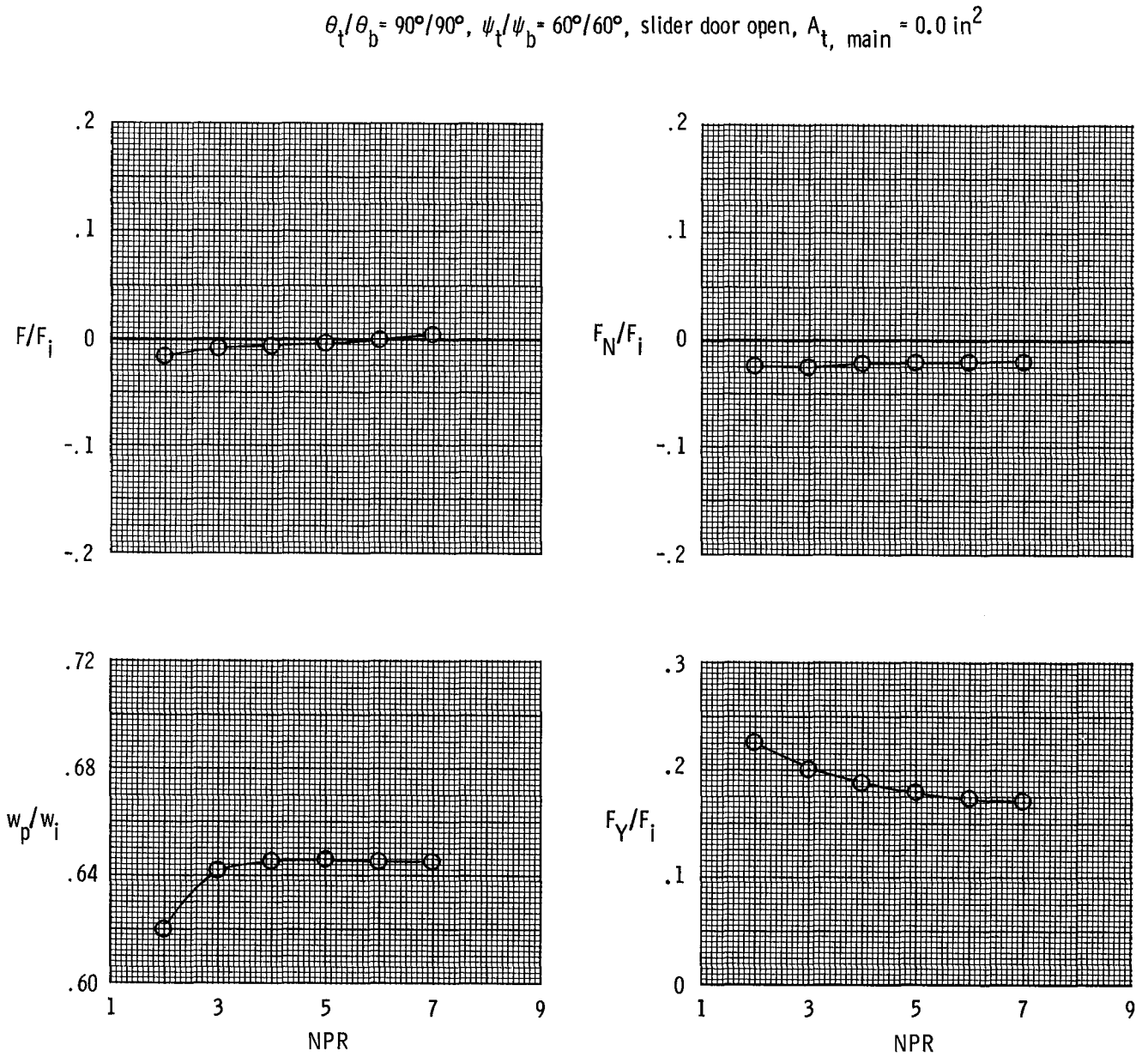

(g) Configuration 4; vertical splitter plate.

Figure 5. Continued.

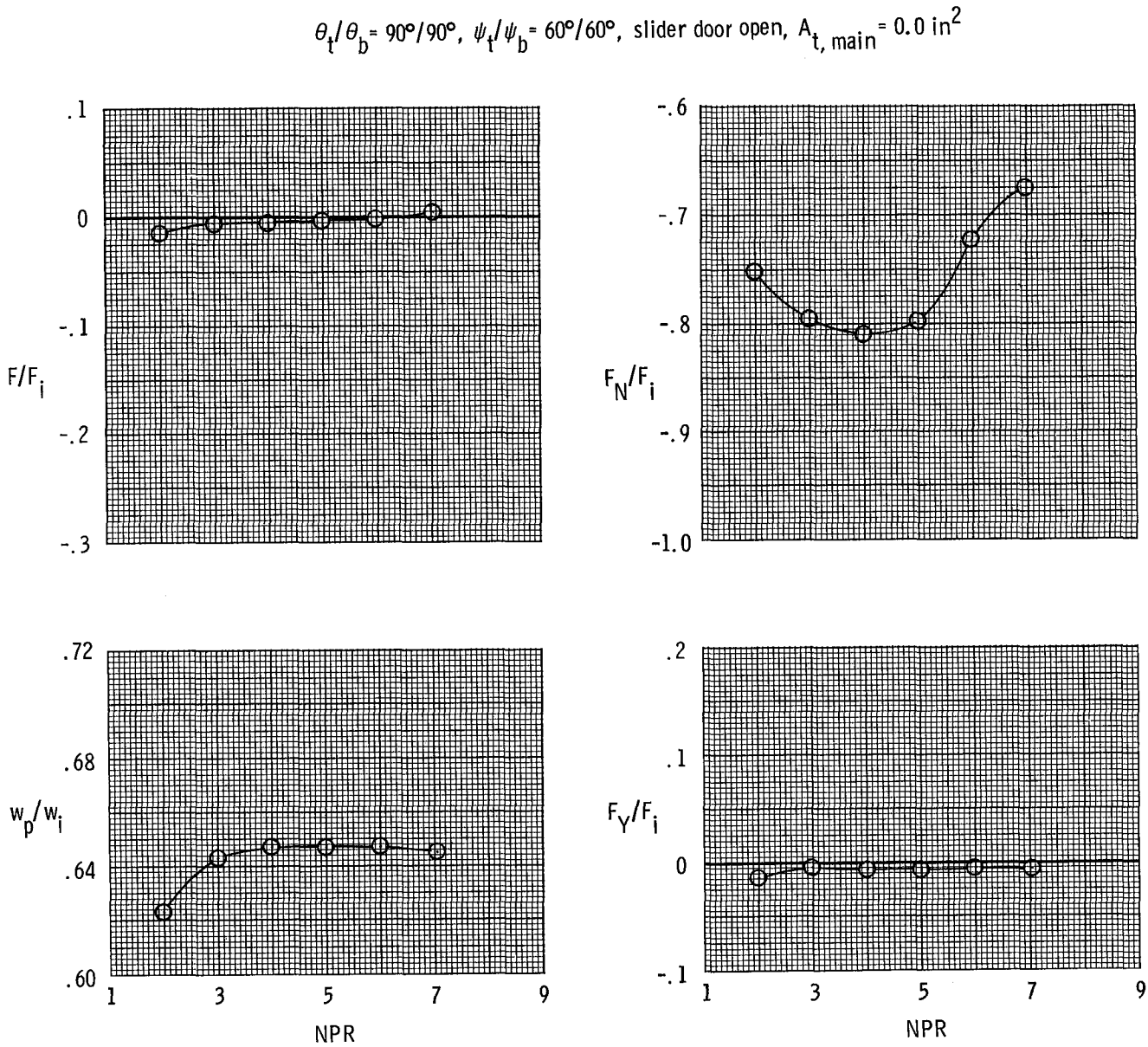

(h) Configuration 4; horizontal splitter plate.

Figure 5. Continued.

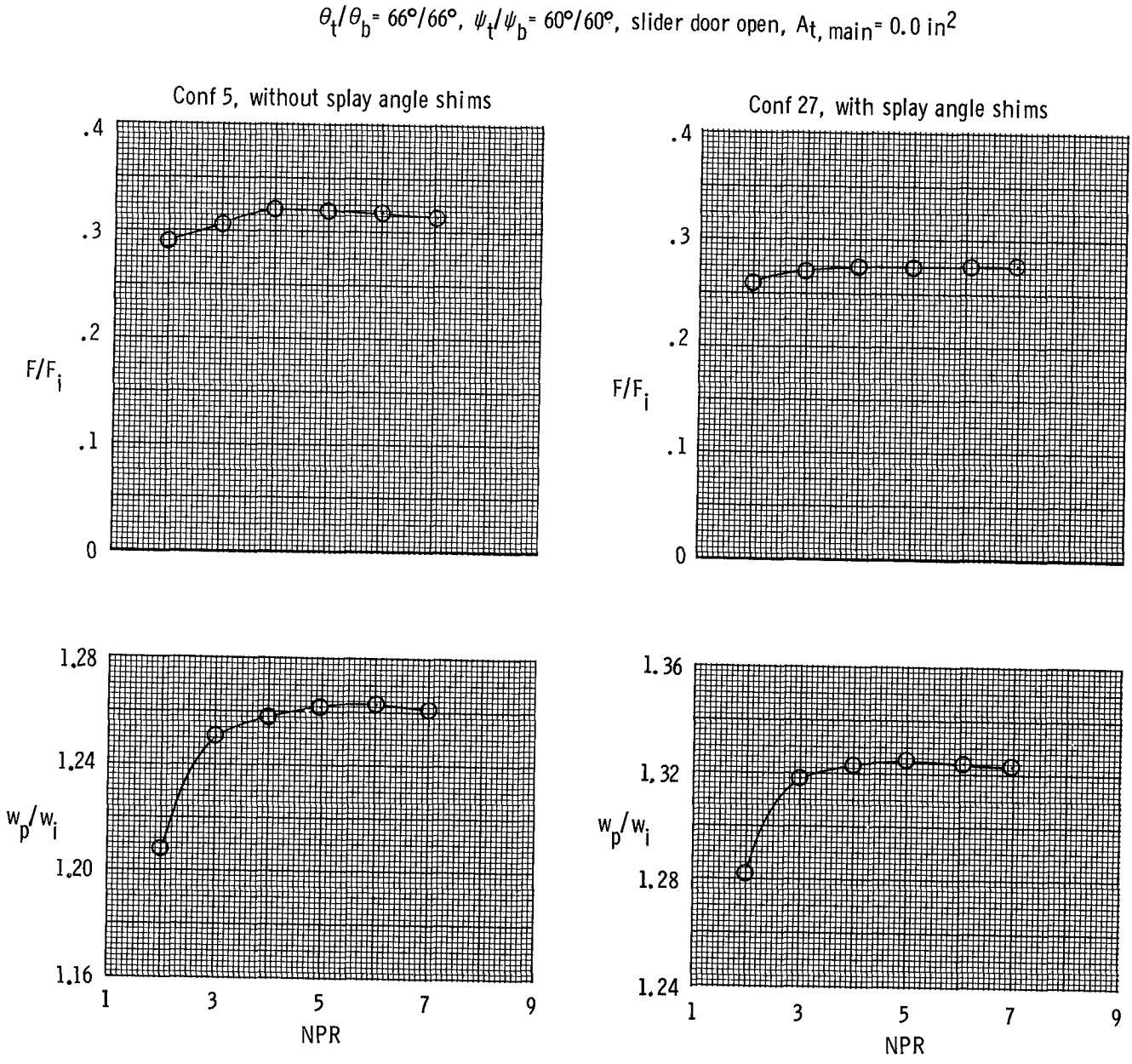

(i) Configurations 5 and 27; no splitter plate.

Figure 5. Continued.

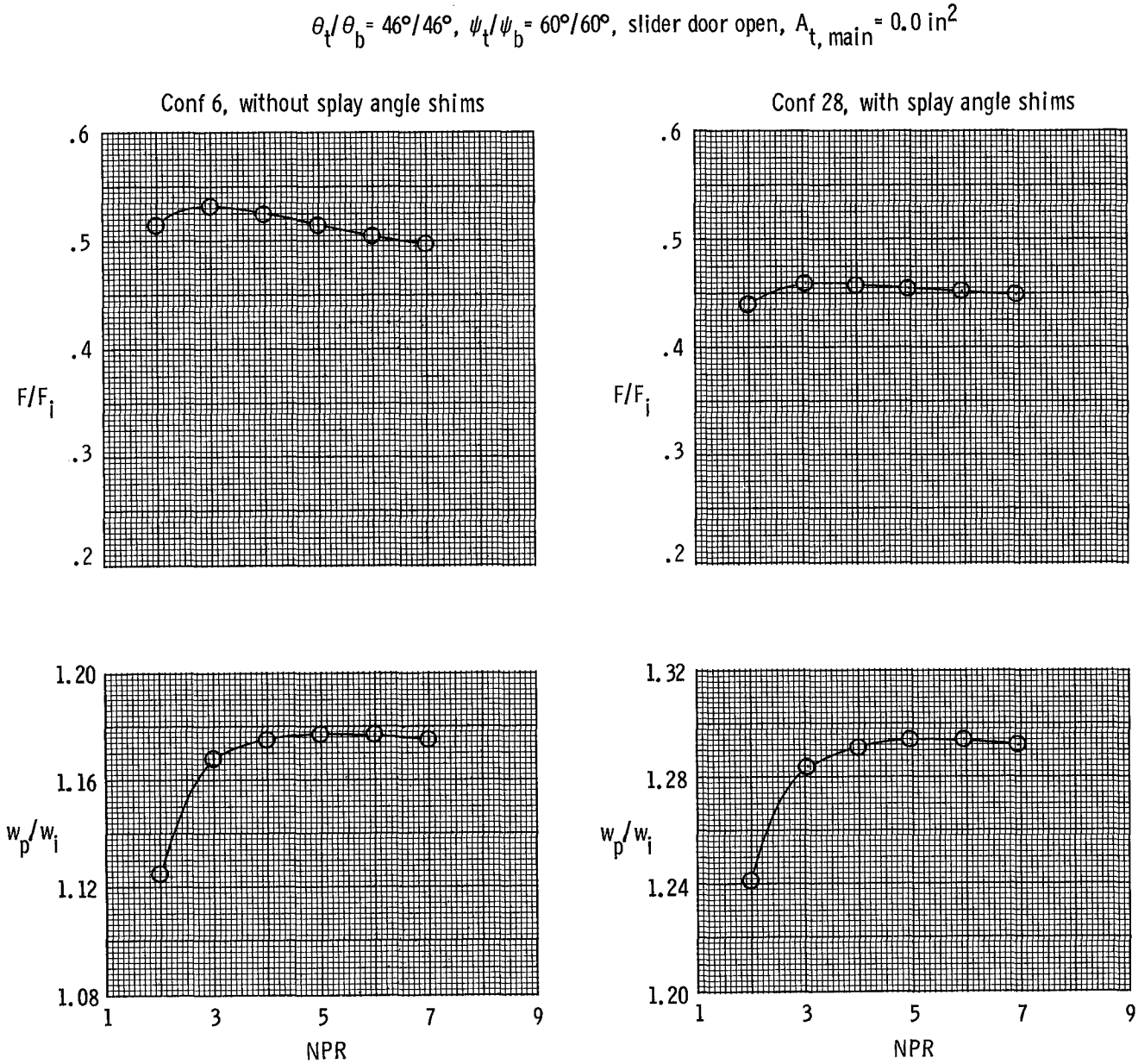

(j) Configurations 6 and 28; no splitter plate.

Figure 5. Continued.

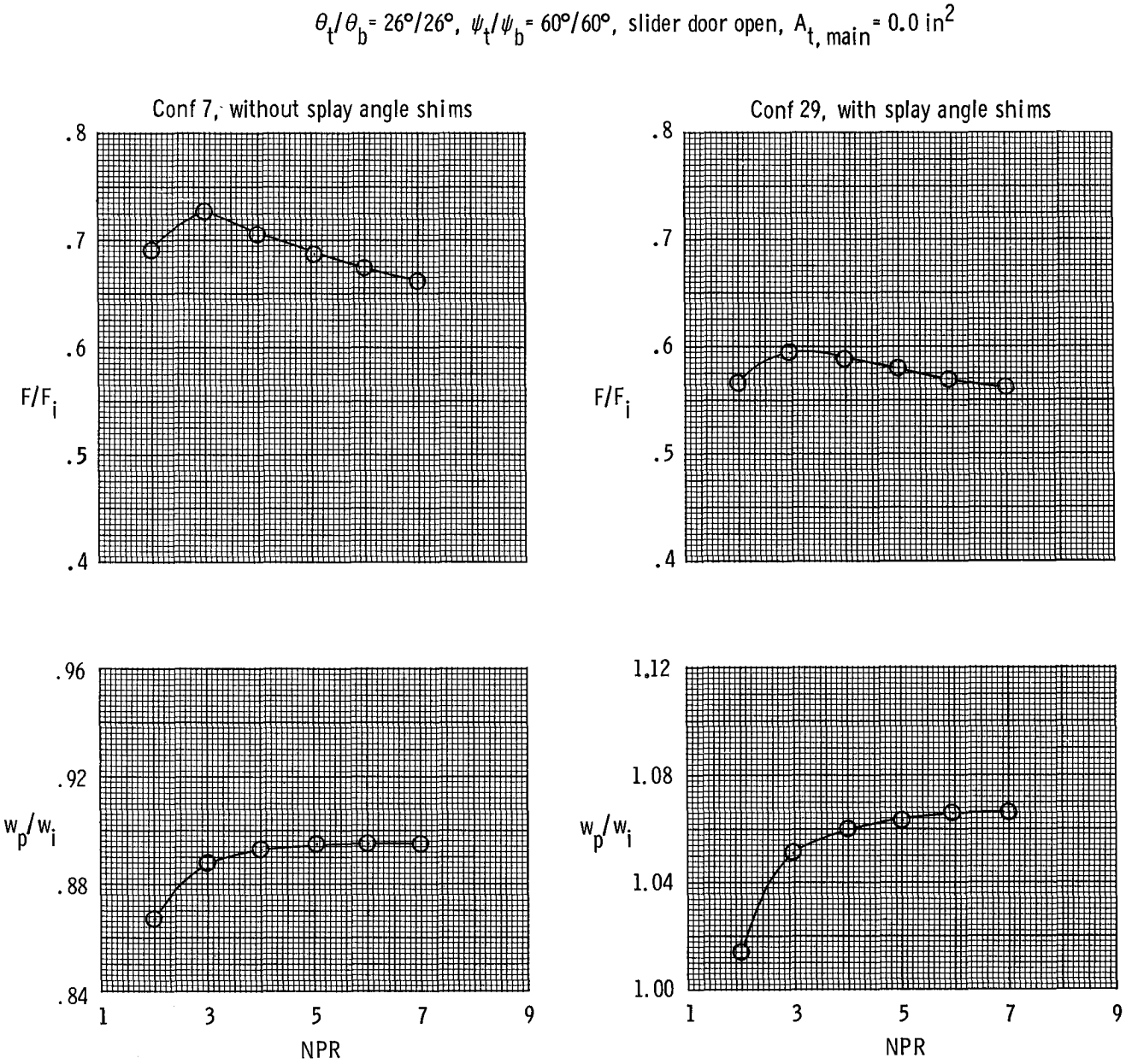

(k) Configurations 7 and 29; no splitter plate.

Figure 5. Continued.

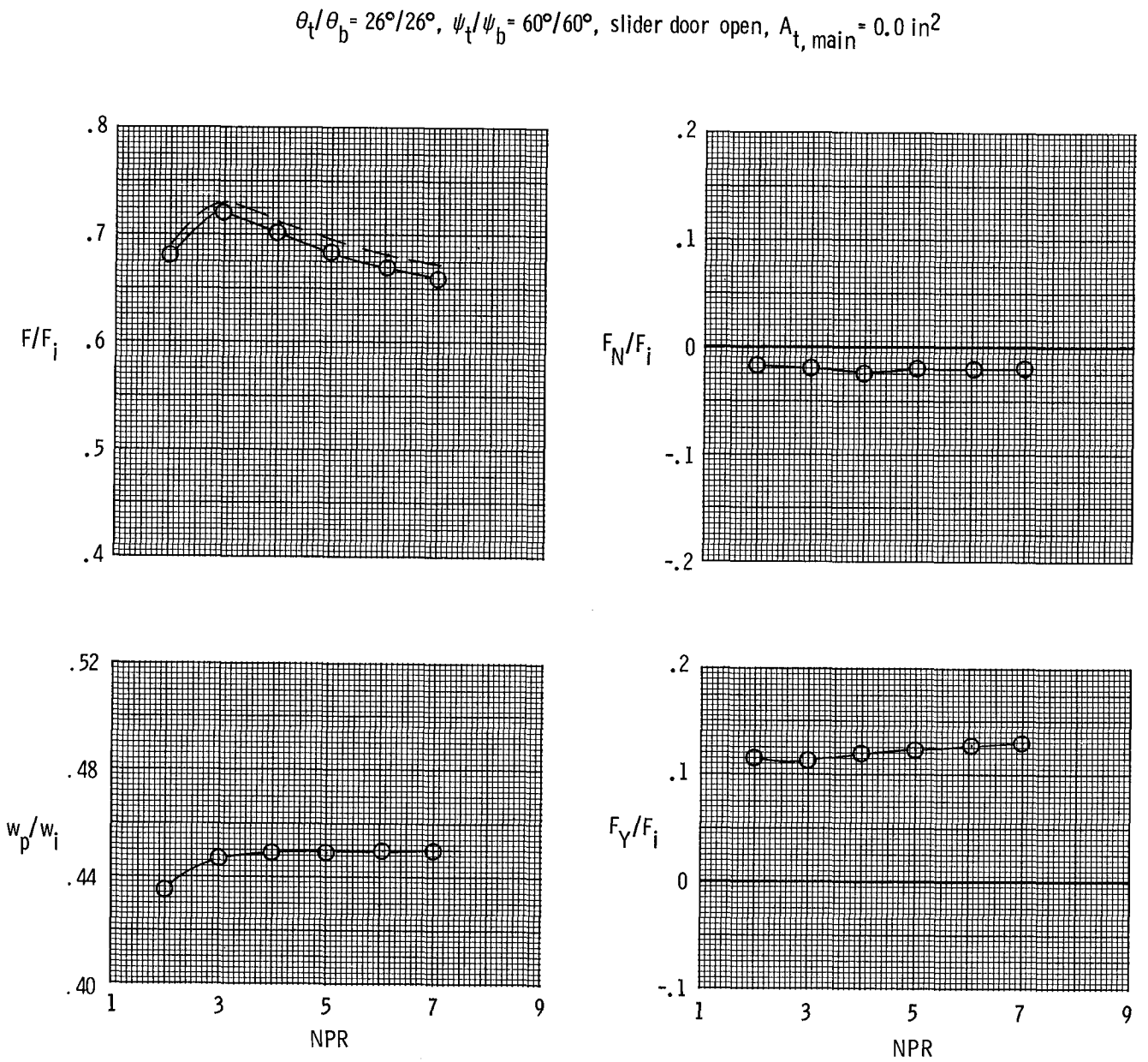

(l) Configuration 7; vertical splitter plate.

Figure 5. Continued.

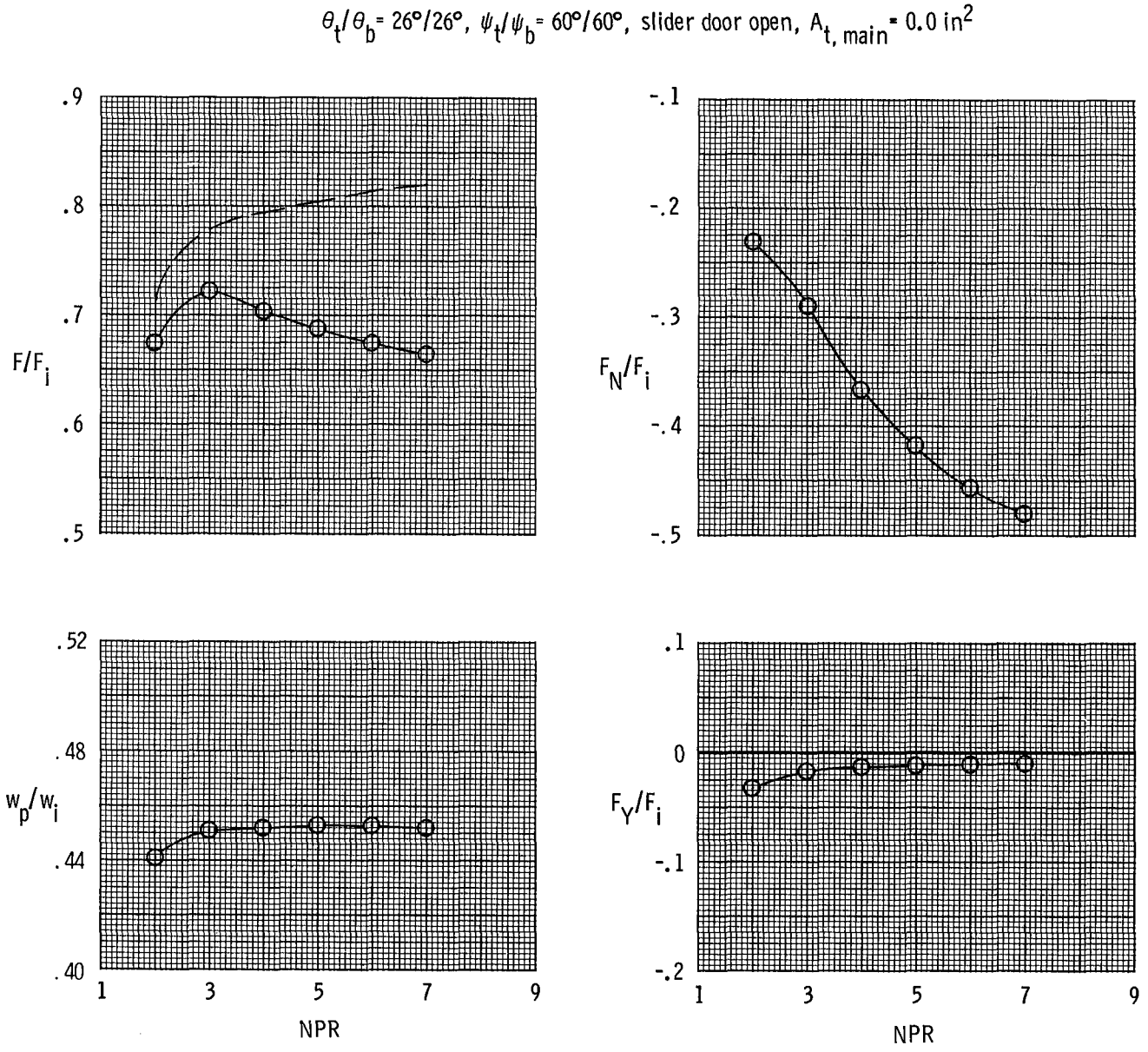

(m) Configuration 7; horizontal splitter plate.

Figure 5. Continued.

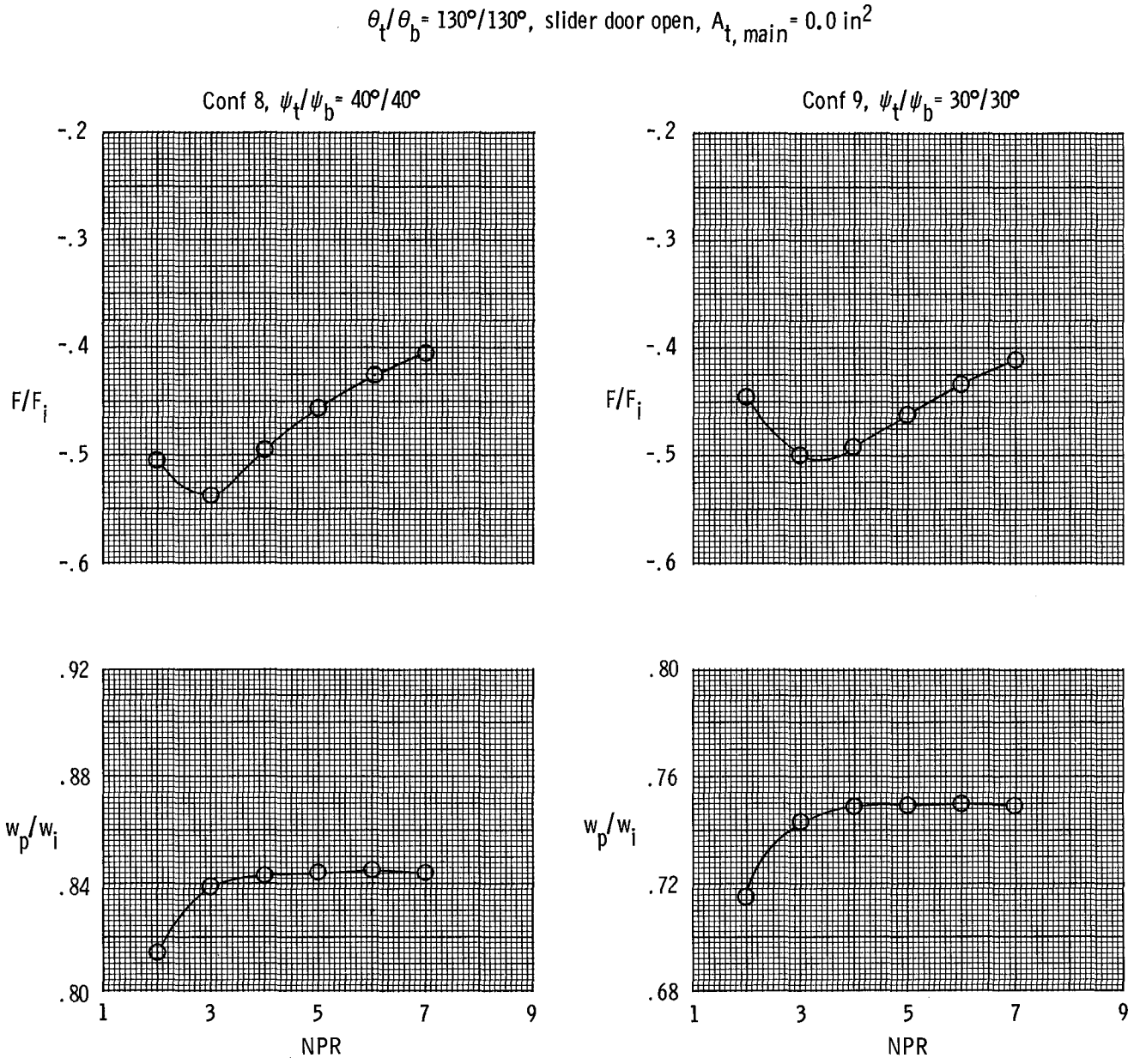

(n) Configurations 8 and 9; no splitter plate.

Figure 5. Continued.

θ_t/θ_b = 130°/130°, ψ_t/ψ_b = 20°/20°, slider door open, $A_{t,\,main}$ = 0.0 in^2

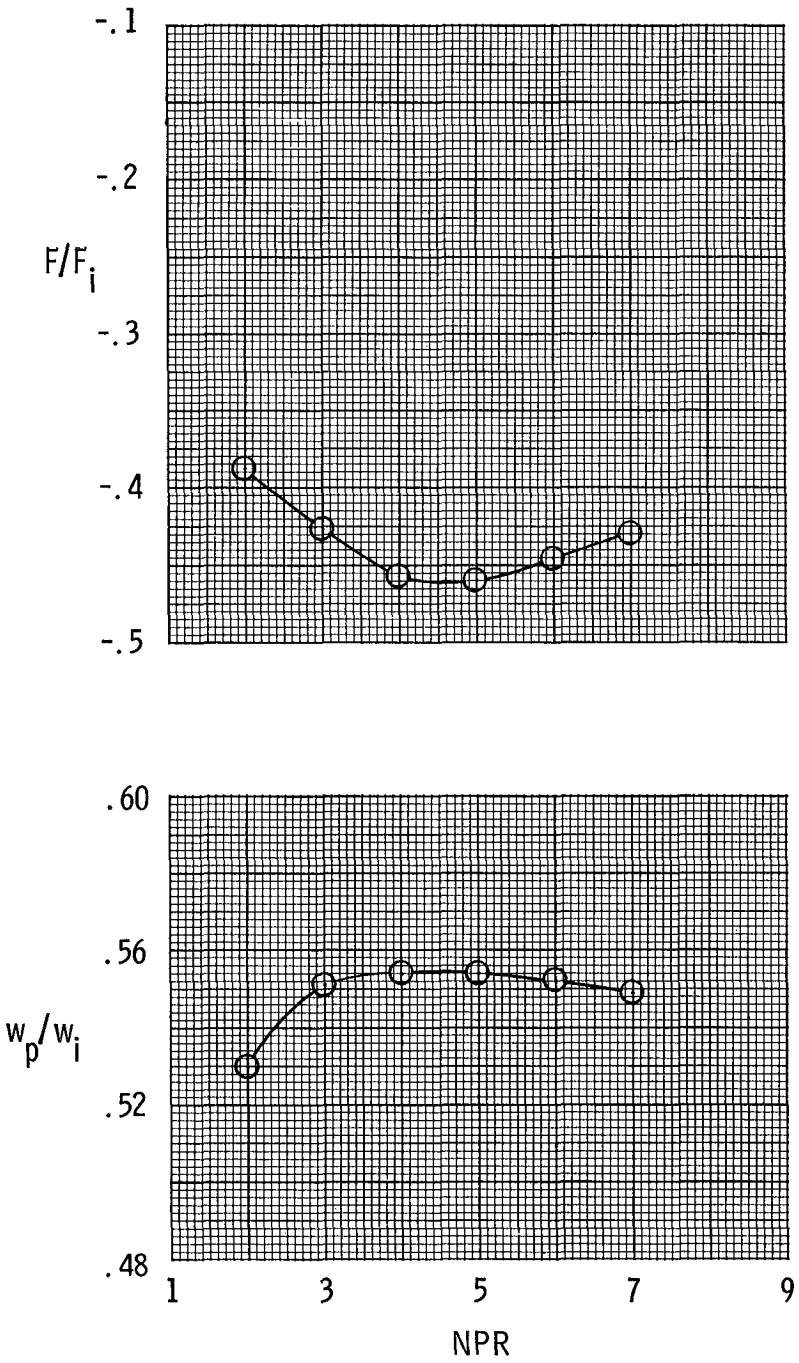

(o) Configuration 10; no splitter plate.

Figure 5. Continued.

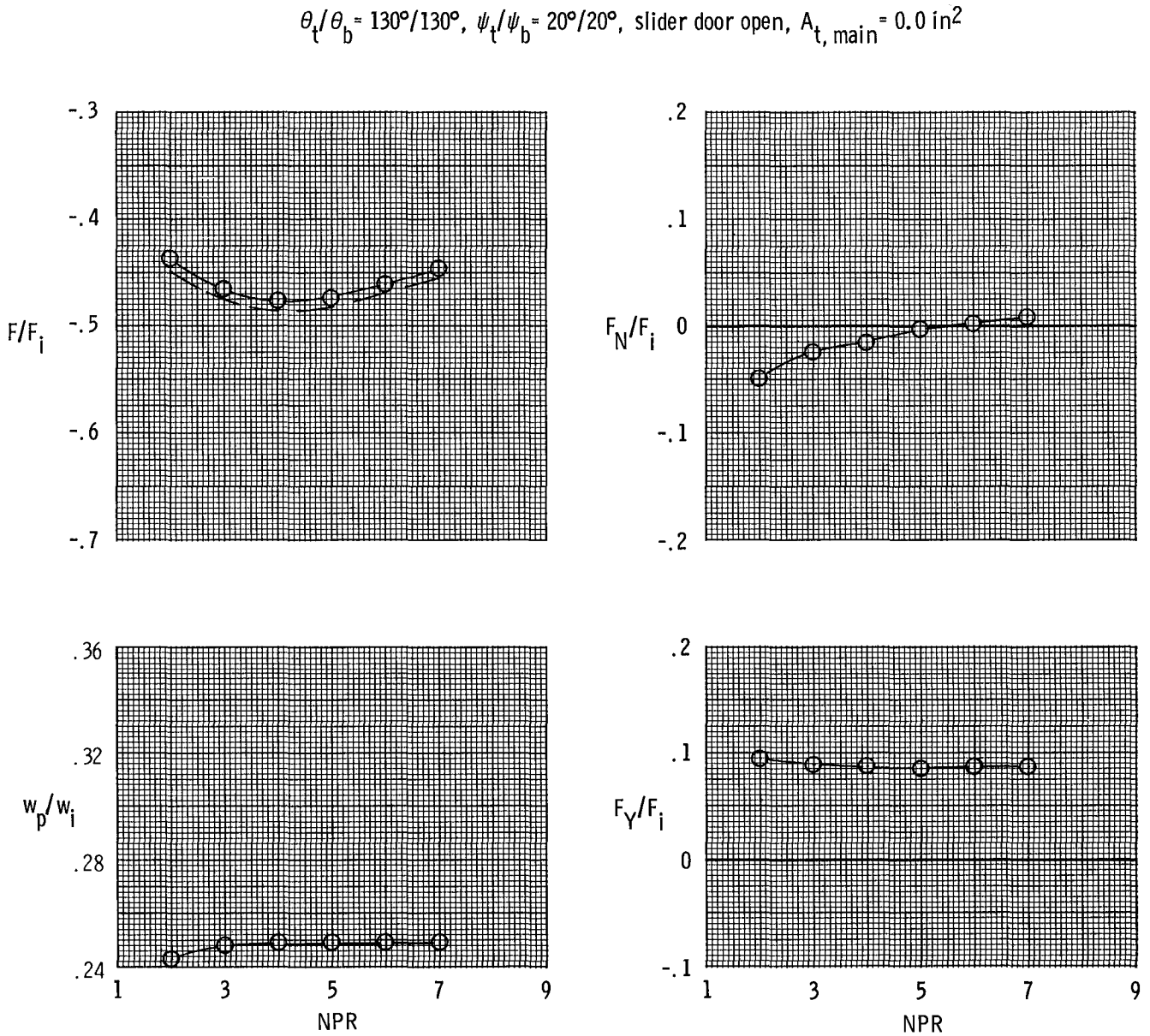

(p) Configuration 10; vertical splitter plate.

Figure 5. Continued.

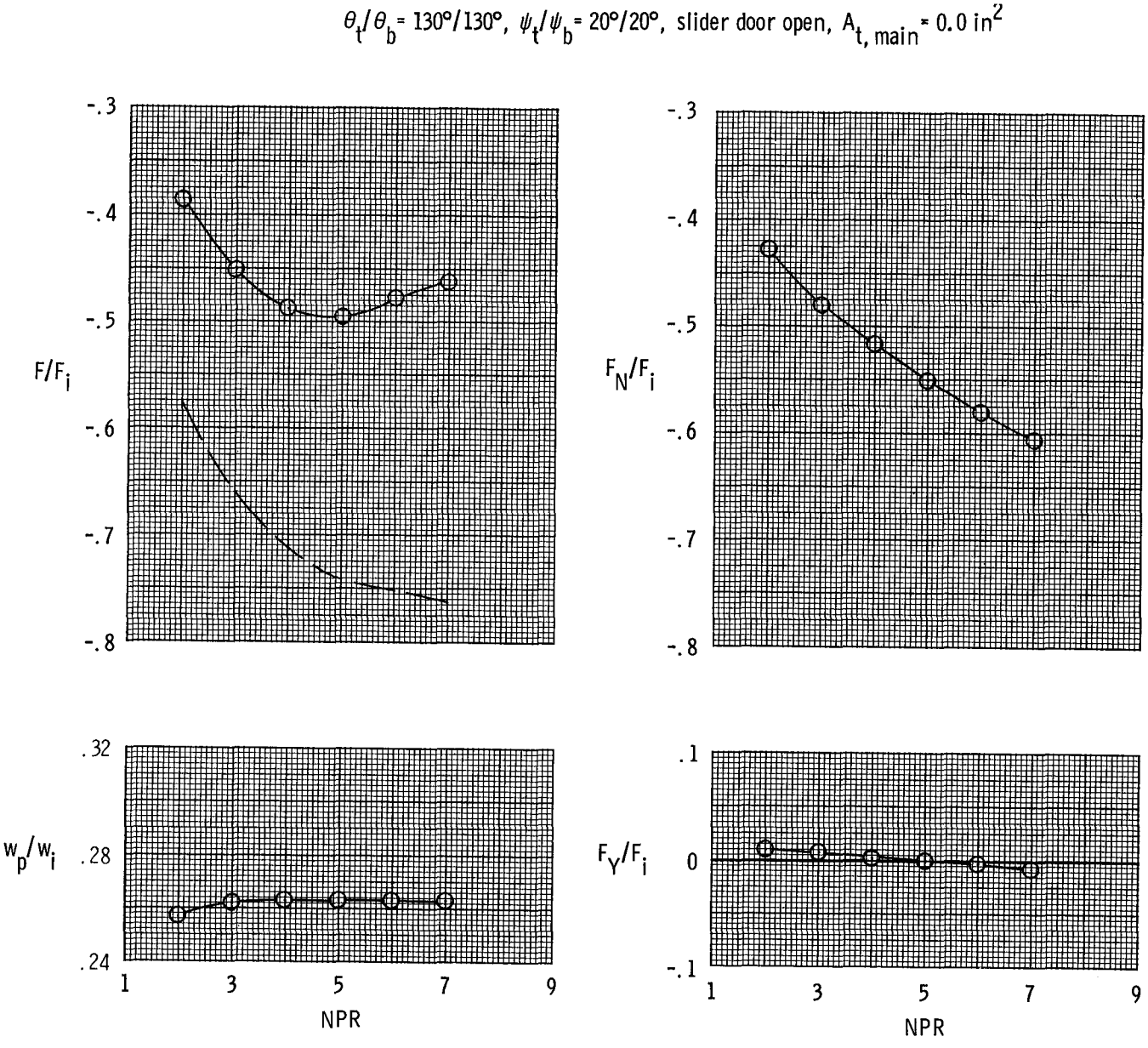

(q) Configuration 10; horizontal splitter plate.

Figure 5. Continued.

θ_t/θ_b = 130°/130°, ψ_t/ψ_b = 10°/10°, slider door open, $A_{t,\,main}$ = 0.0 in^2

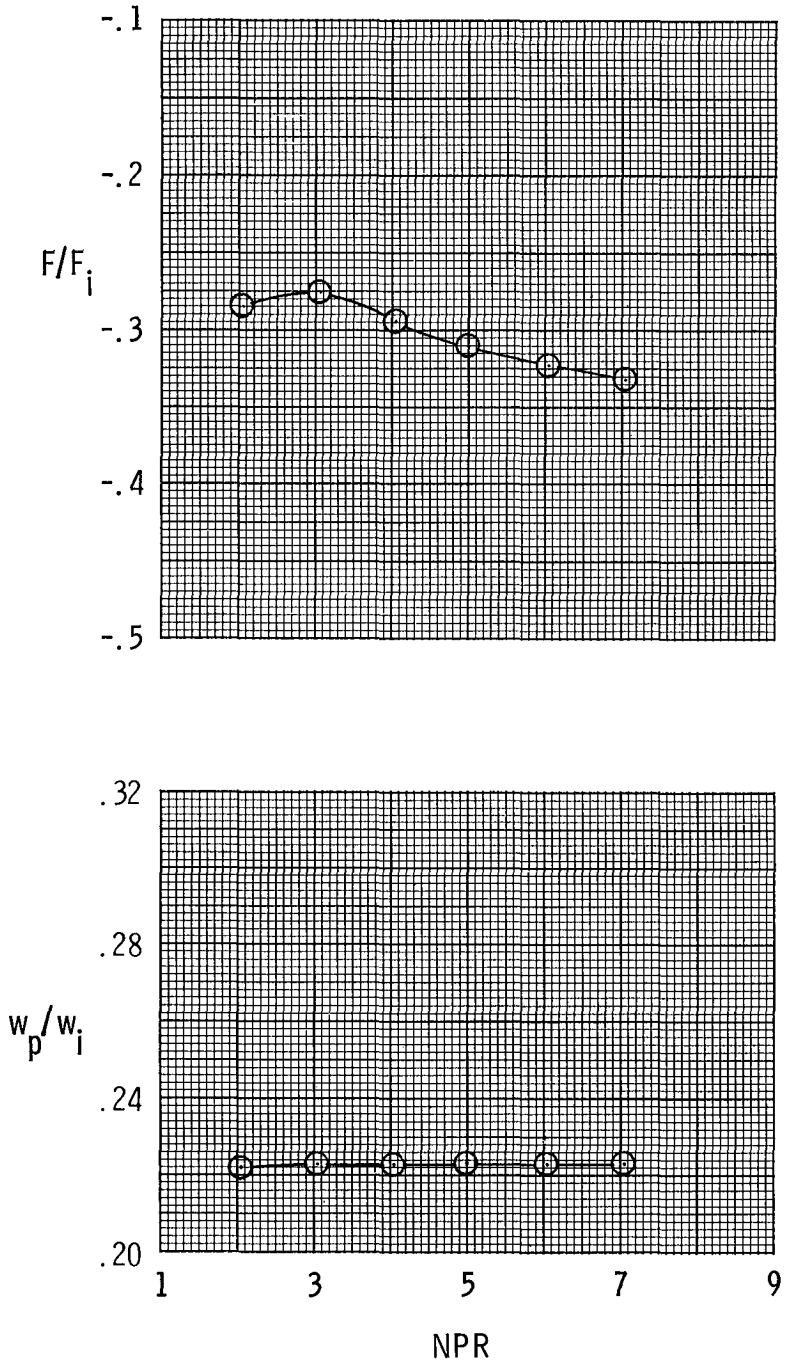

(r) Configuration 11; no splitter plate.

Figure 5. Continued.

θ_t/θ_b = 130°/130°, ψ_t/ψ_b = off/off, slider door open, $A_{t,\,main}$ = 0.0 in^2

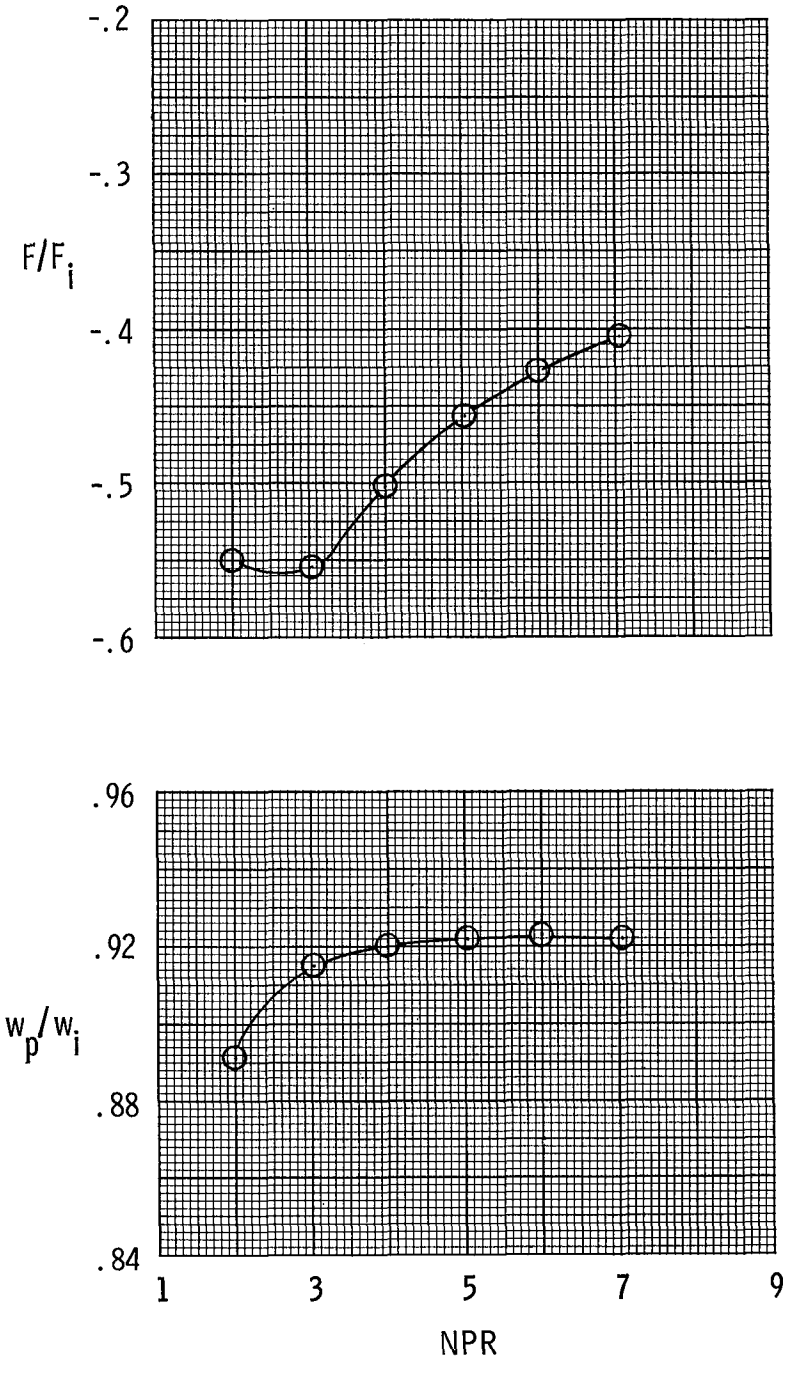

(s) Configuration 12; no splitter plate.

Figure 5. Continued.

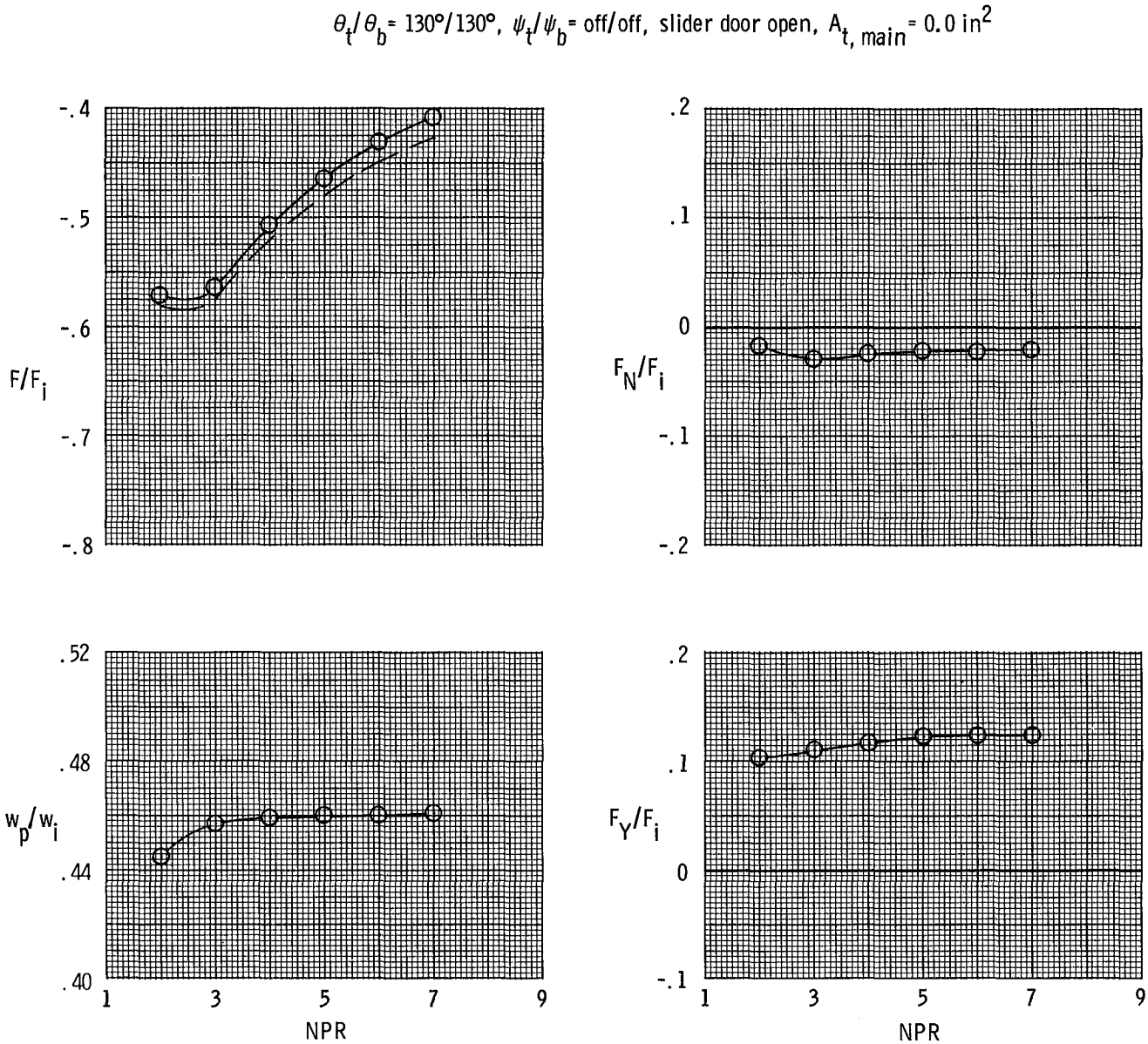

(t) Configuration 12; vertical splitter plate.

Figure 5. Continued.

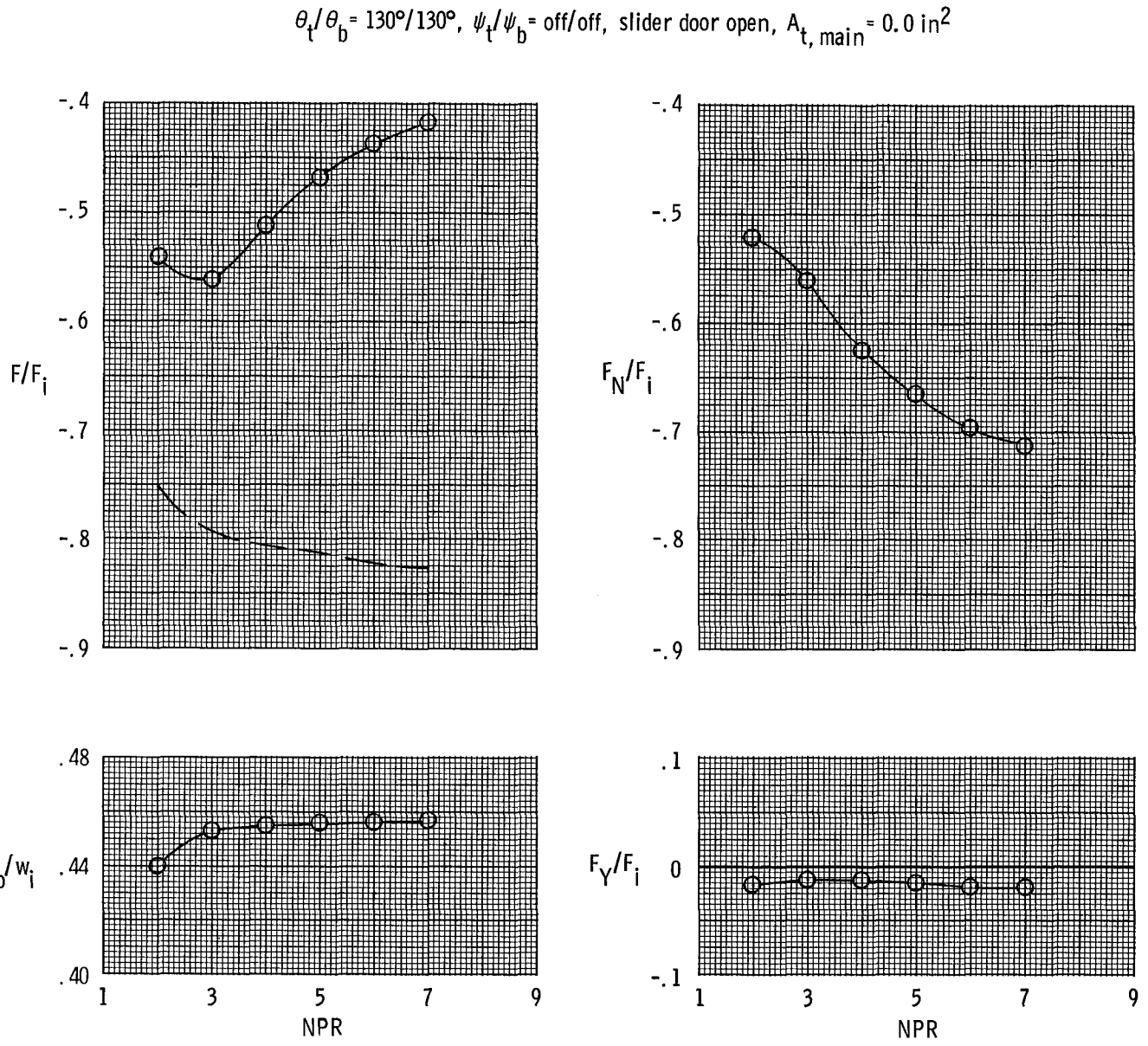

(u) Configuration 12; horizontal splitter plate.

Figure 5. Continued.

θ_t/θ_b = off/off, ψ_t/ψ_b = 60°/60°, slider door open, $A_{t,\,main}$ = 0.0 in^2

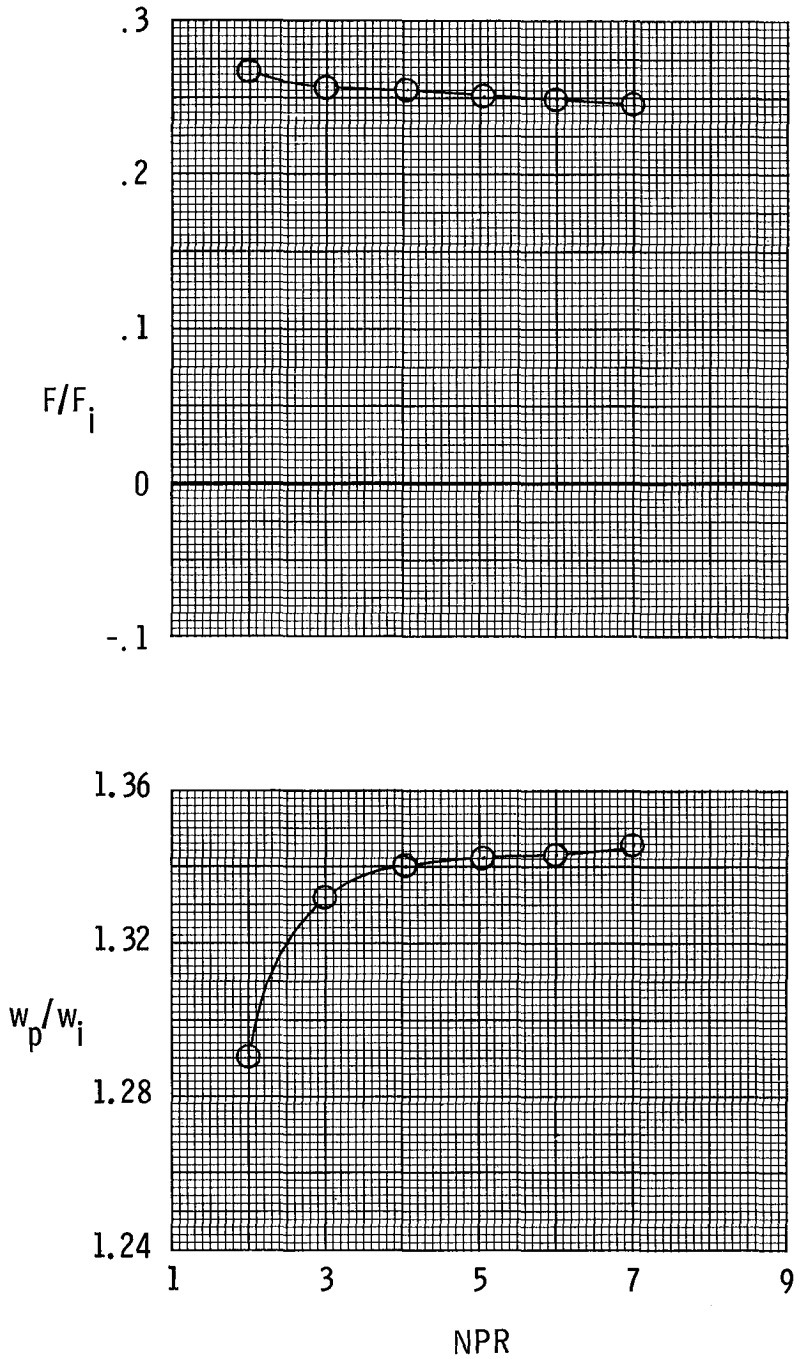

(v) Configuration 13; no splitter plate.

Figure 5. Continued.

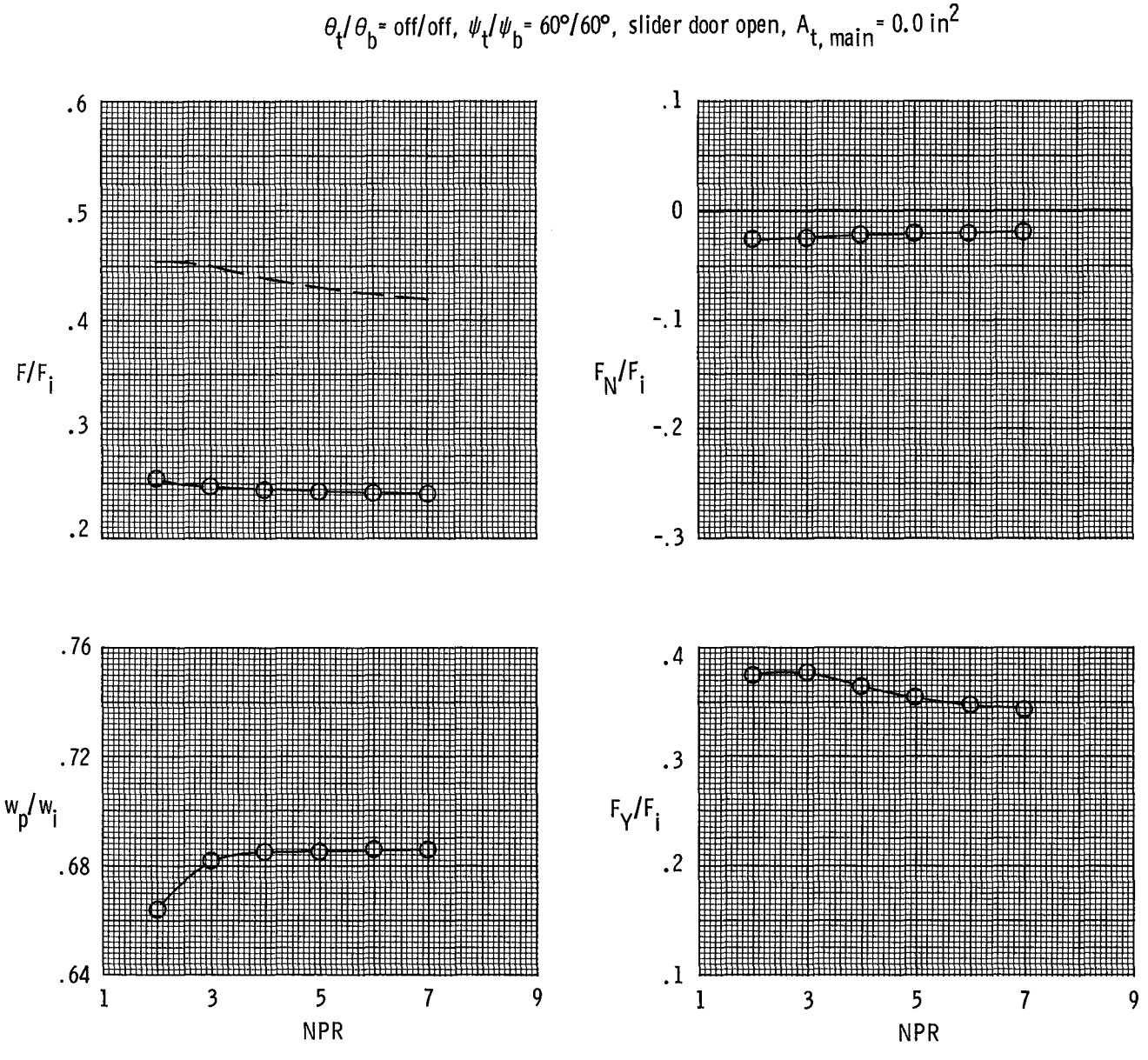

(w) Configuration 13; vertical splitter plate.

Figure 5. Continued.

θ_t/θ_b = 130°/130°, ψ_t/ψ_b = 60°/60°, slider door closed, $A_{t,main}$ = 0.0 in^2

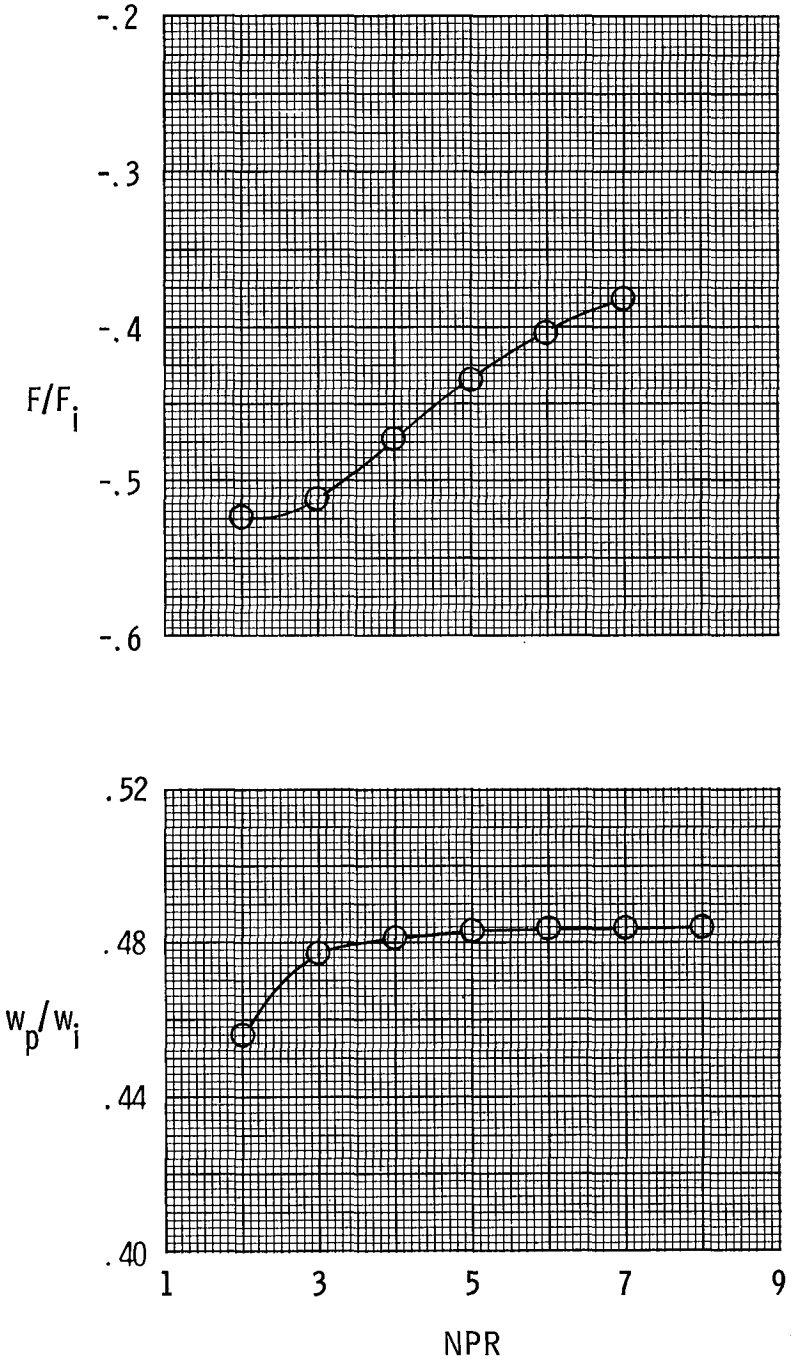

(x) Configuration 14; no splitter plate.

Figure 5. Continued.

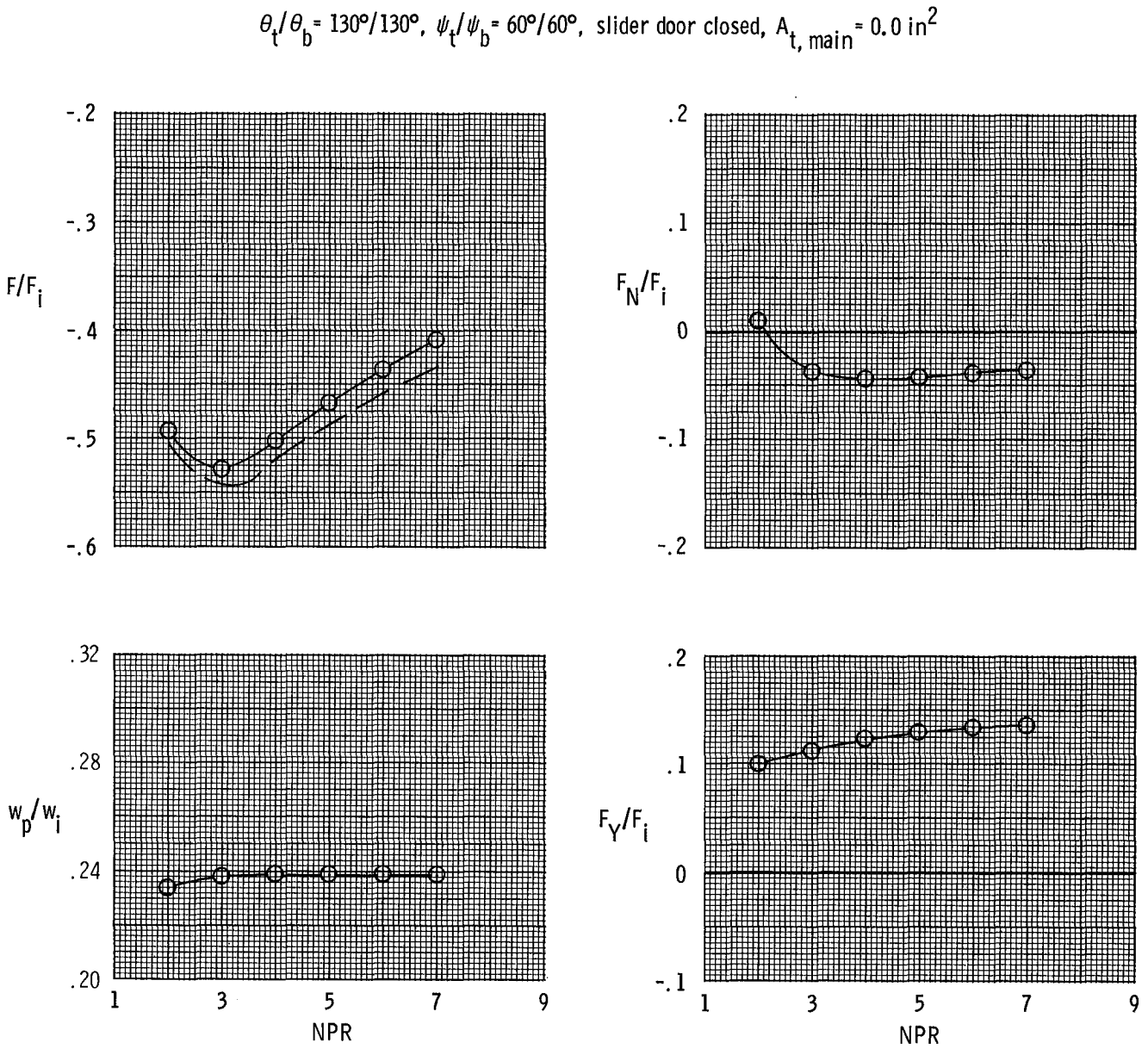

(y) Configuration 14; vertical splitter plate.

Figure 5. Continued.

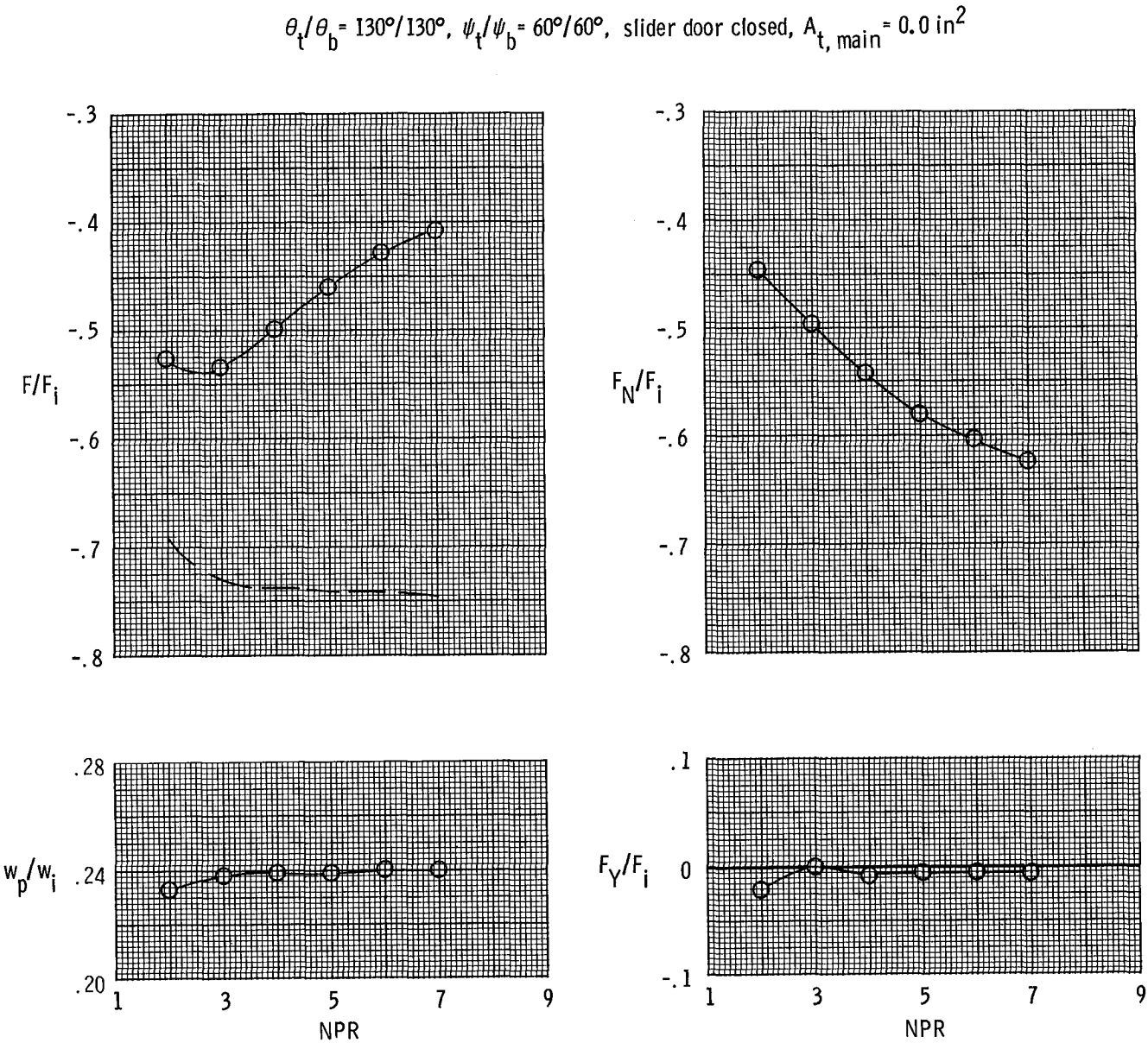

(z) Configuration 14; horizontal splitter plate.

Figure 5. Continued.

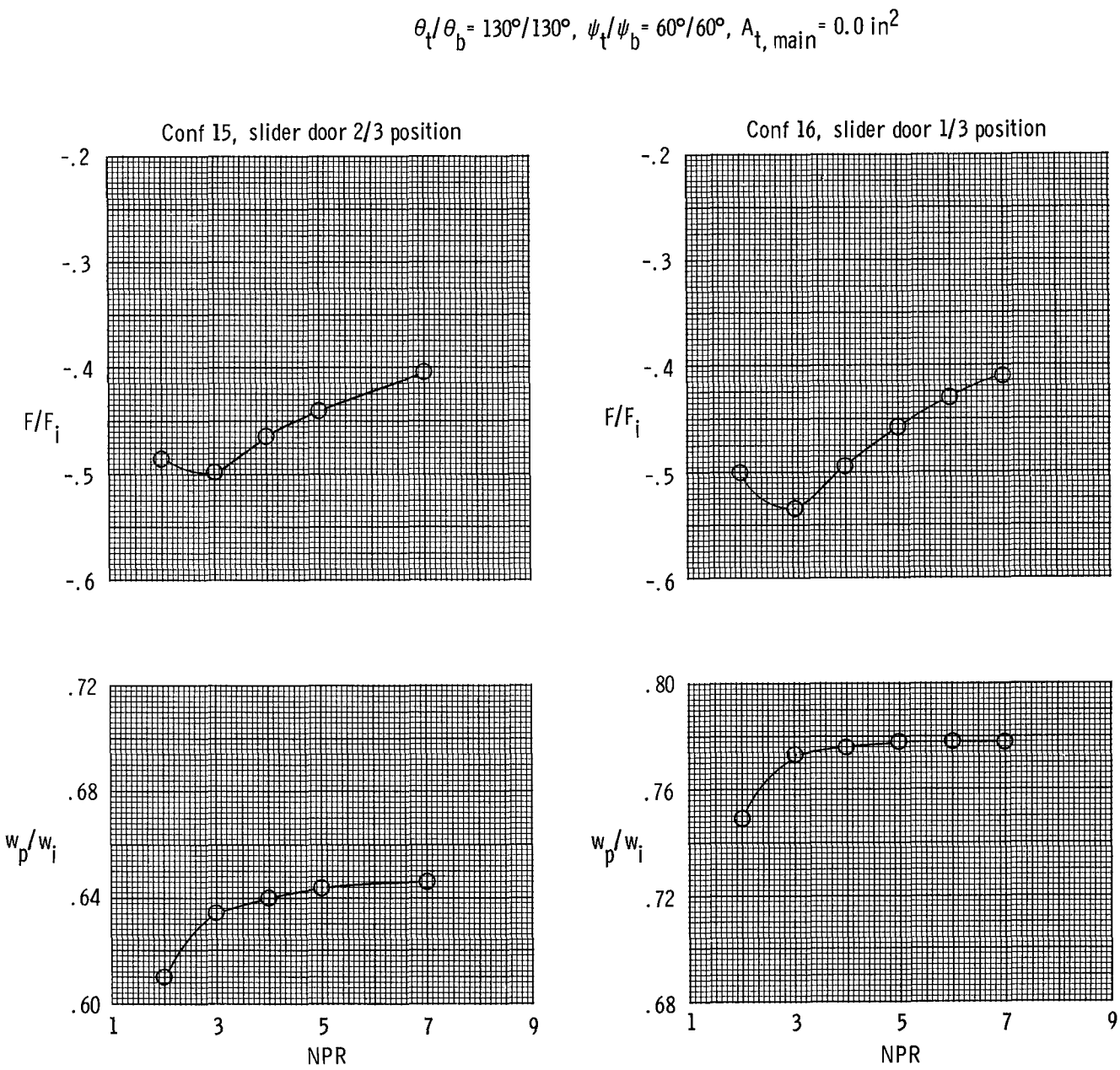

(aa) Configurations 15 and 16; no splitter plate.

Figure 5. Continued.

$\theta_t/\theta_b = 90°/90°$, $\psi_t/\psi_b = 60°/60°$, slider door closed, $A_{t,\,main} = 0.0\ in^2$

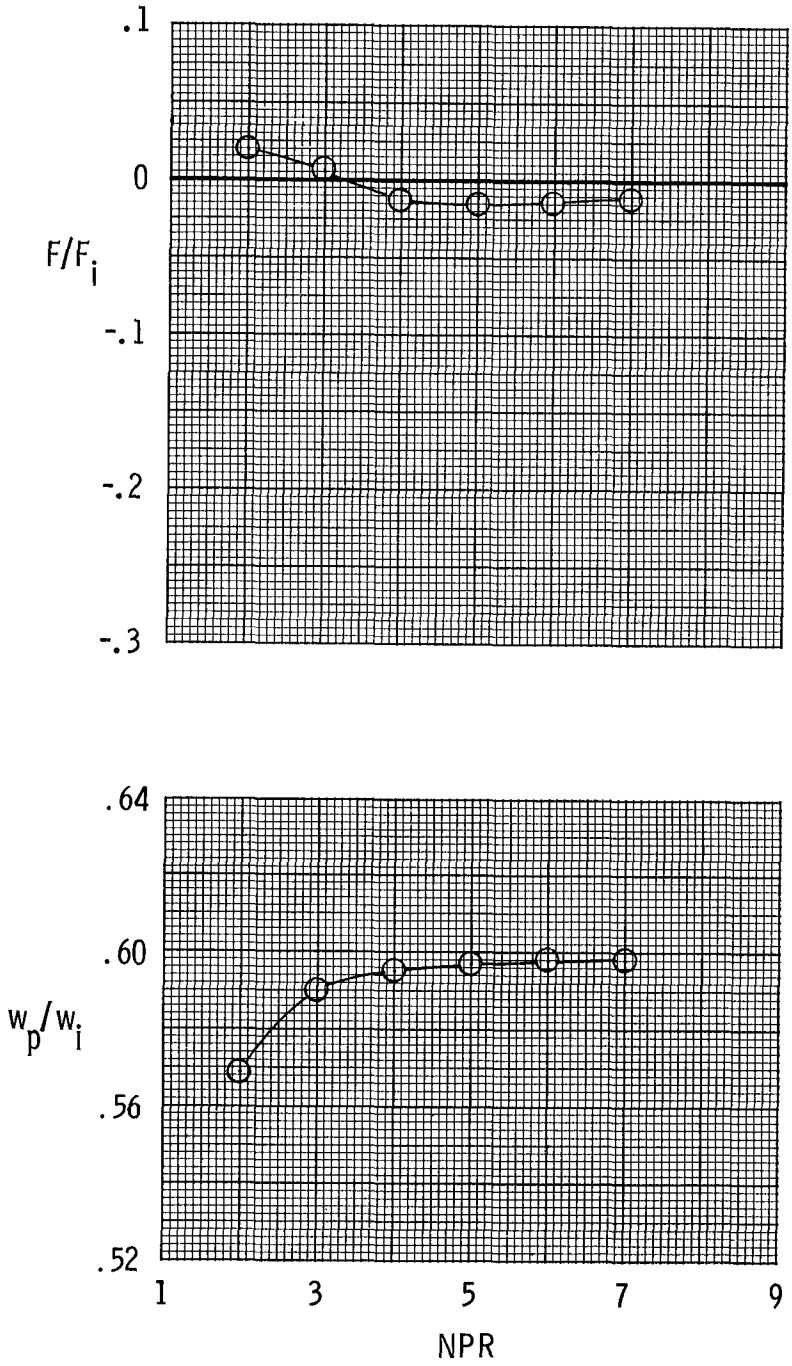

(bb) Configuration 17; no splitter plate.

Figure 5. Continued.

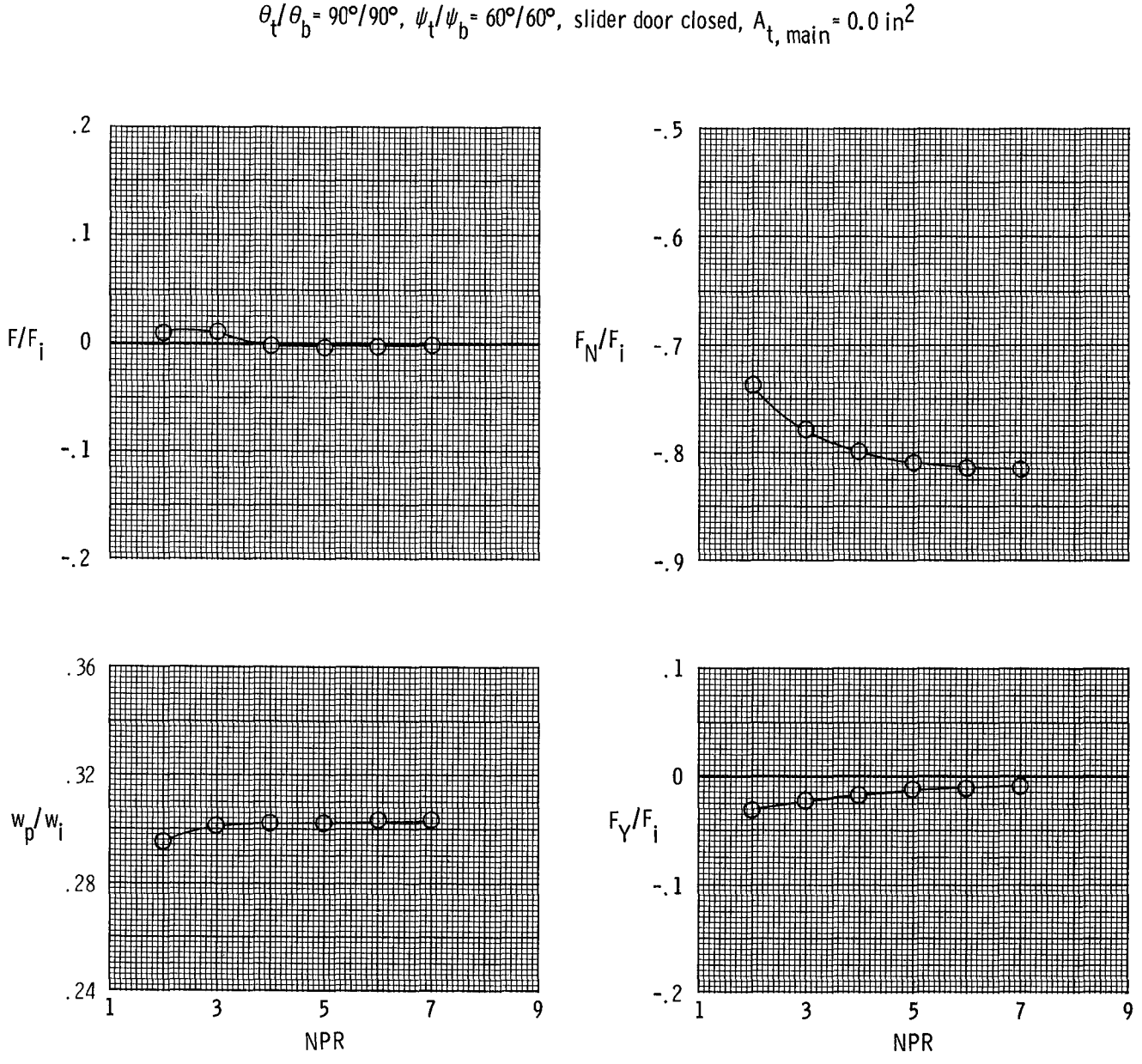

(cc) Configuration 17; horizontal splitter plate.

Figure 5. Continued.

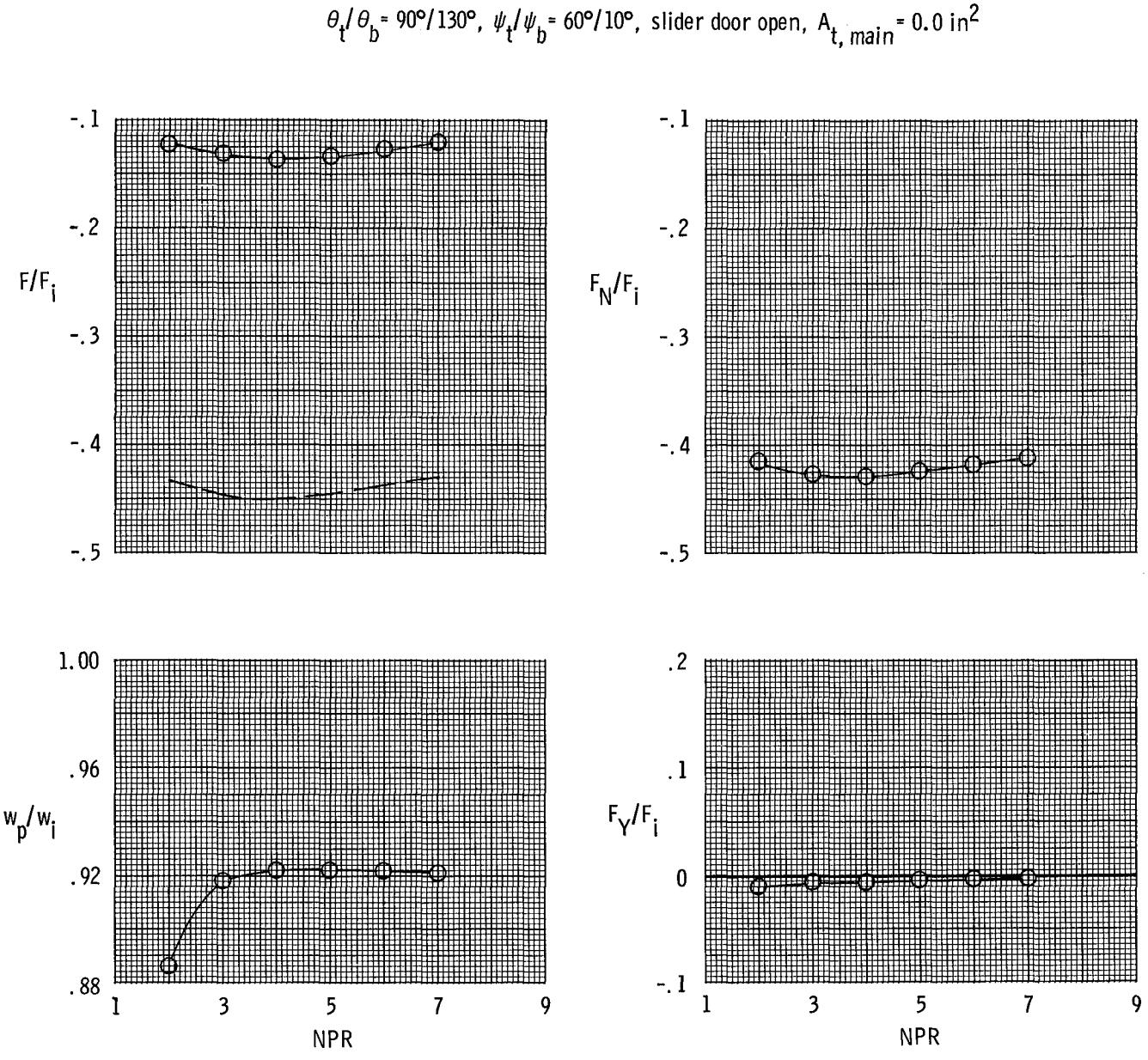

(dd) Configuration 18; no splitter plate.

Figure 5. Continued.

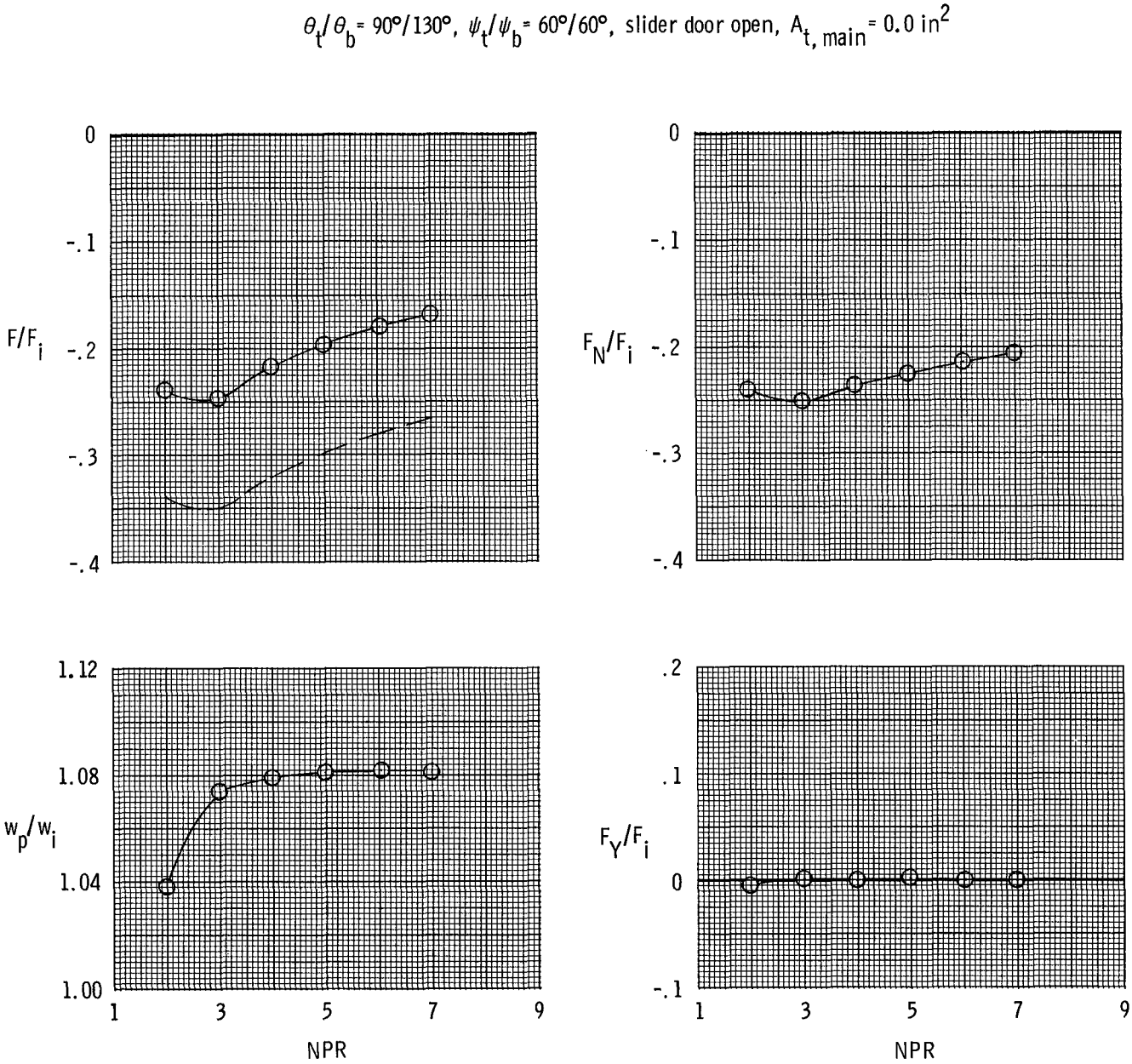

(ee) Configuration 19; no splitter plate.

Figure 5. Continued.

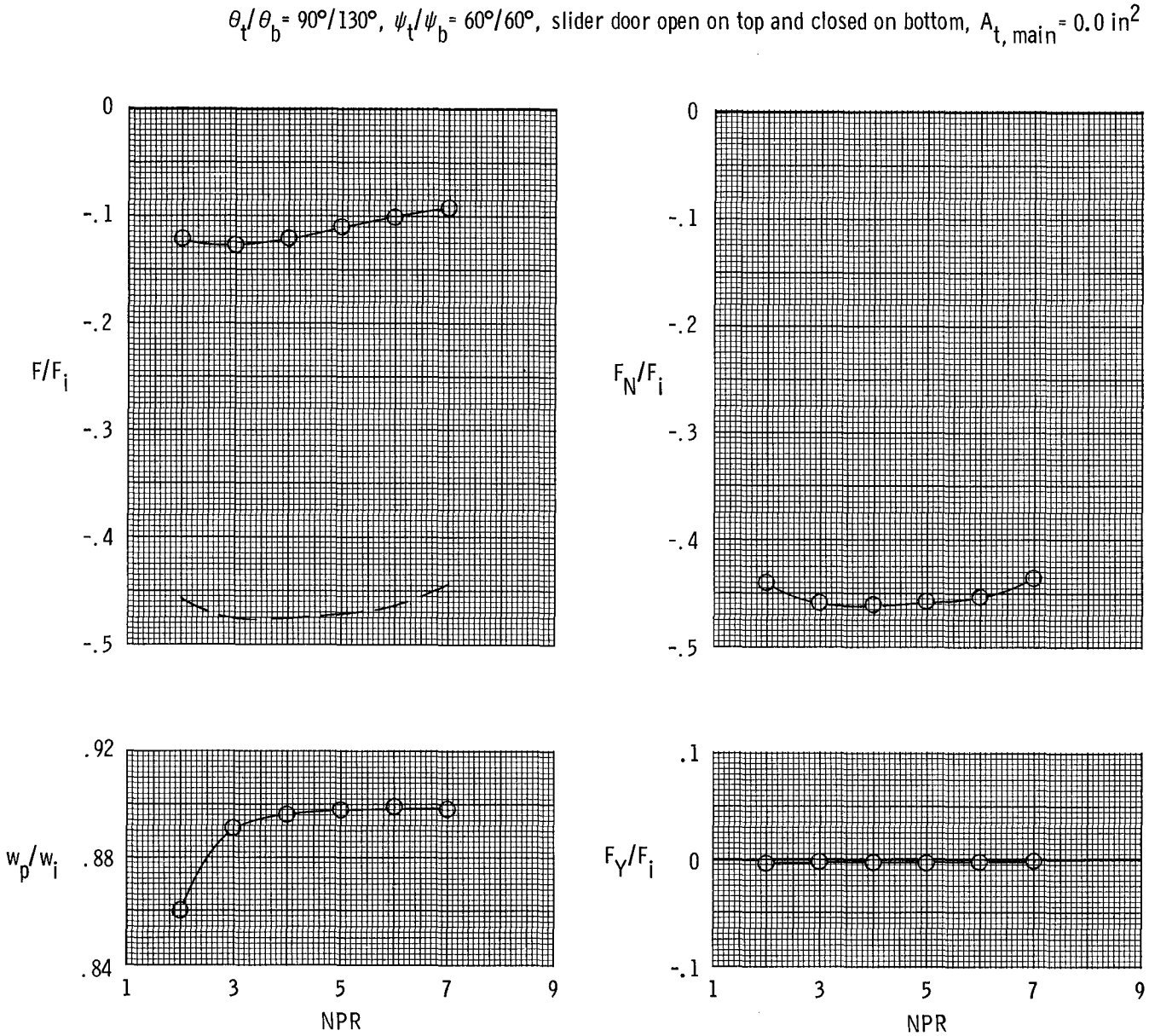

(ff) Configuration 20; no splitter plate.

Figure 5. Continued.

$\theta_t/\theta_b = 130°/130°$, $\psi_t/\psi_b = 60°/60°$, slider door open, $A_{t,\,main} = 0.0\ in^2$,

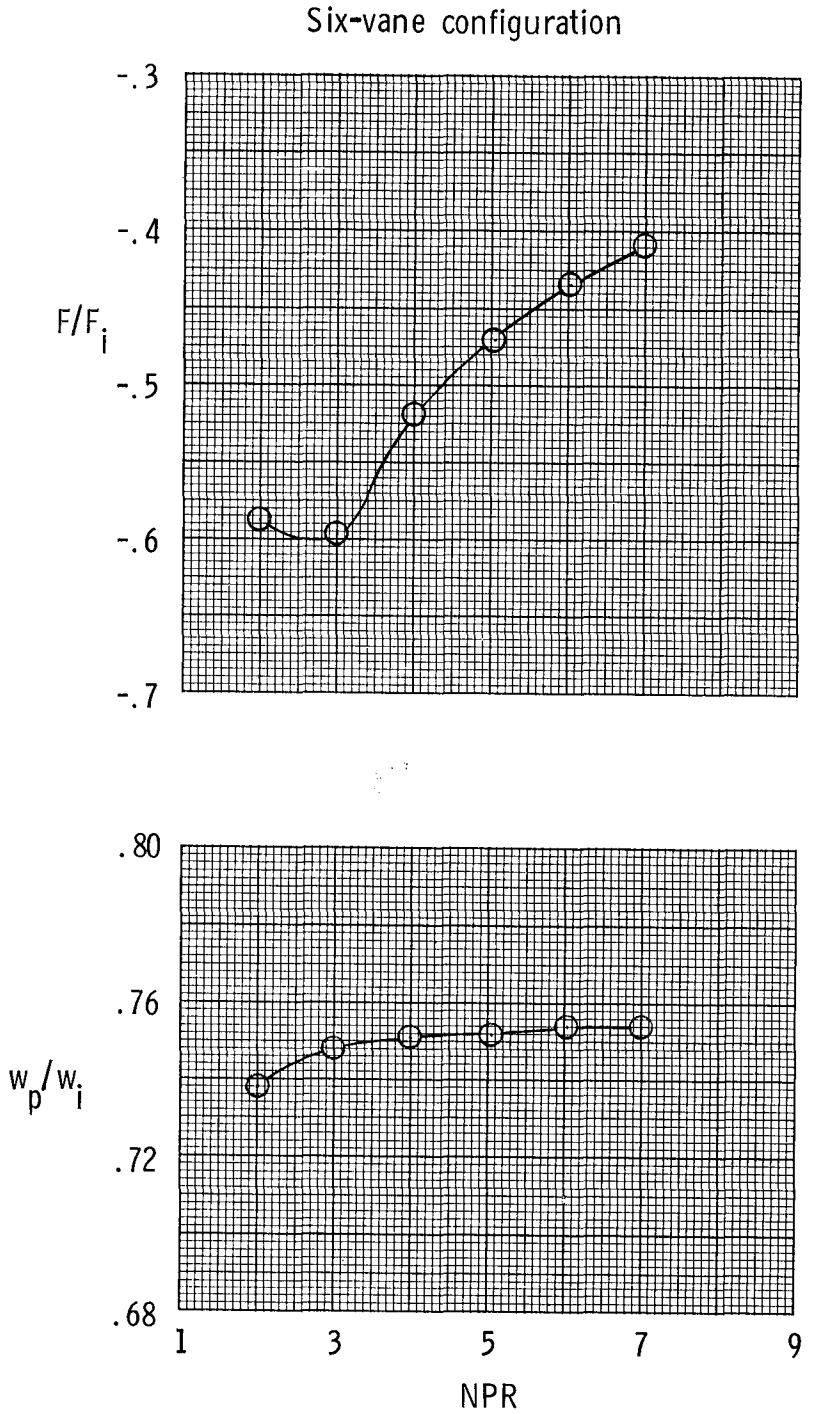

(gg) Configuration 21; no splitter plate.

Figure 5. Continued.

$\theta_t/\theta_b = 130°/130°$, $\psi_t/\psi_b = 60°/60°$, slider door open, $A_{t,\,main} = 0.0\ in^2$, port tab removed

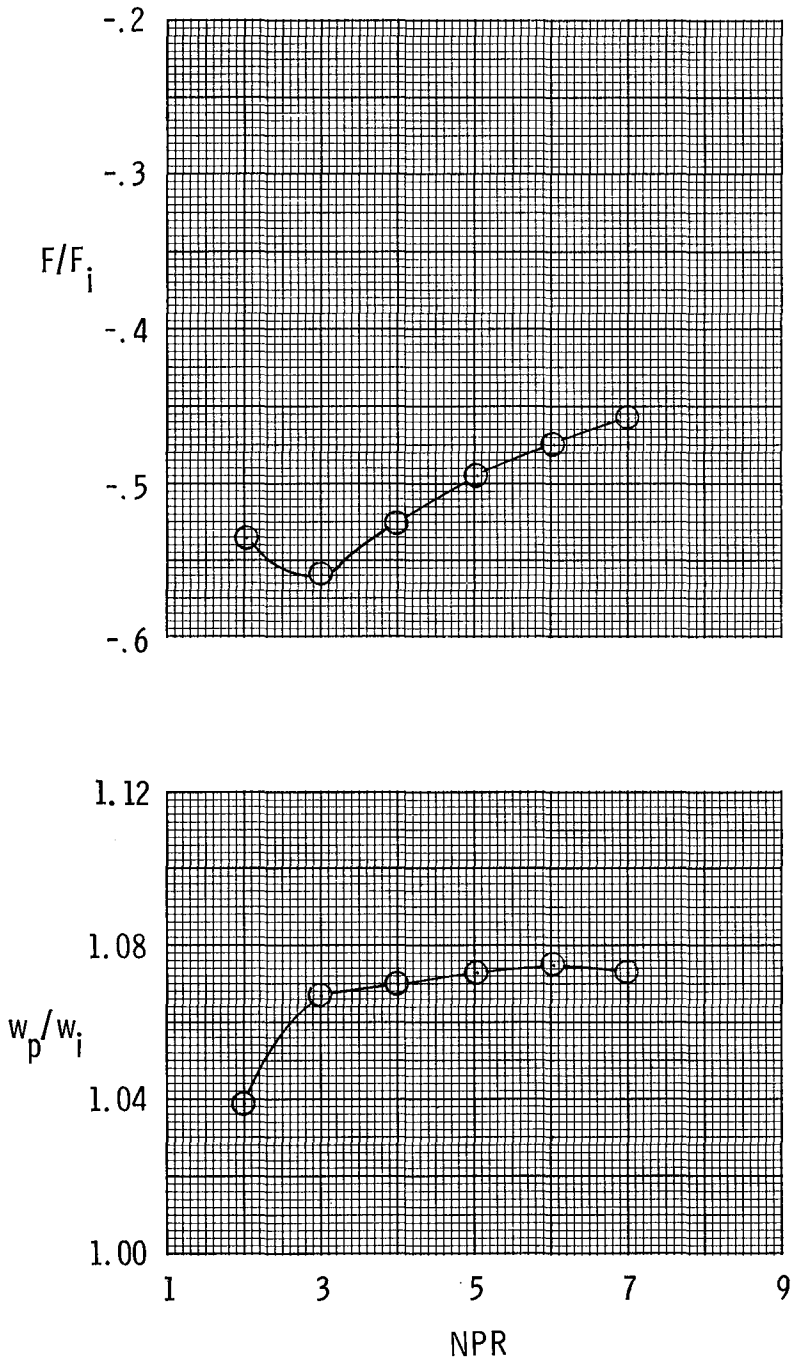

(hh) Configuration 22; no splitter plate.

Figure 5. Continued.

θ_t/θ_b = 130°/130°, ψ_t/ψ_b = 60°/60°, slider door open, $A_{t,\,main}$ = 0.0 in^2, vane box sideplates installed

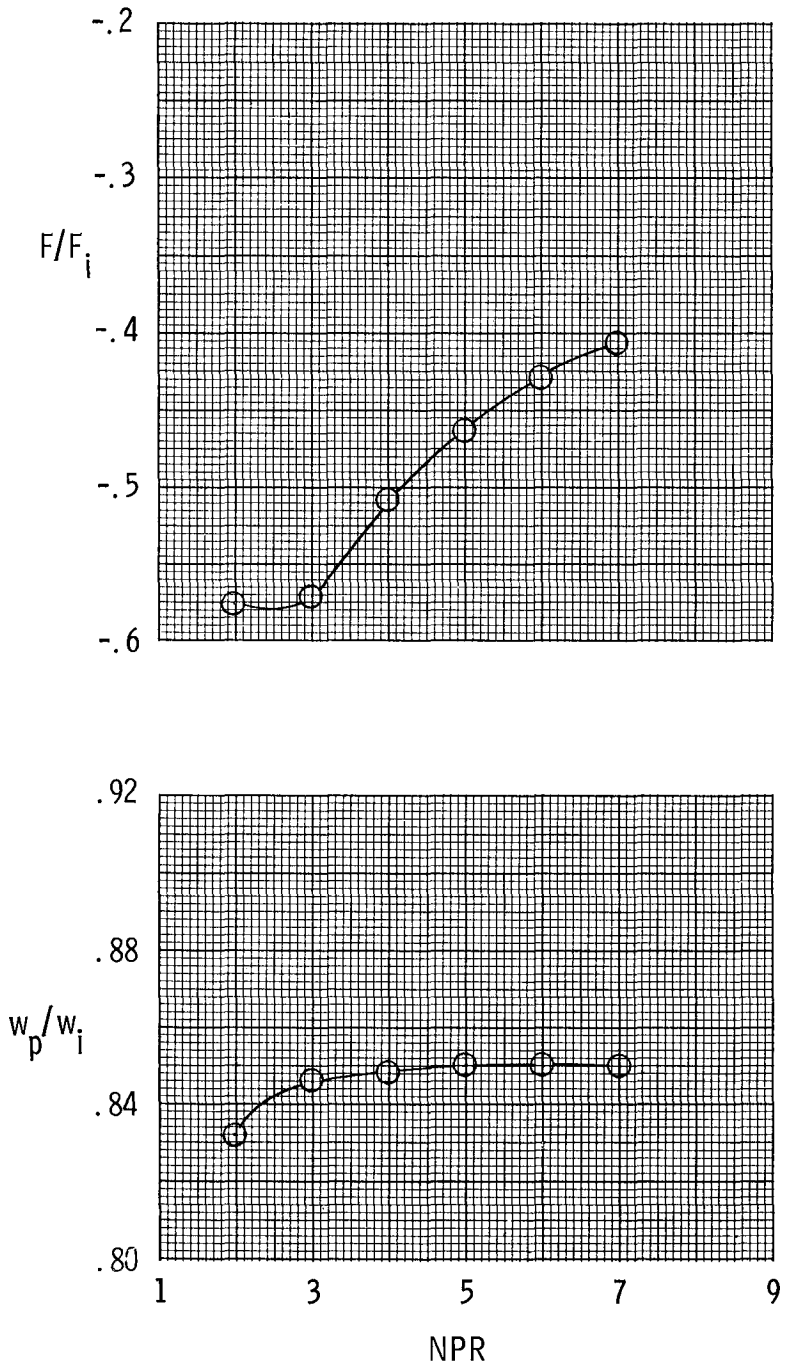

(ii) Configuration 23; no splitter plate.

Figure 5. Continued.

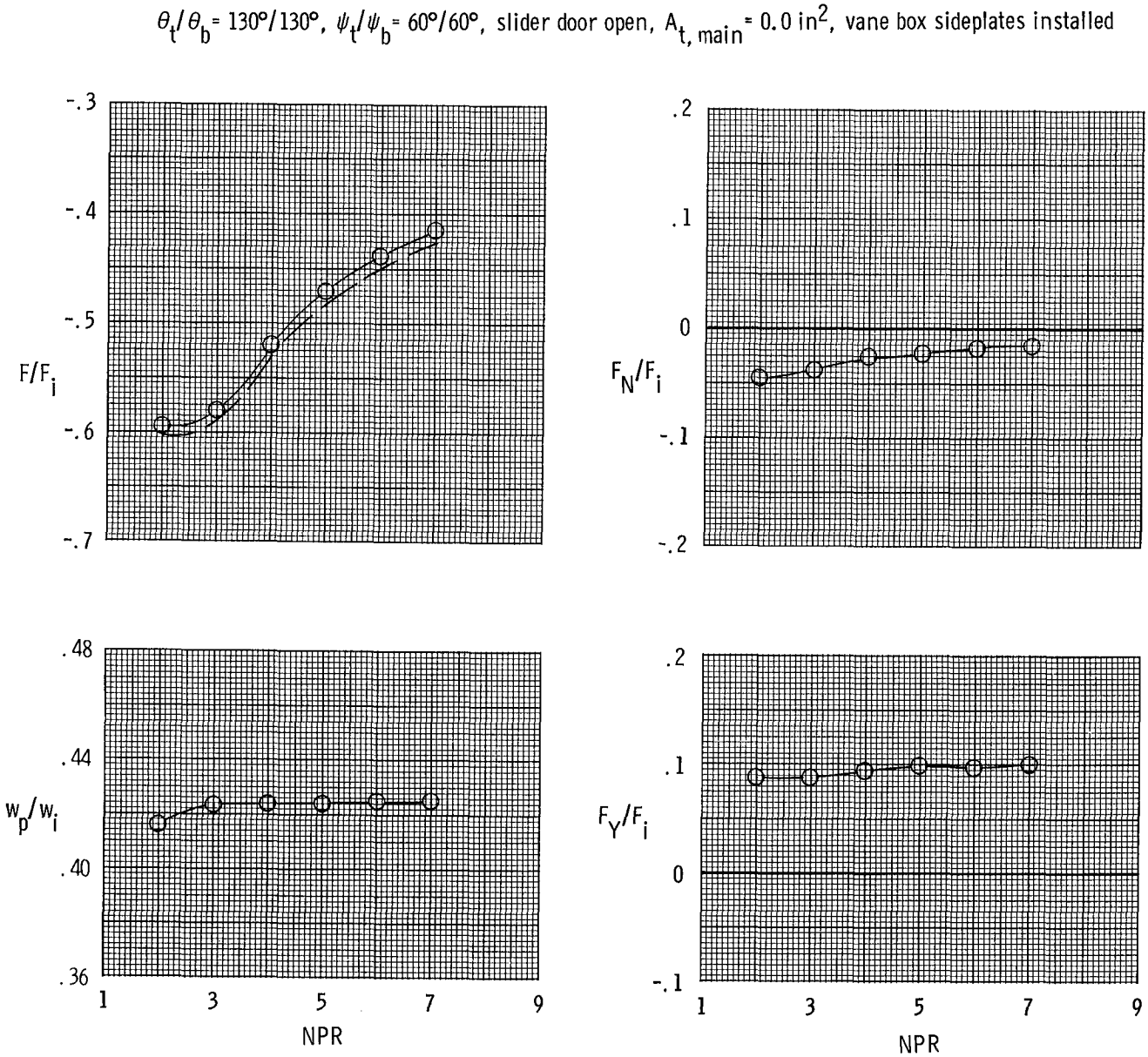

(jj) Configuration 23; vertical splitter plate.

Figure 5. Continued.

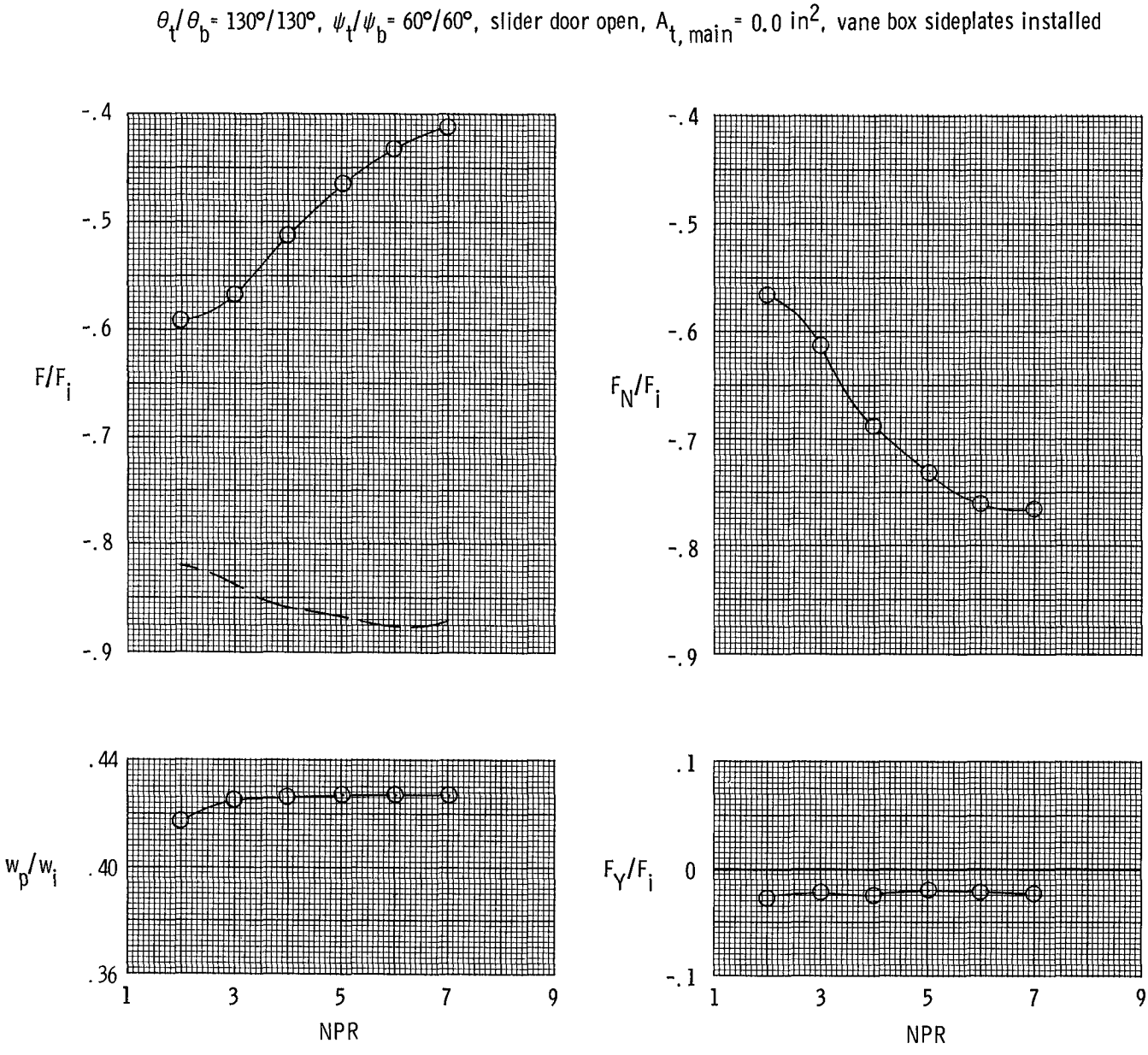

(kk) Configuration 23; horizontal splitter plate.

Figure 5. Continued.

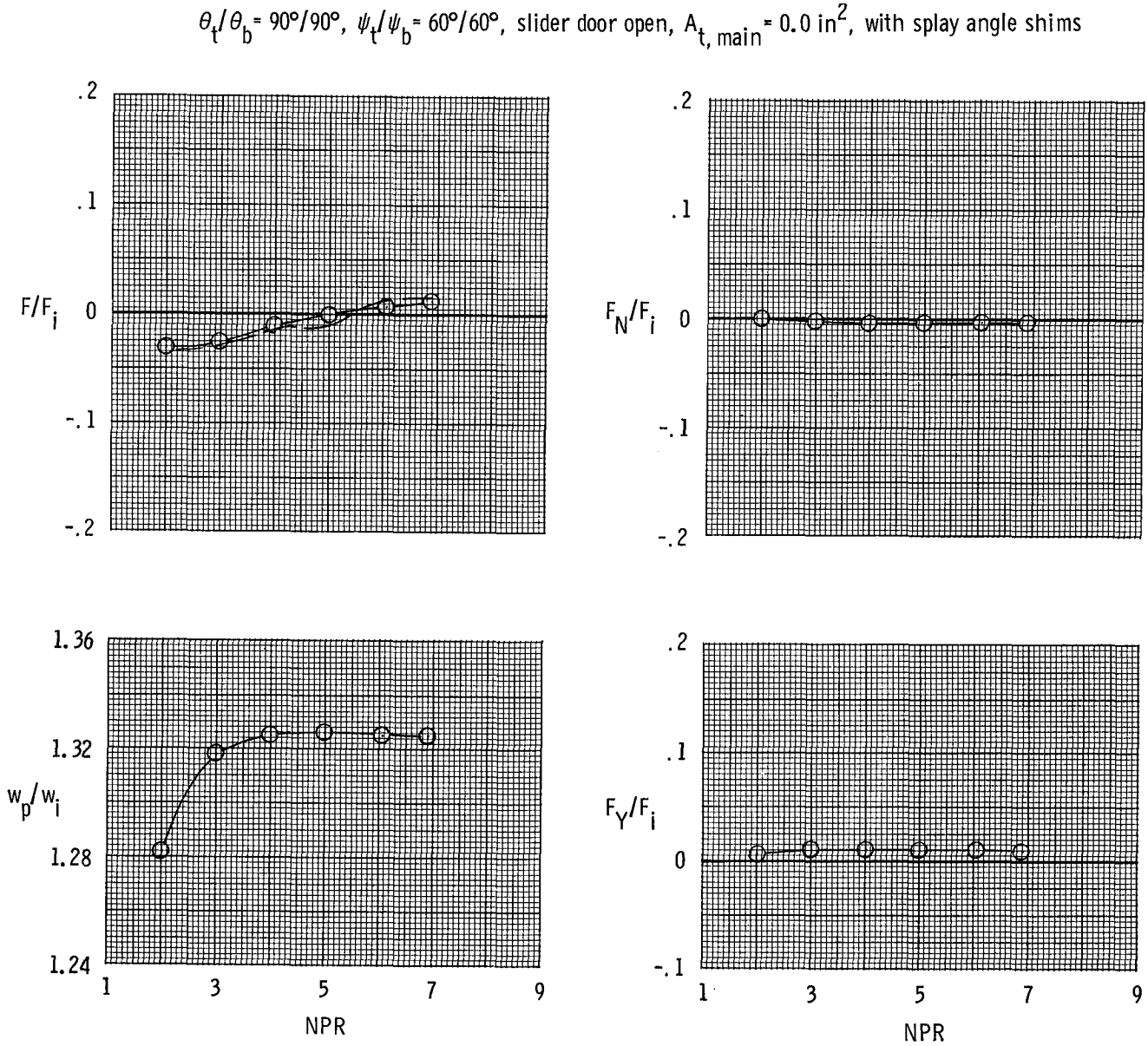

(ll) Configuration 26; no splitter plate.

Figure 5. Continued.

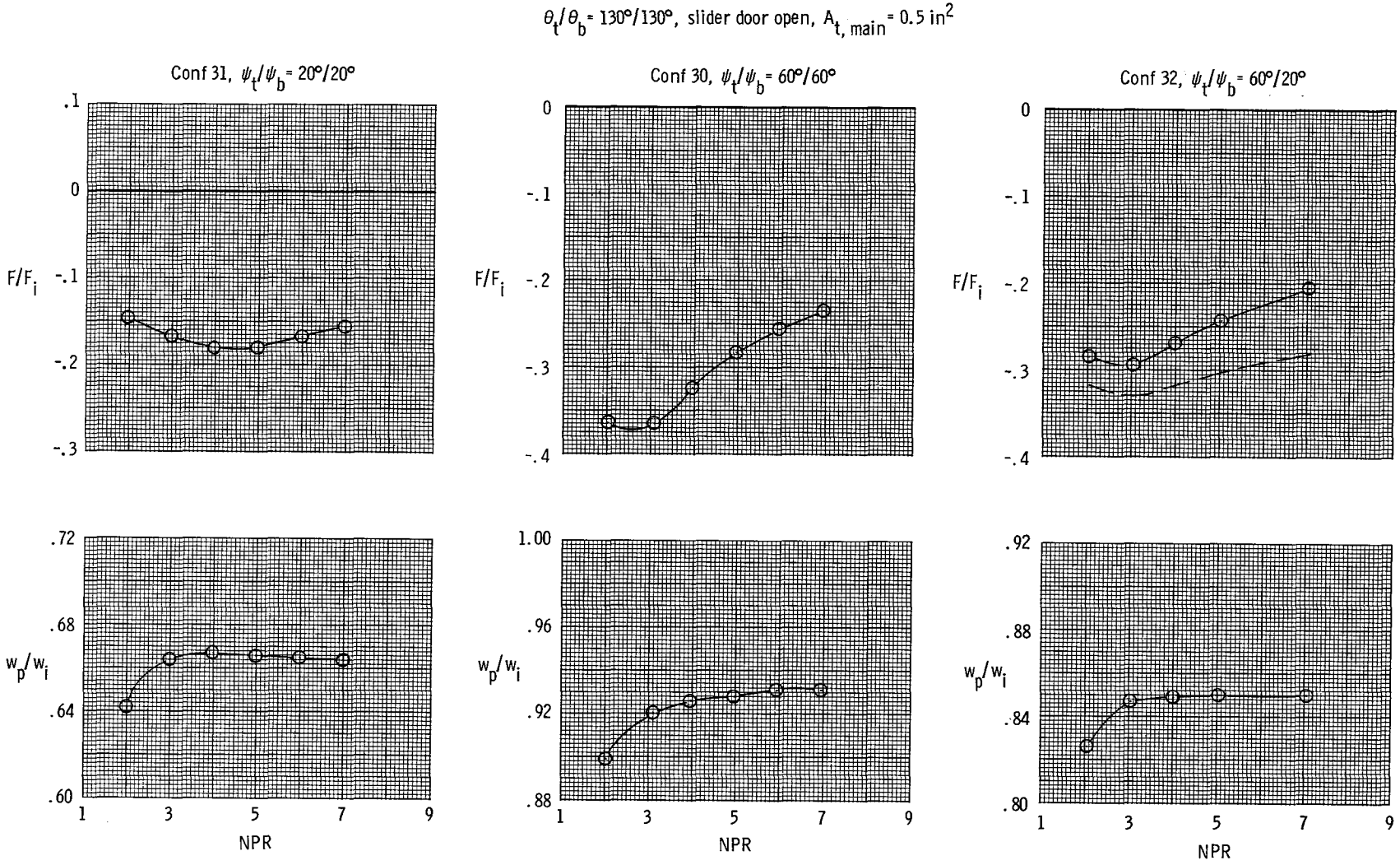

(mm) Configurations 30, 31, and 32; no splitter plate.

Figure 5. Continued.

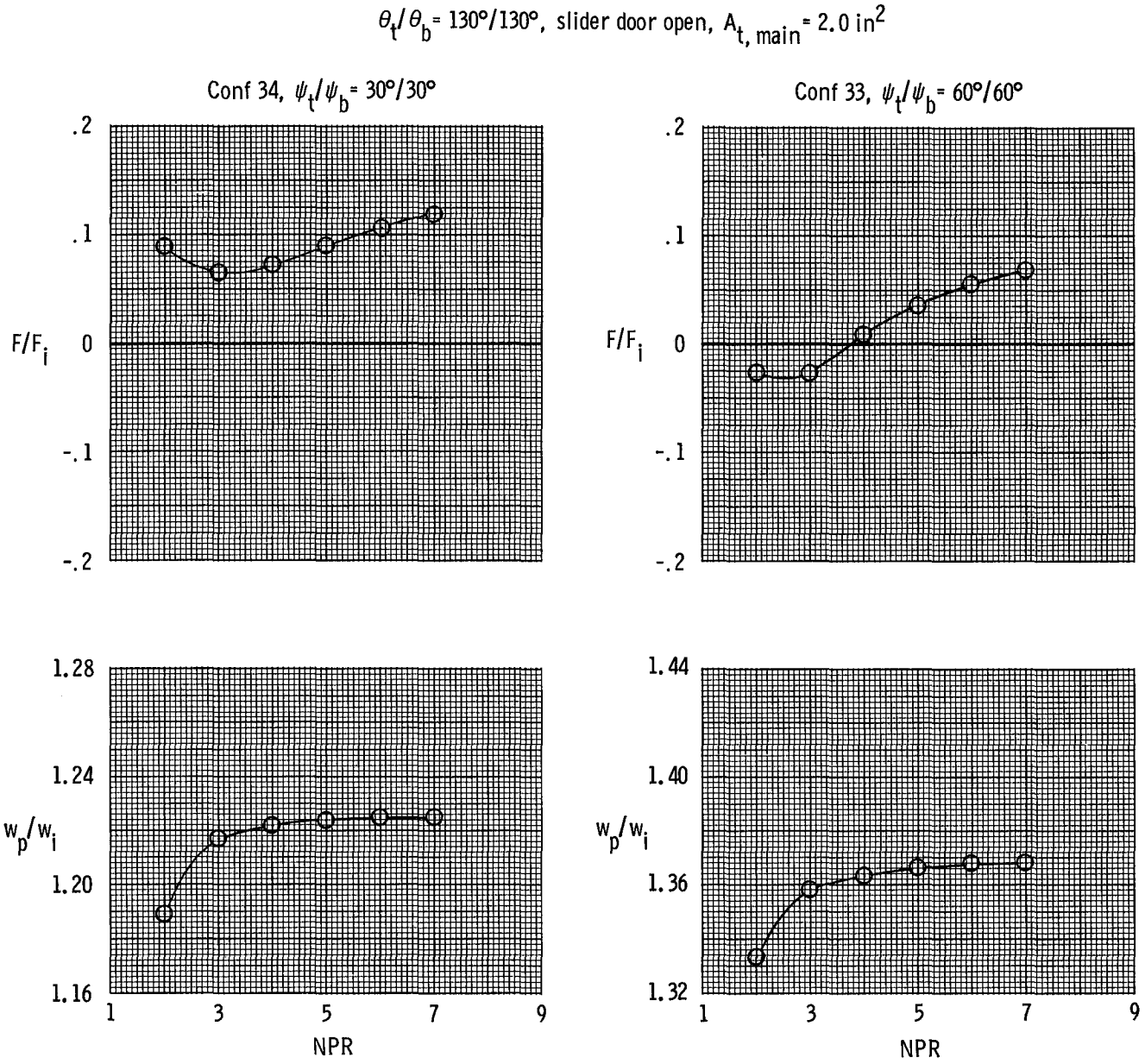

(nn) Configurations 33 and 34; no splitter plate.

Figure 5. Continued.

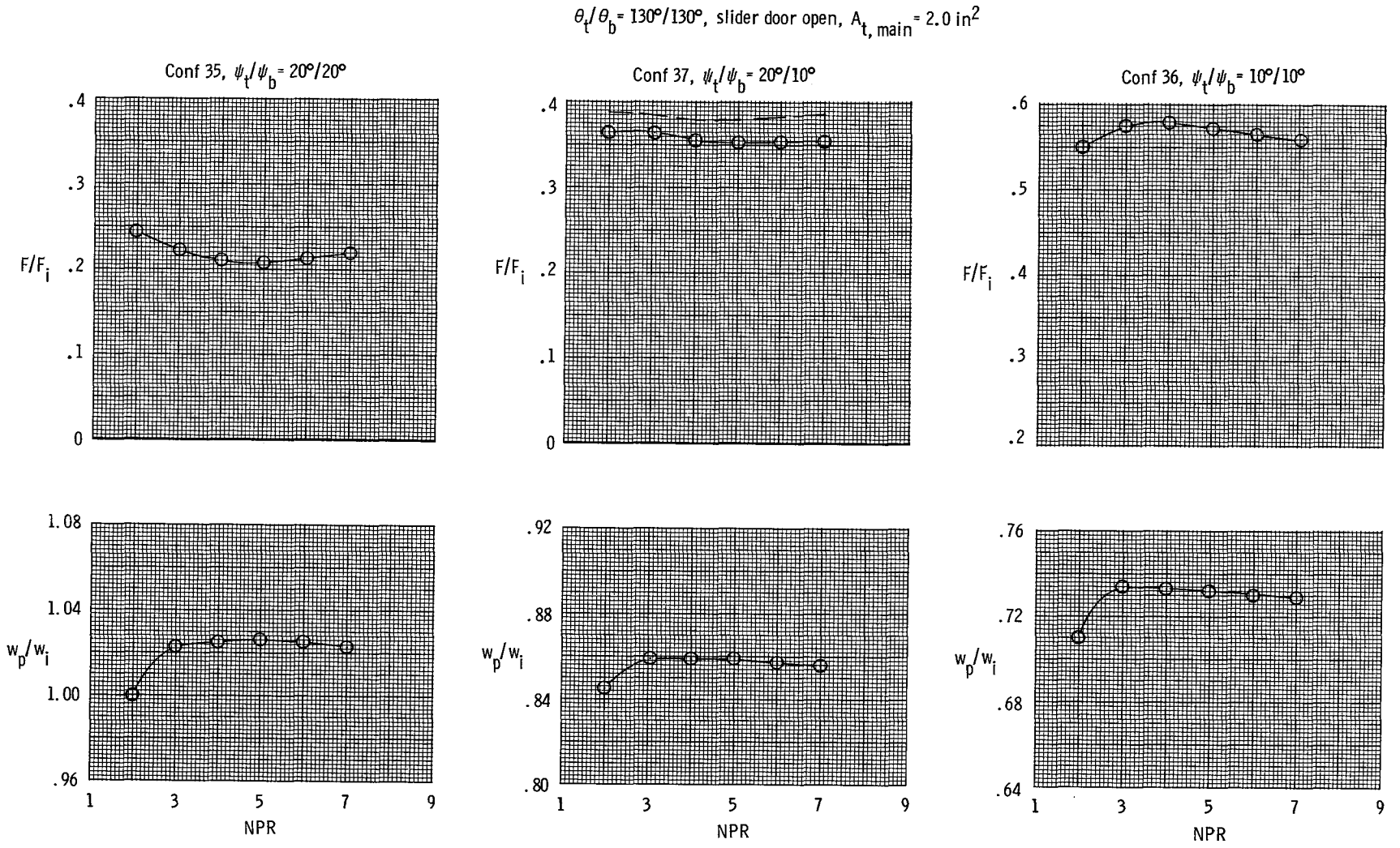

(oo) Configurations 35, 36, and 37; no splitter plate.

Figure 5. Continued.

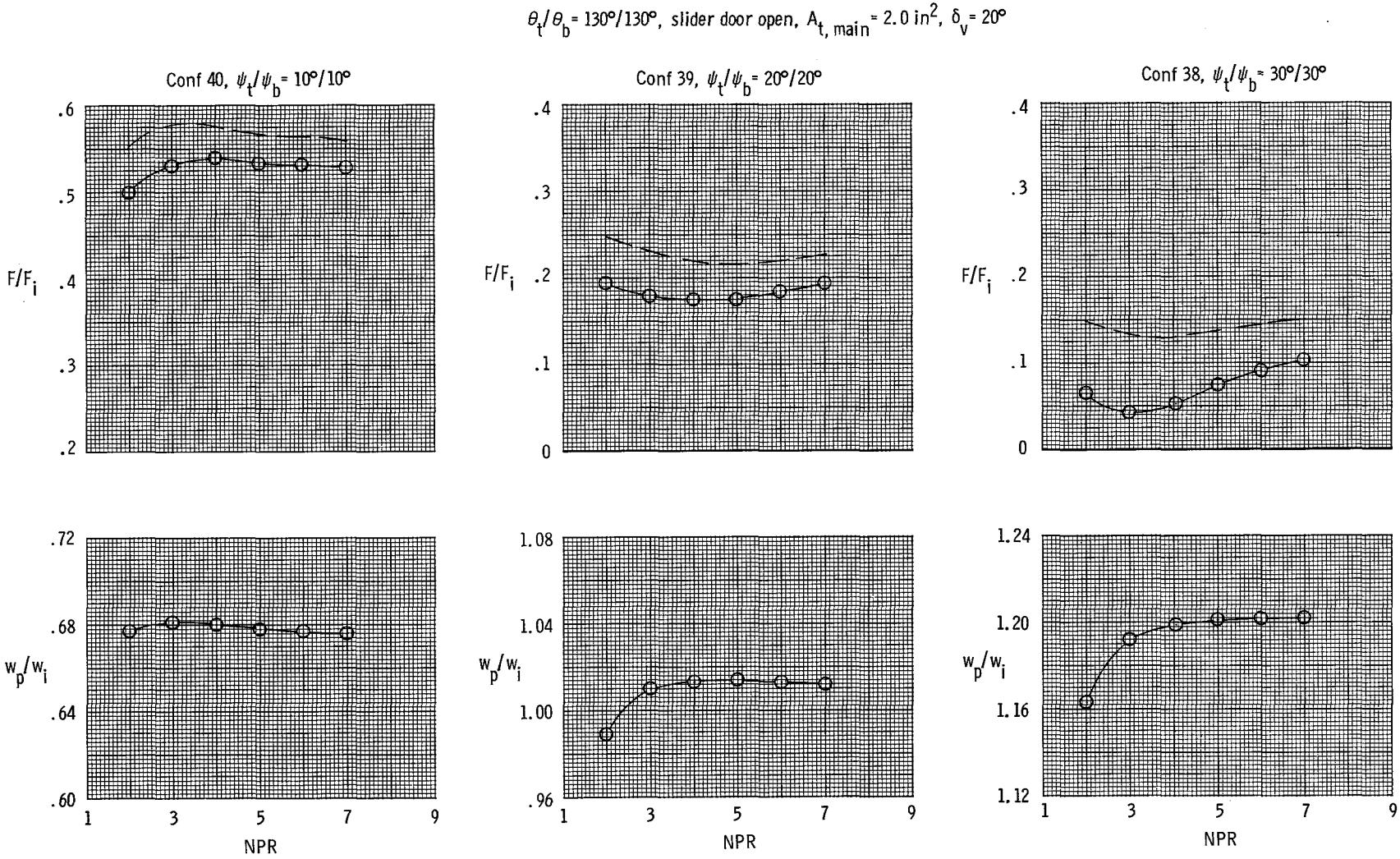

(pp) Configurations 38, 39, and 40; no splitter plate.

Figure 5. Continued.

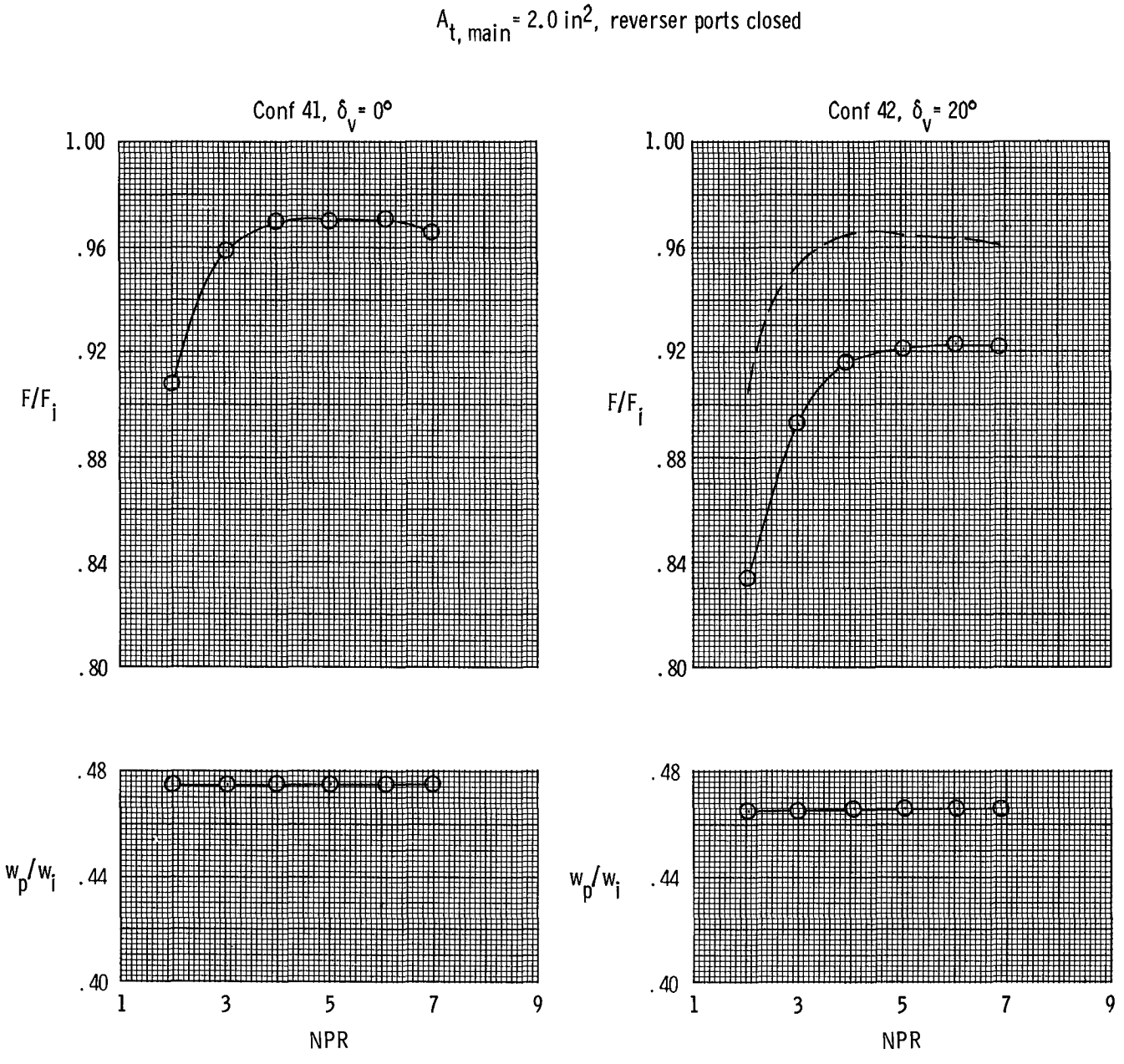

(qq) Configurations 41 and 42; no splitter plate.

Figure 5. Continued.

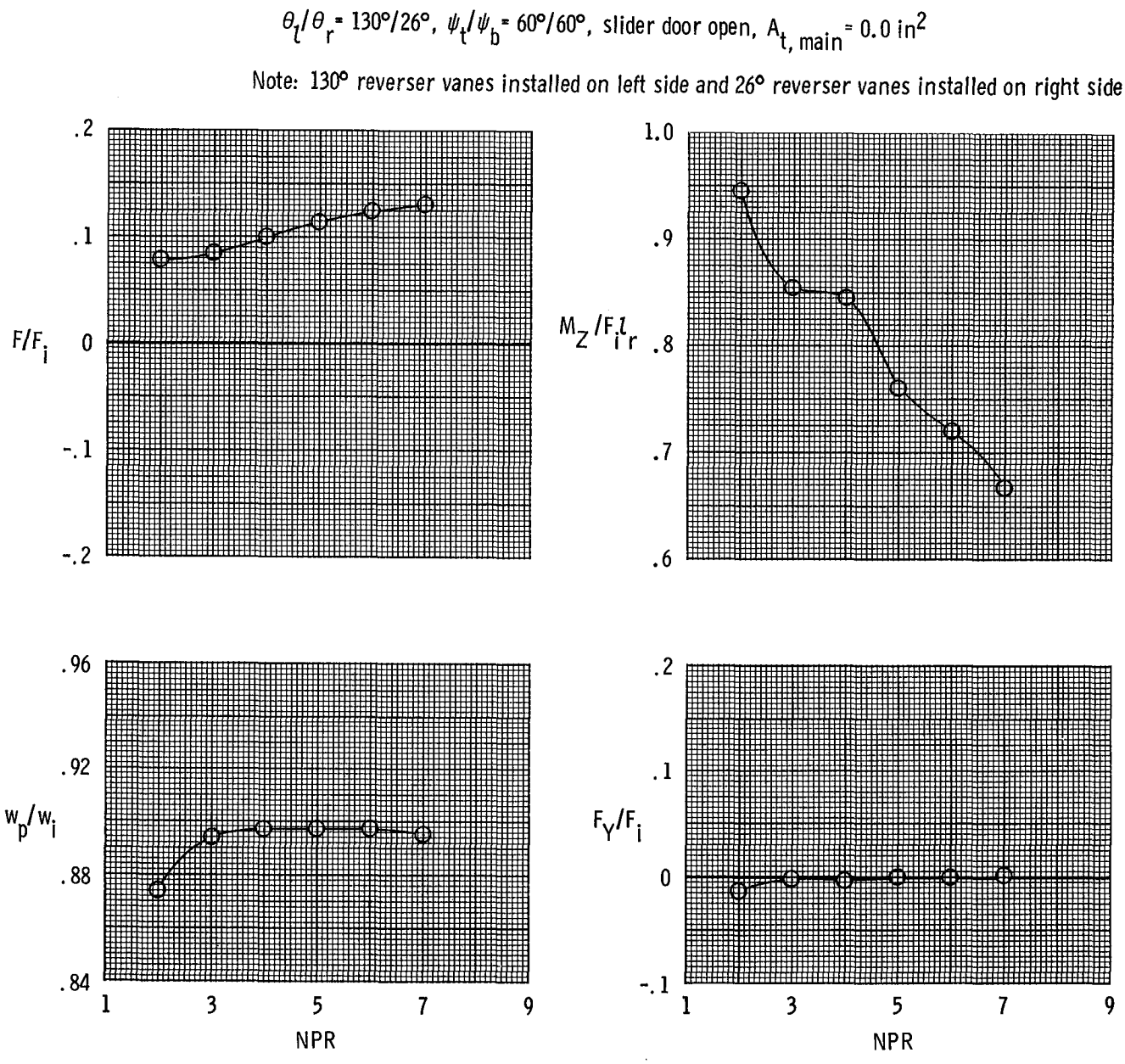

(rr) Configuration 43; no splitter plate.

Figure 5. Concluded.

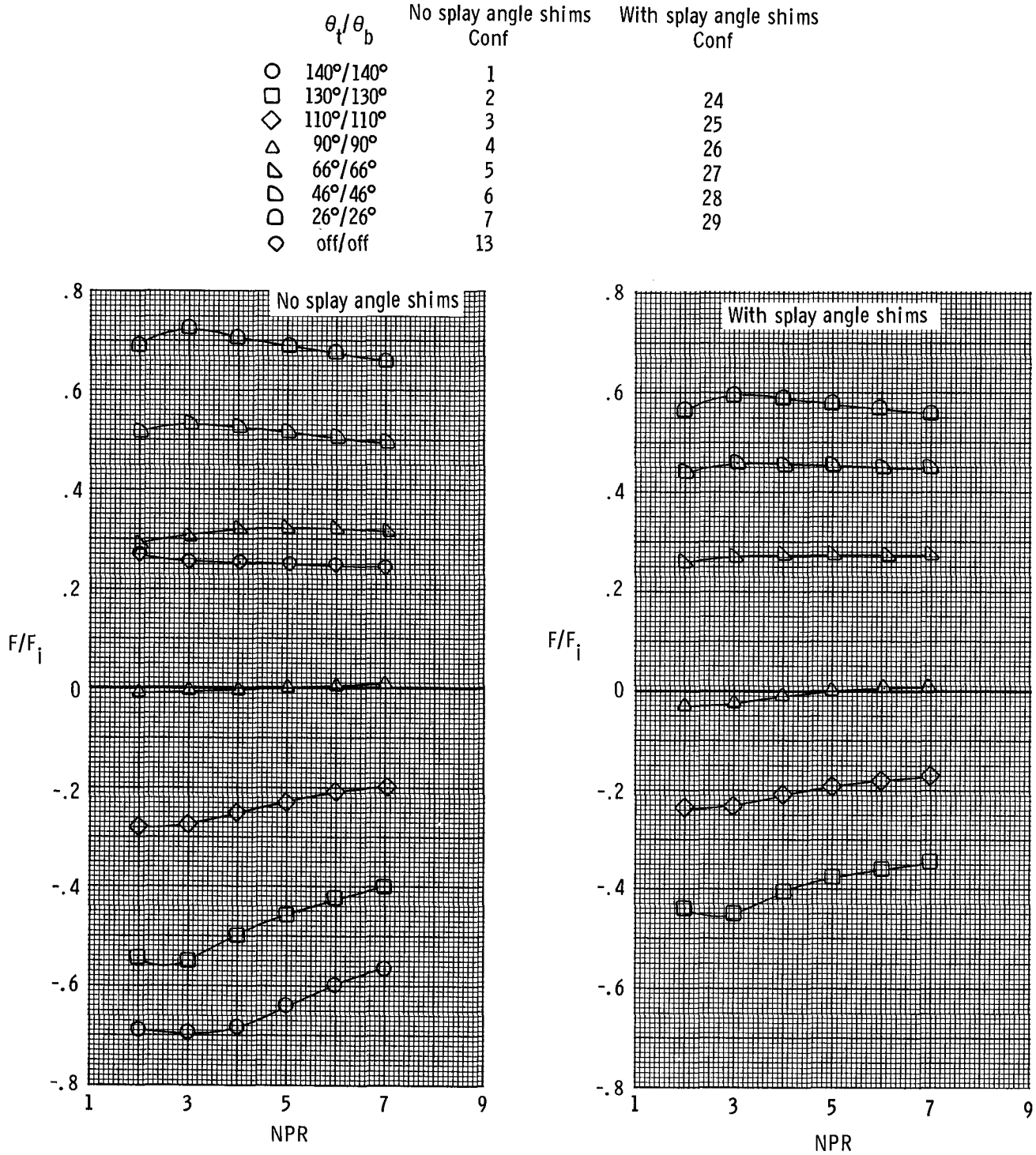

Figure 6. Effect of geometric efflux angle on thrust ratio. ψ_t/ψ_b = 60°/60°; slider door open; $A_{t,\text{main}} = 0.0$ in^2.

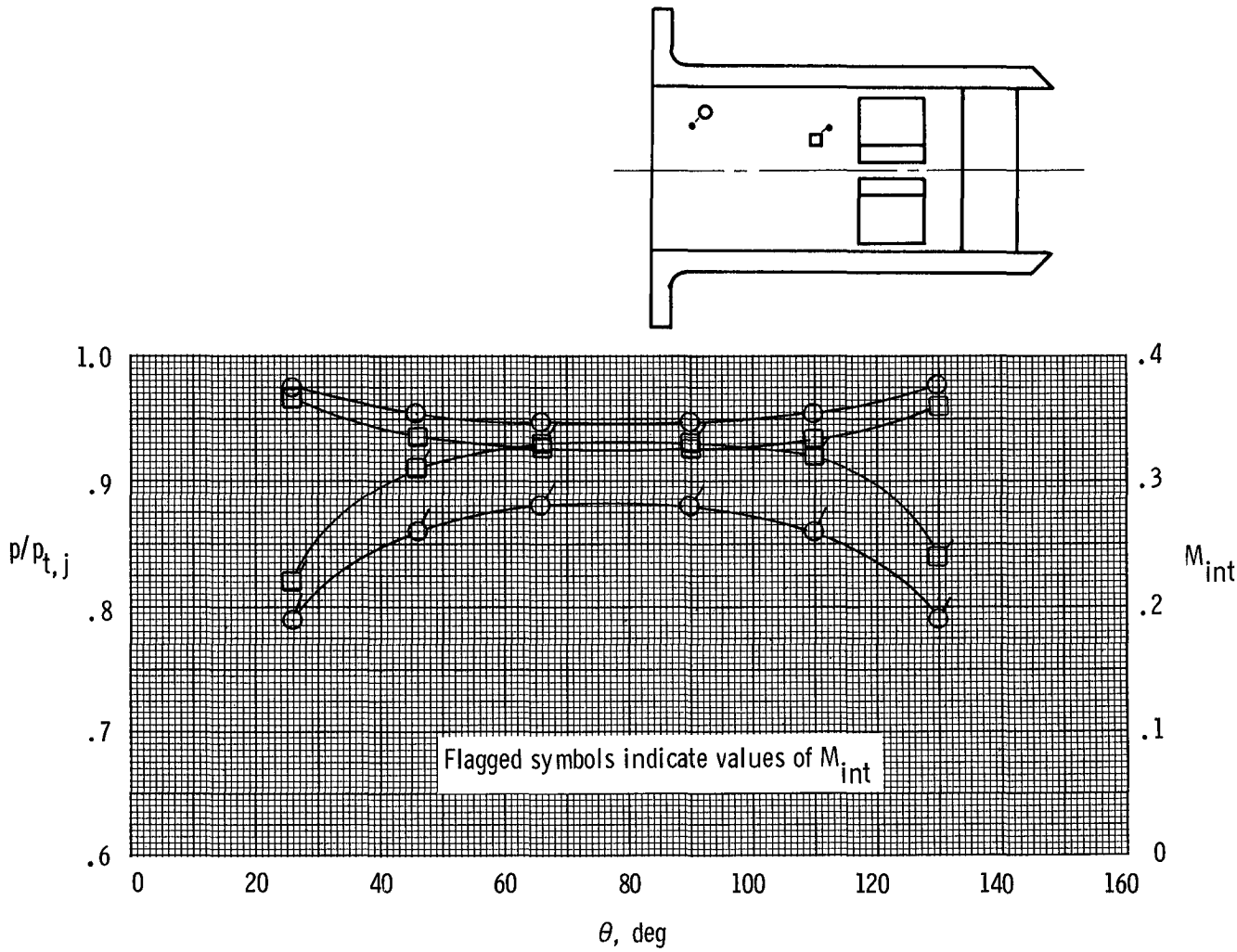

(a) Upper flap pressures and Mach numbers; splay angle shims off.

Figure 7. Effect of geometric efflux angle and splay angle shims on reverser static-pressure ratios and internal Mach numbers. $\psi_t/\psi_b = 60°/60°$; slider door open; $A_{t,\text{main}} = 0.0$ in^2; NPR = 3.0.

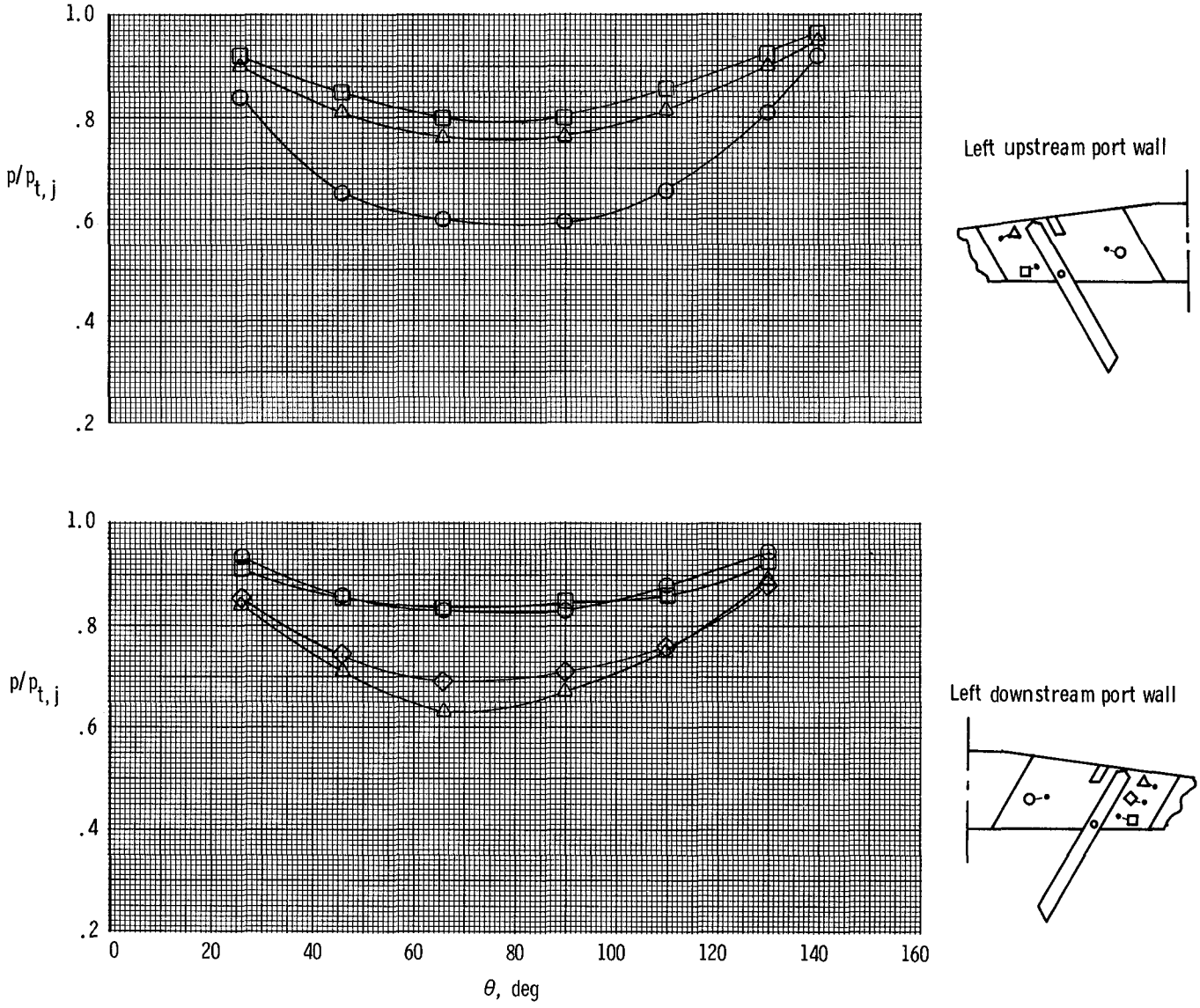

(b) Port pressures; splay angle shims off.

Figure 7. Continued.

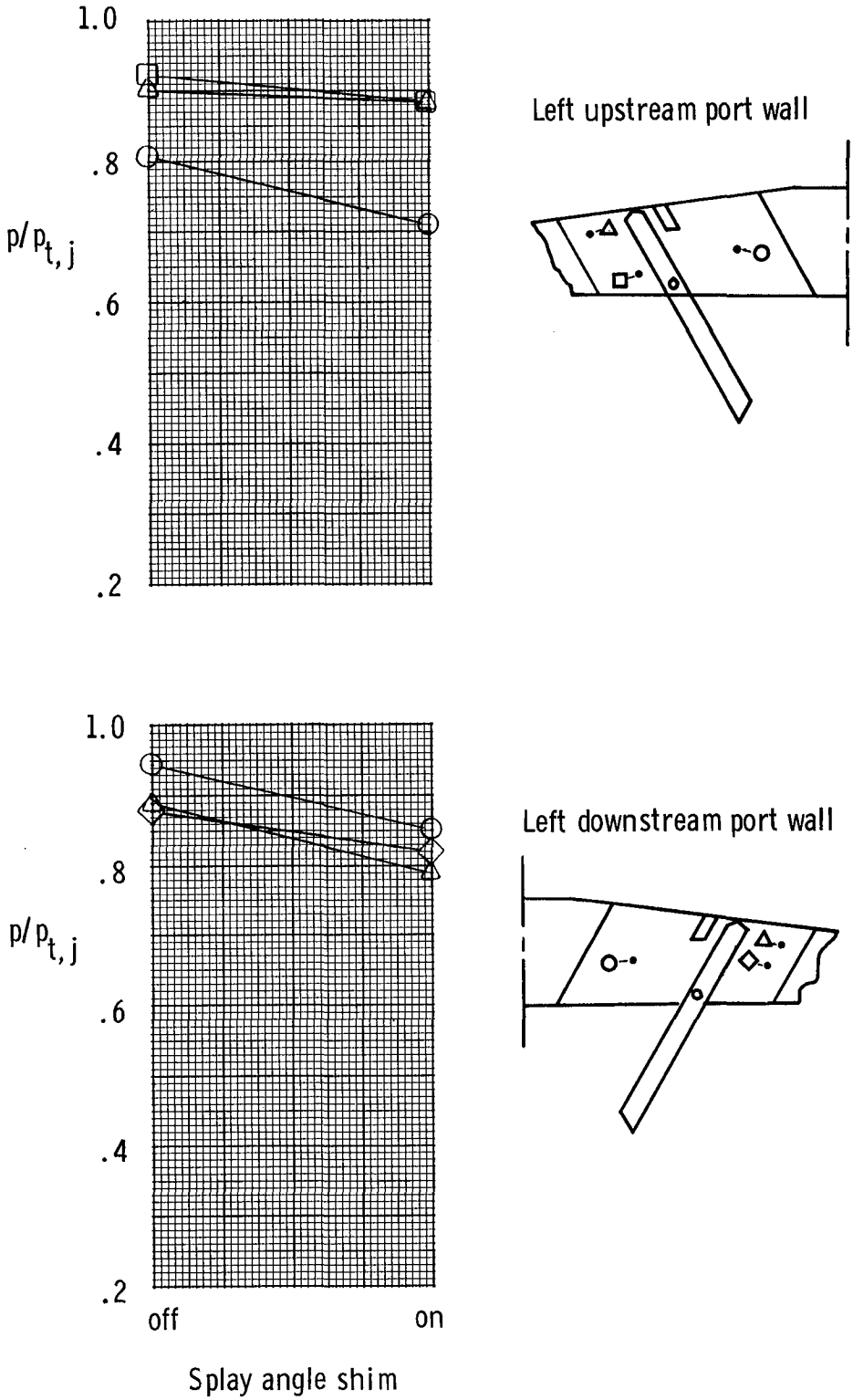

(c) Port pressures; $\theta_t/\theta_b = 130°/130°$.

Figure 7. Concluded.

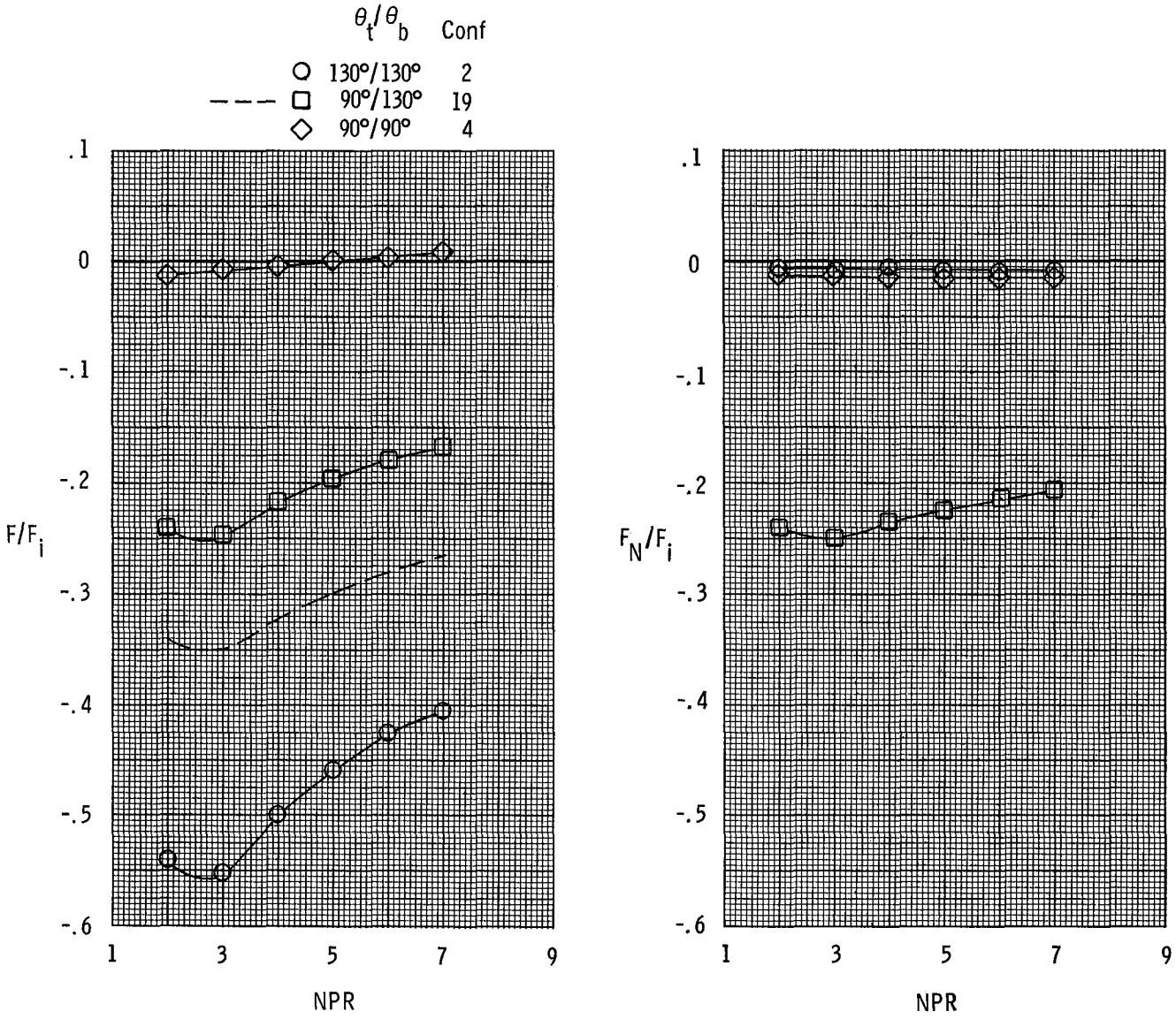

(a) Differential efflux angles for generating normal force.

Figure 8. Effect of differential geometric efflux angles on thrust ratio, normal-force ratio, and yawing-moment ratio. $\psi_t/\psi_b = 60°/60°$; slider door open; $A_{t,\text{main}} = 0.0$ in^2. Line with no symbols indicates resultant thrust ratio F_r/F_i.

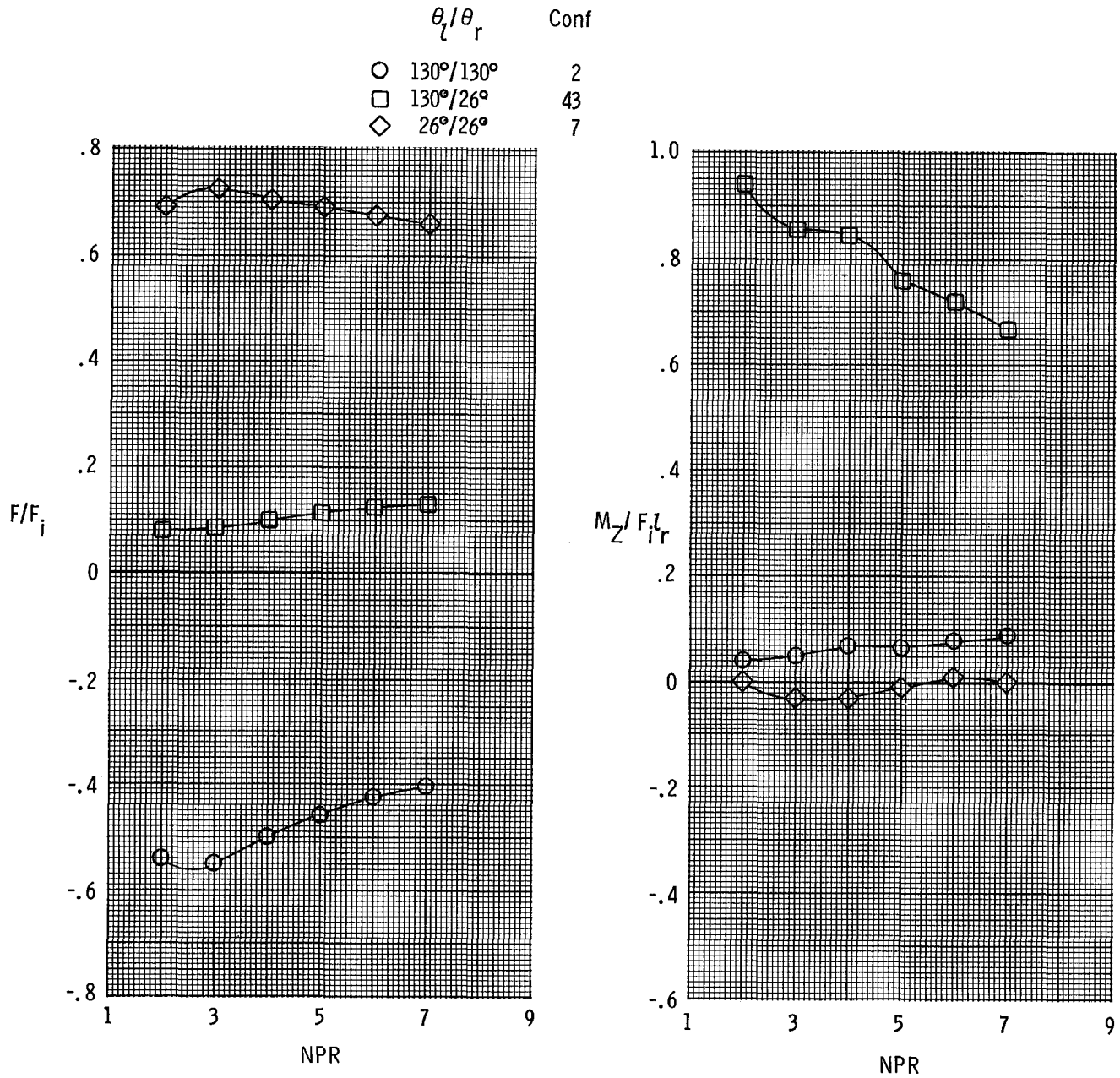

(b) Differential efflux angles for generating yawing moment.

Figure 8. Concluded.

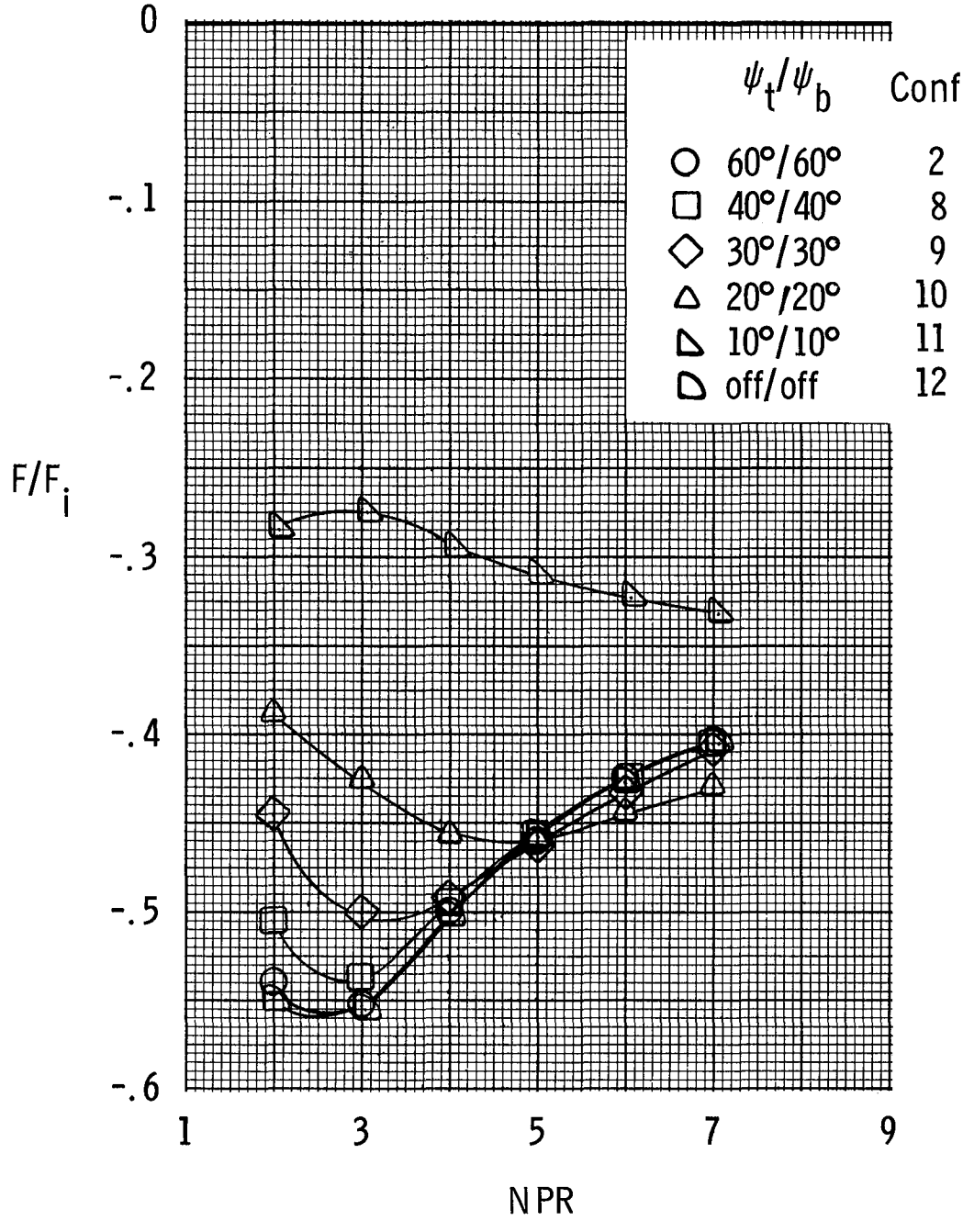

Figure 9. Effect of inner door angle on thrust ratio. $\theta_t/\theta_b = 130°/130°$; slider door open; $A_{t,\text{main}} = 0.0$ in^2.

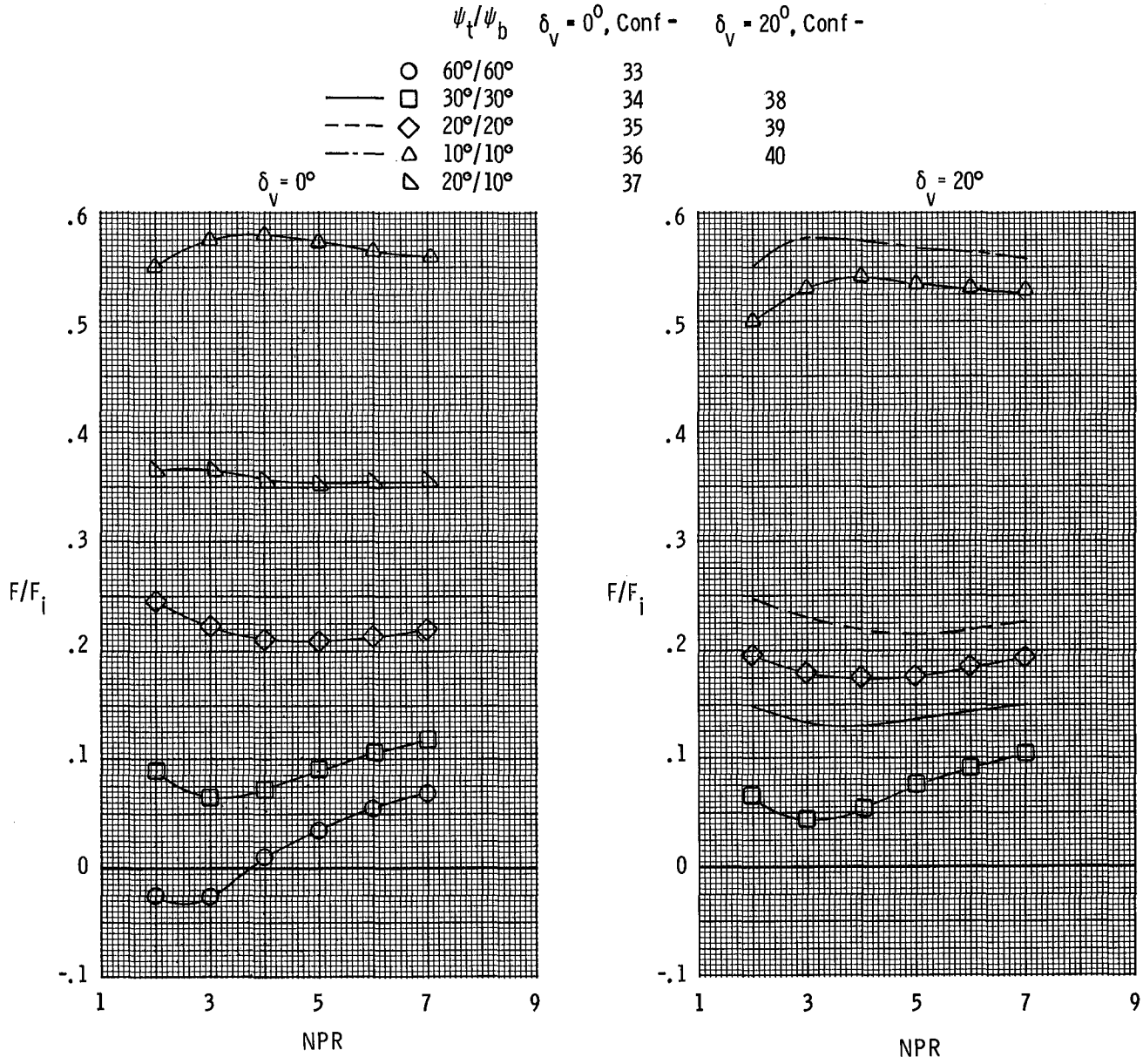

Figure 10. Effect of inner door angle on thrust ratio for approach configuration. θ_t/θ_b = 130°/130°; slider door open; $A_{t,\text{main}} = 2.0$ in^2. Lines with no symbols indicate resultant thrust ratio F_r/F_i.

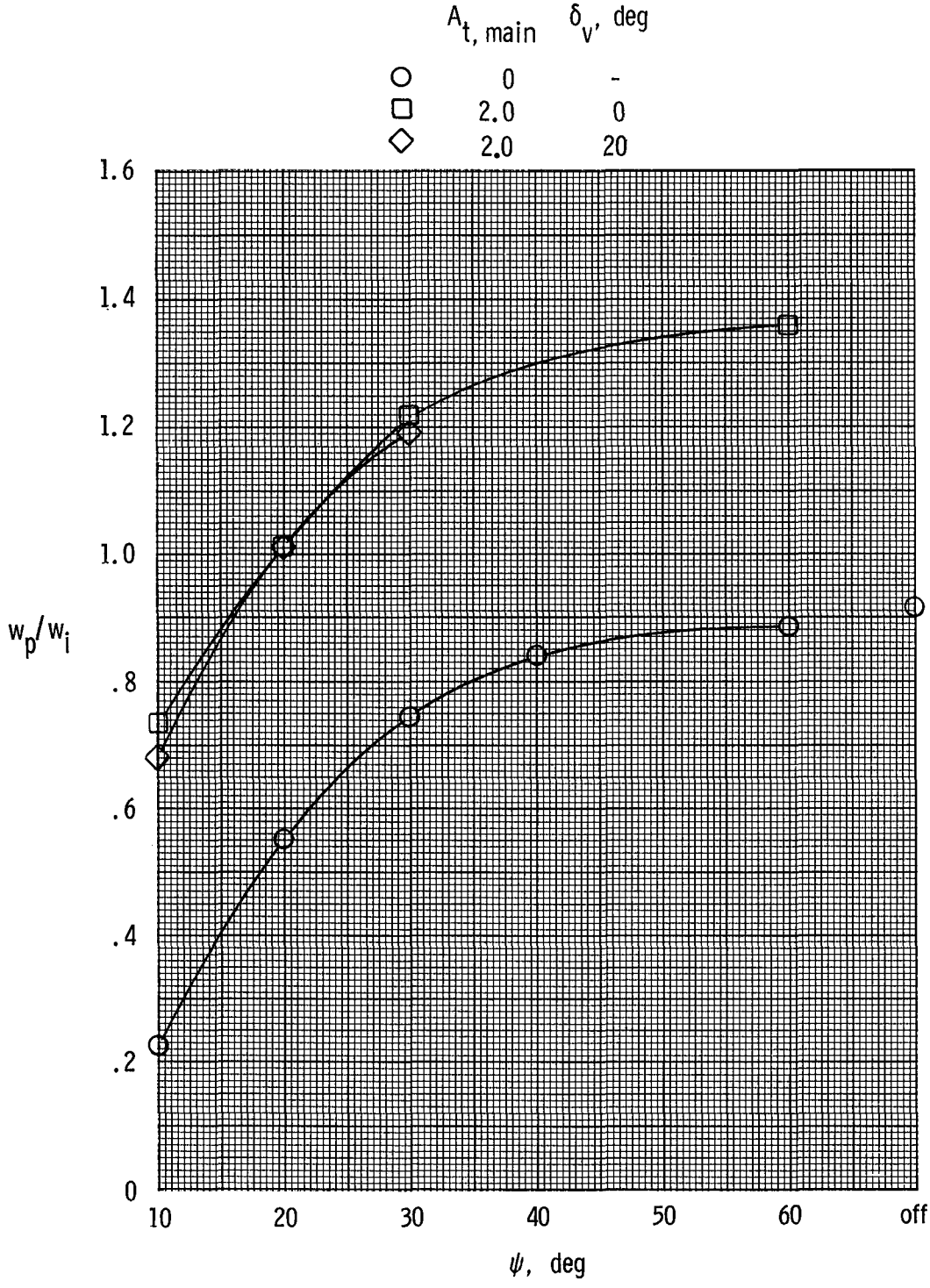

Figure 11. Summary of the effect of inner door angle on nozzle discharge coefficient for various reverser configurations. $\theta_t/\theta_b = 130°/130°$; slider door open; NPR = 3.0.

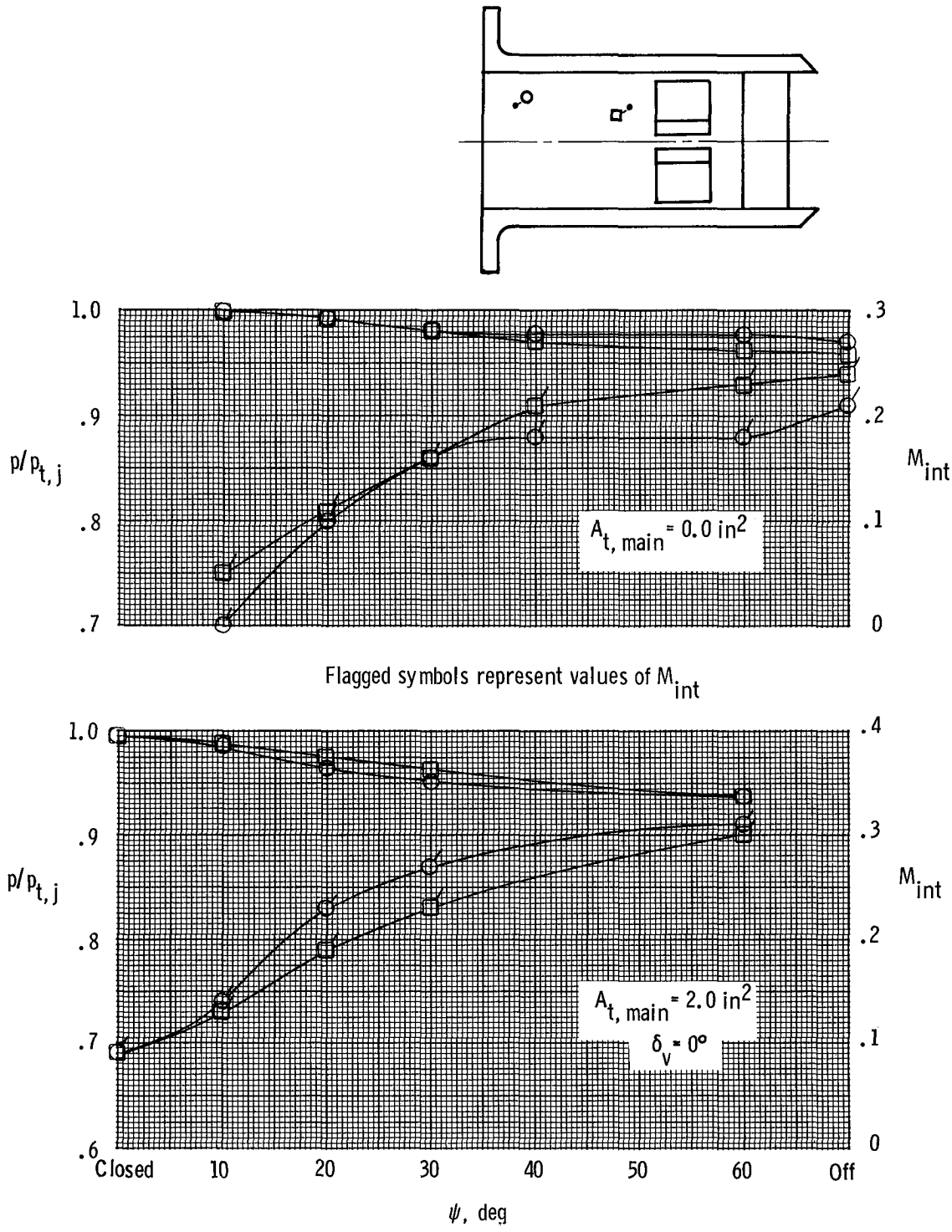

(a) Upper flap pressures and Mach numbers.

Figure 12. Effect of inner door angle on reverser static-pressure ratios and internal Mach numbers. θ_t/θ_b = 130°/130°; slider door open; NPR = 3.0.

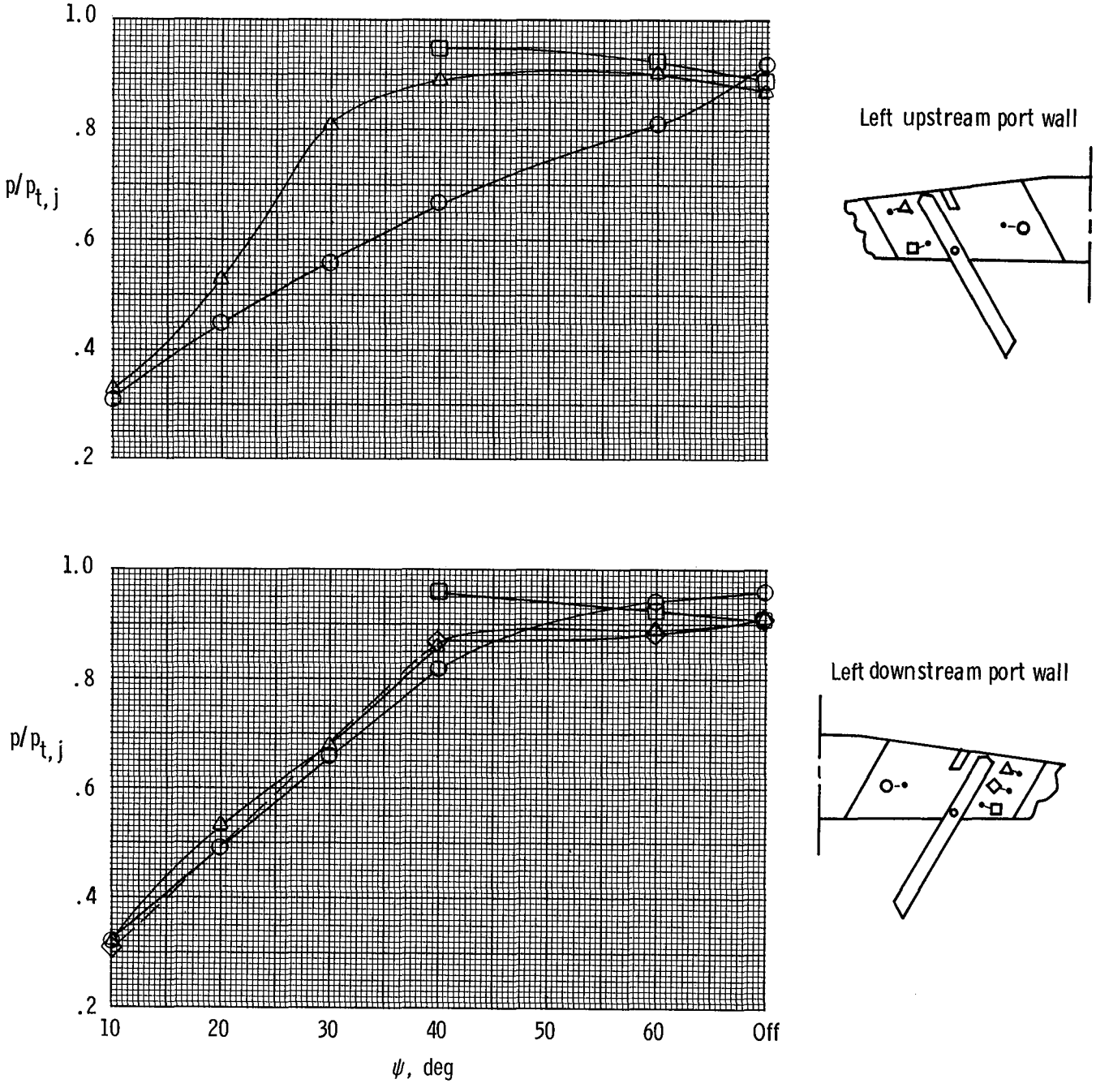

(b) Port pressures; $A_{t,\text{main}} = 0.0$ in^2.

Figure 12. Continued.

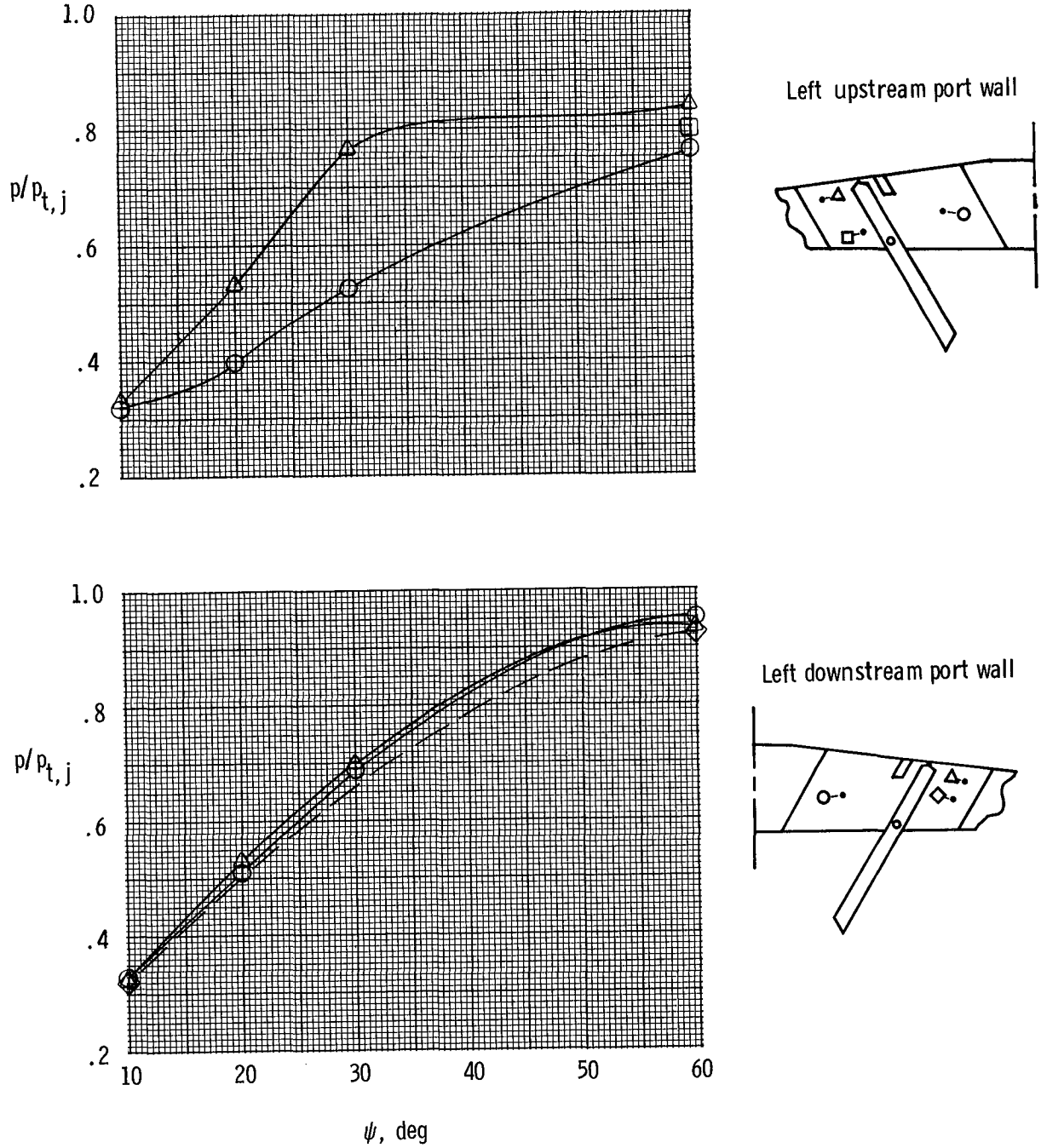

(c) Port pressures; $A_{t,\text{main}} = 2.0$ in^2; $\delta_v = 0°$.

Figure 12. Continued.

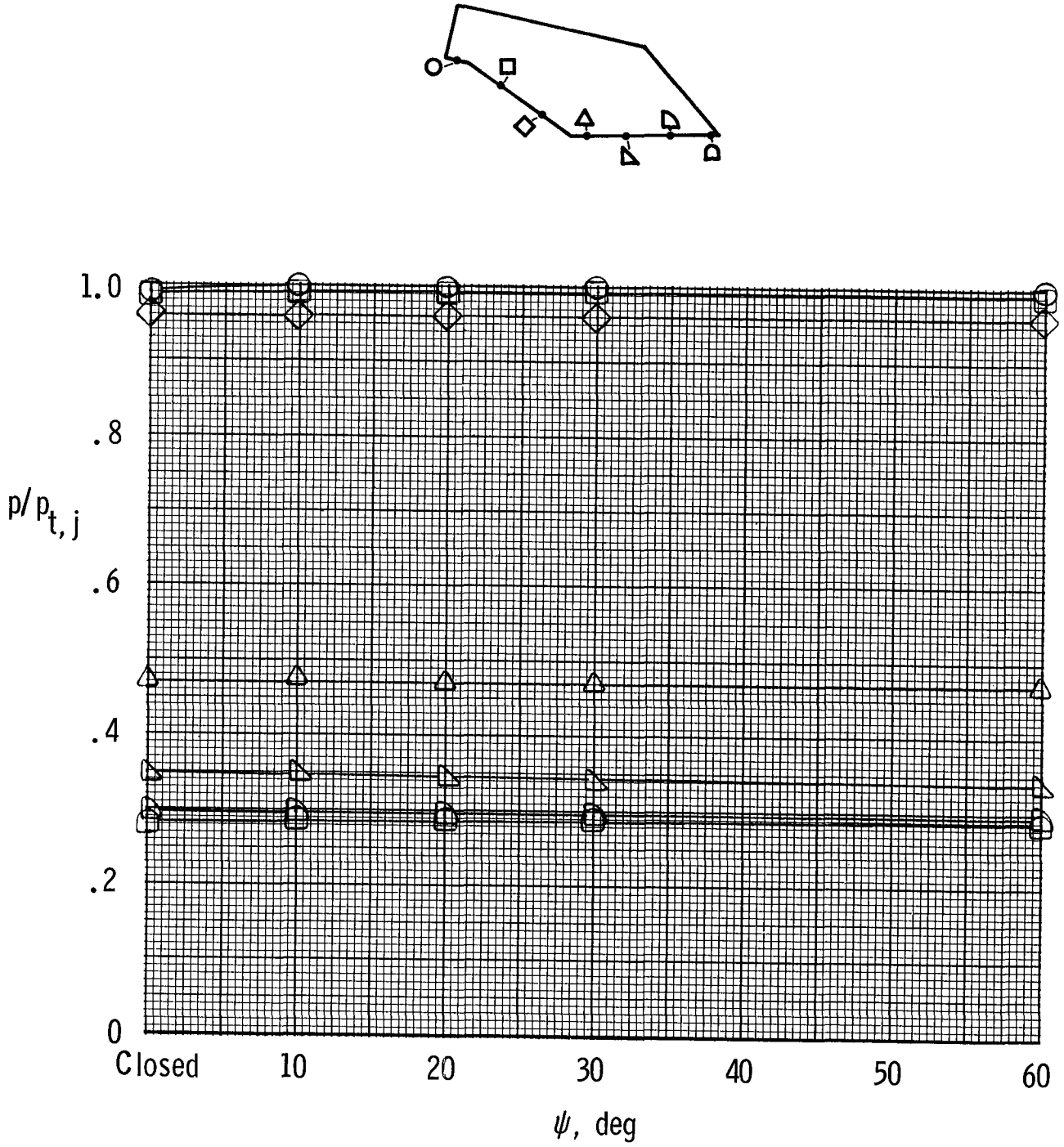

(d) Main exhaust nozzle upper flap pressures; $A_{t,\text{main}} = 2.0$ in^2; $\delta_v = 0°$.

Figure 12. Concluded.

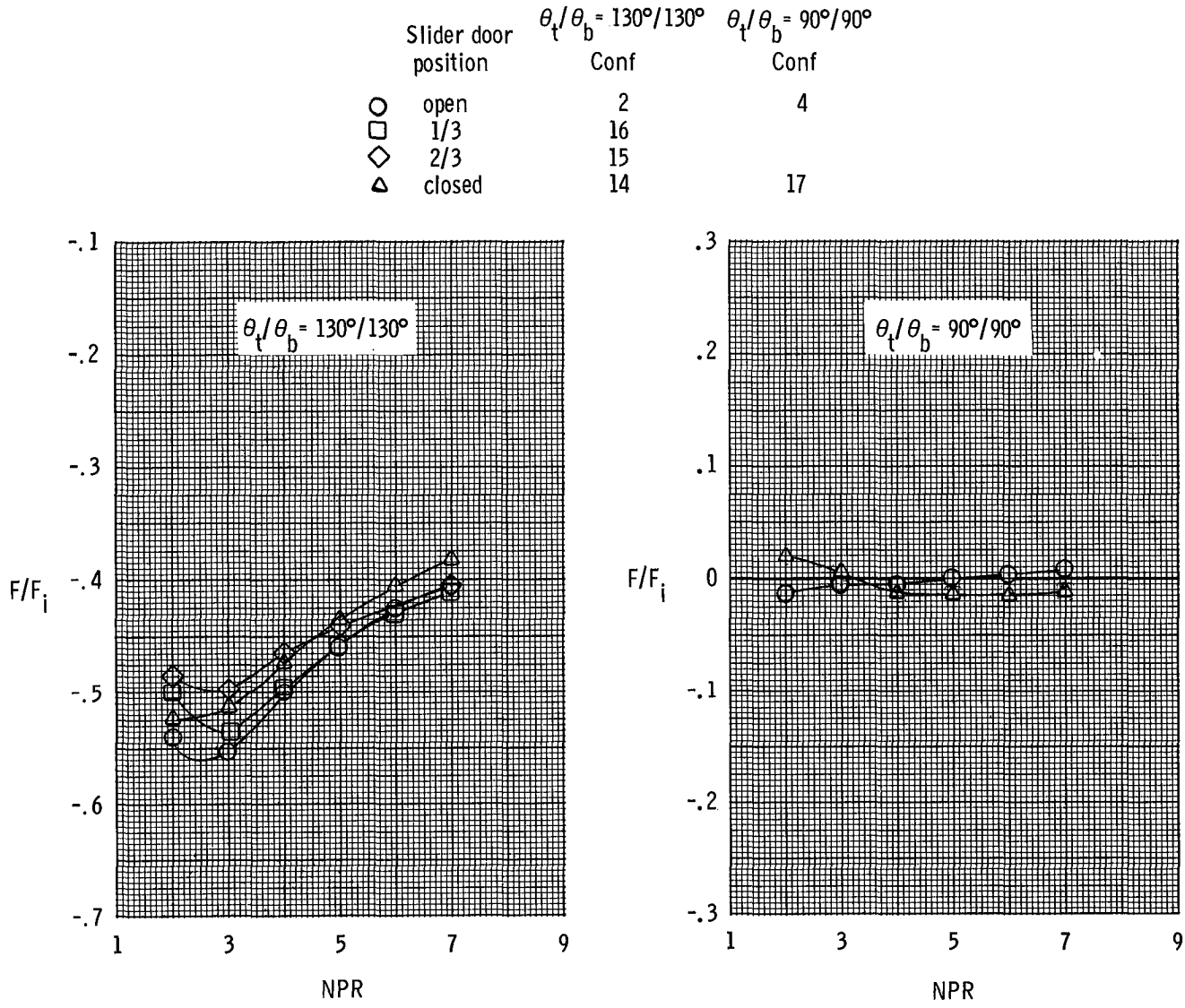

Figure 13. Effect of slider door position on thrust ratio. $\psi_t/\psi_b = 60°/60°$; $A_{t,\text{main}} = 0.0$ in^2.

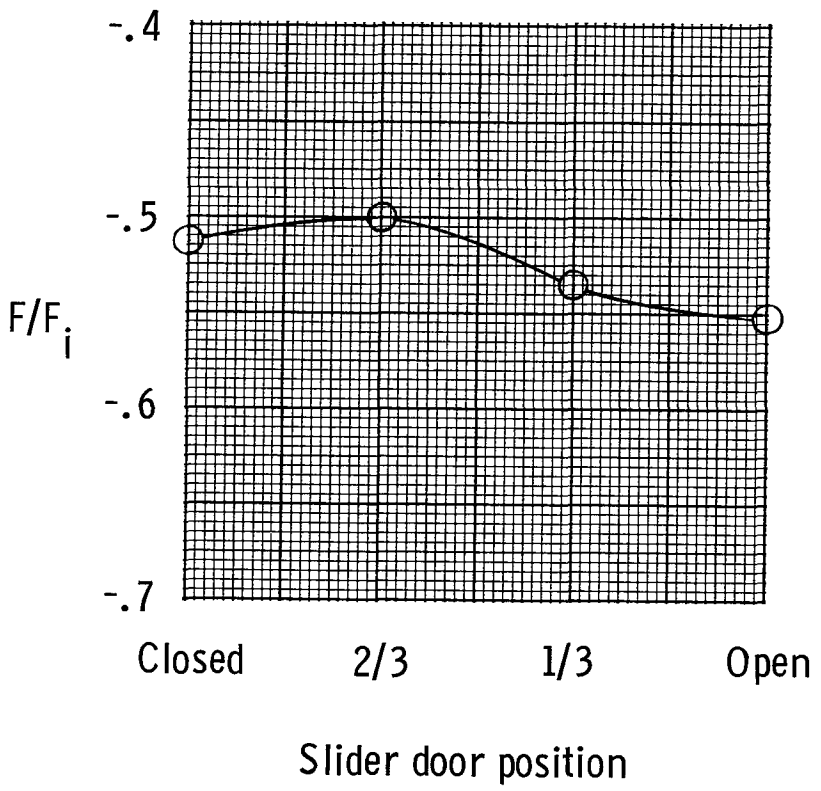

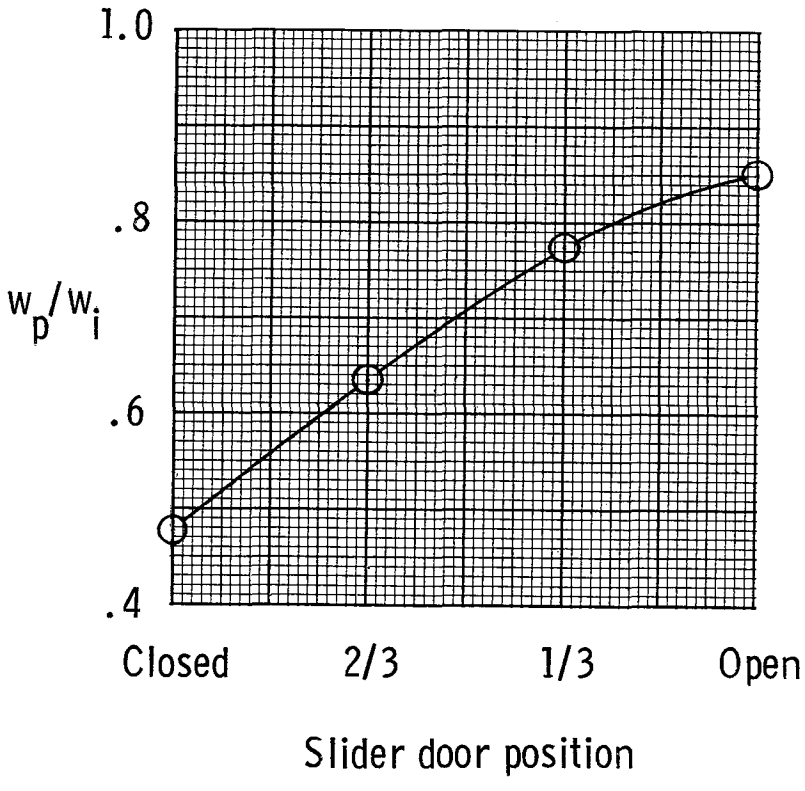

Figure 14. Summary of the effects of slider door position on thrust ratio and nozzle discharge coefficient. $\theta_t/\theta_b = 130°/130°$; $\psi_t/\psi_b = 60°/60°$; $A_{t,\text{main}} = 0.0$ in^2; NPR = 3.0.

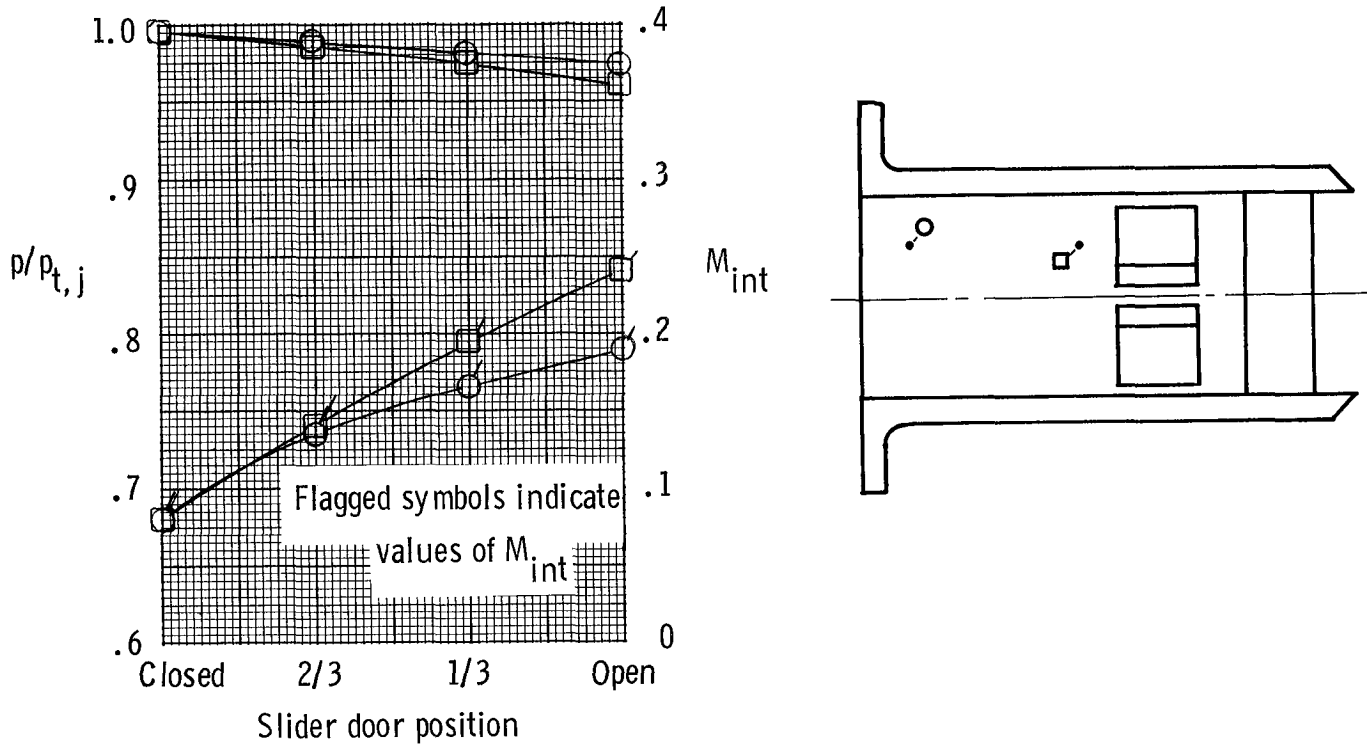

(a) Upper flap pressures and Mach numbers.

Figure 15. Effect of slider door position on reverser static-pressure ratios and internal Mach numbers. $\theta_t/\theta_b = 130°/130°$; $\psi_t/\psi_b = 60°/60°$; $A_{t,\text{main}} = 0.0$ in^2; NPR = 3.0.

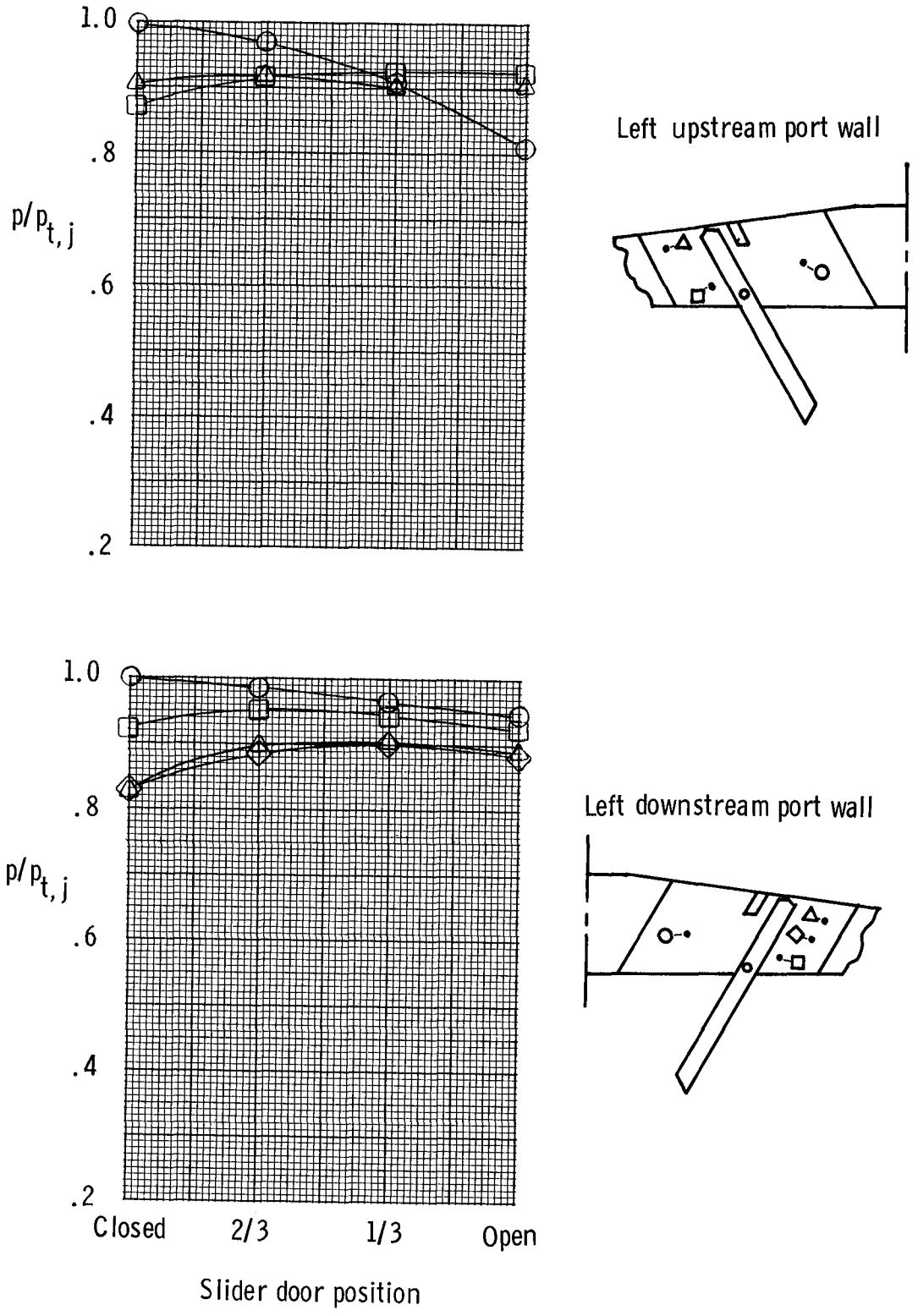

(b) Port pressures.

Figure 15. Concluded.

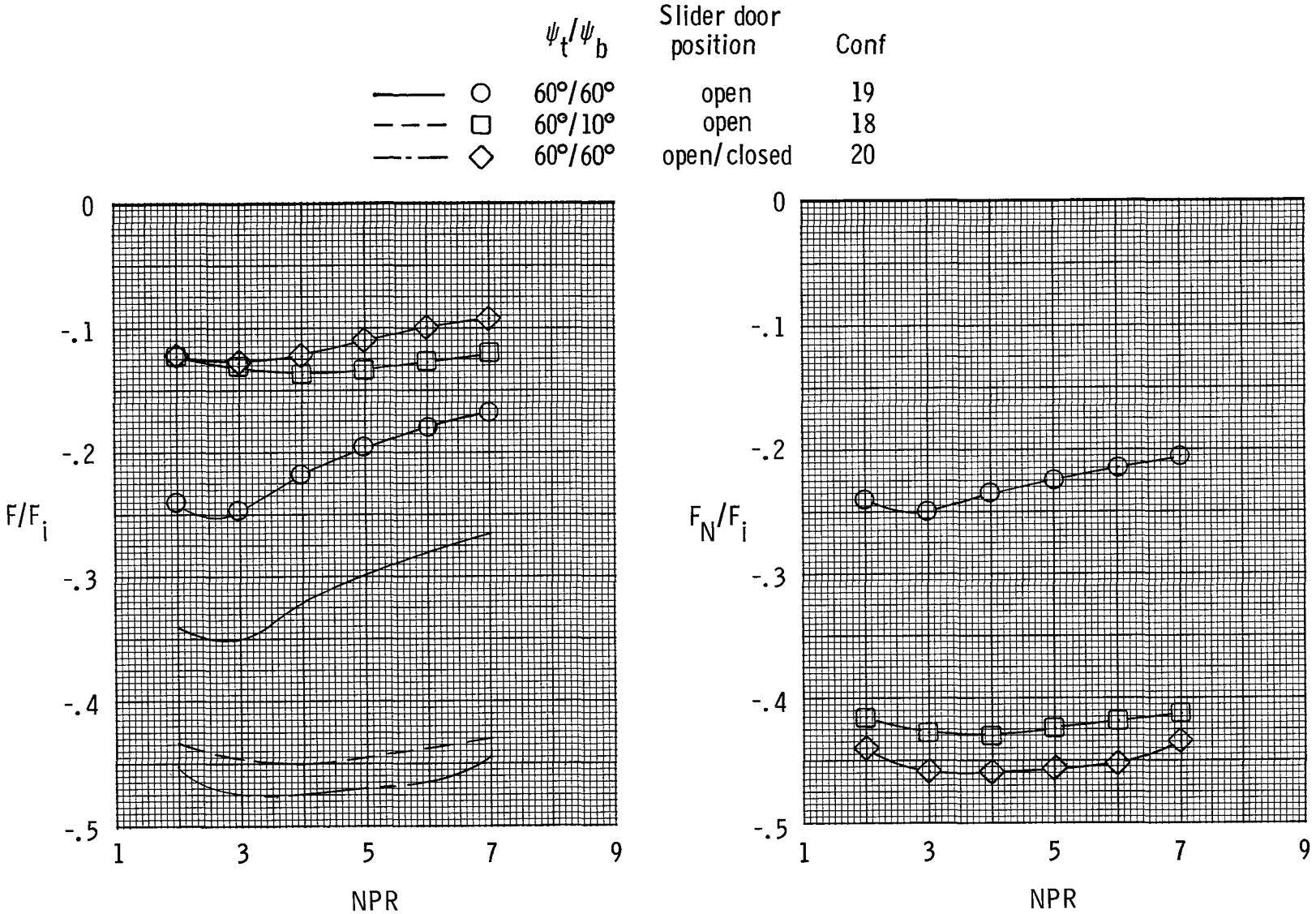

Figure 16. Effect of inner door angle and slider door position on thrust and normal-force ratios. θ_t/θ_b = 90°/130°; $A_{t,\text{main}} = 0.0$ in^2. Lines with no symbols indicate resultant thrust ratio F_r/F_i.

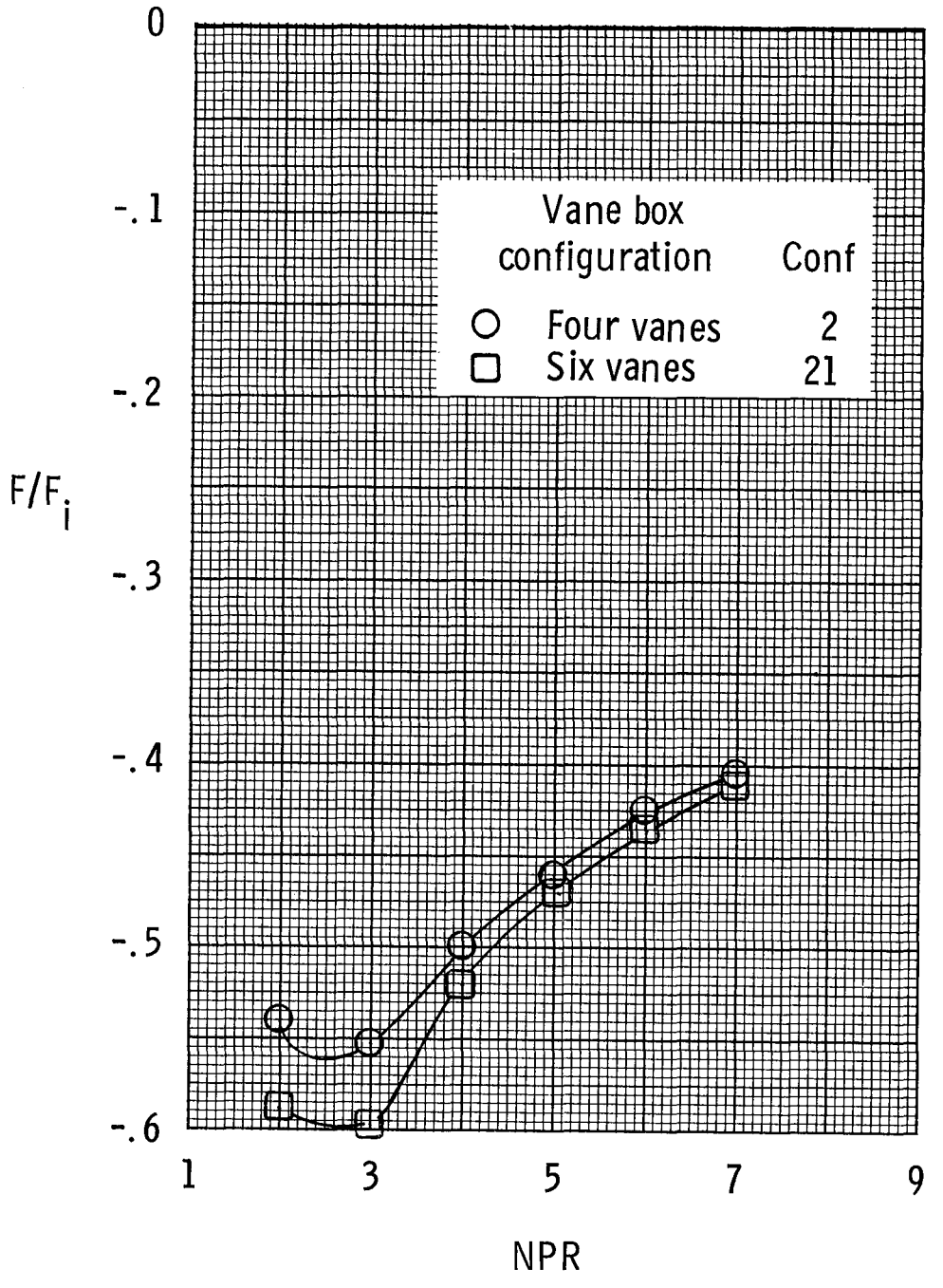

Figure 17. Effect of vane box configuration on thrust ratio. $\theta_t/\theta_b = 130°/130°$; $\psi_t/\psi_b = 60°/60°$; slider door open; $A_{t,\text{main}} = 0.0$ in^2.

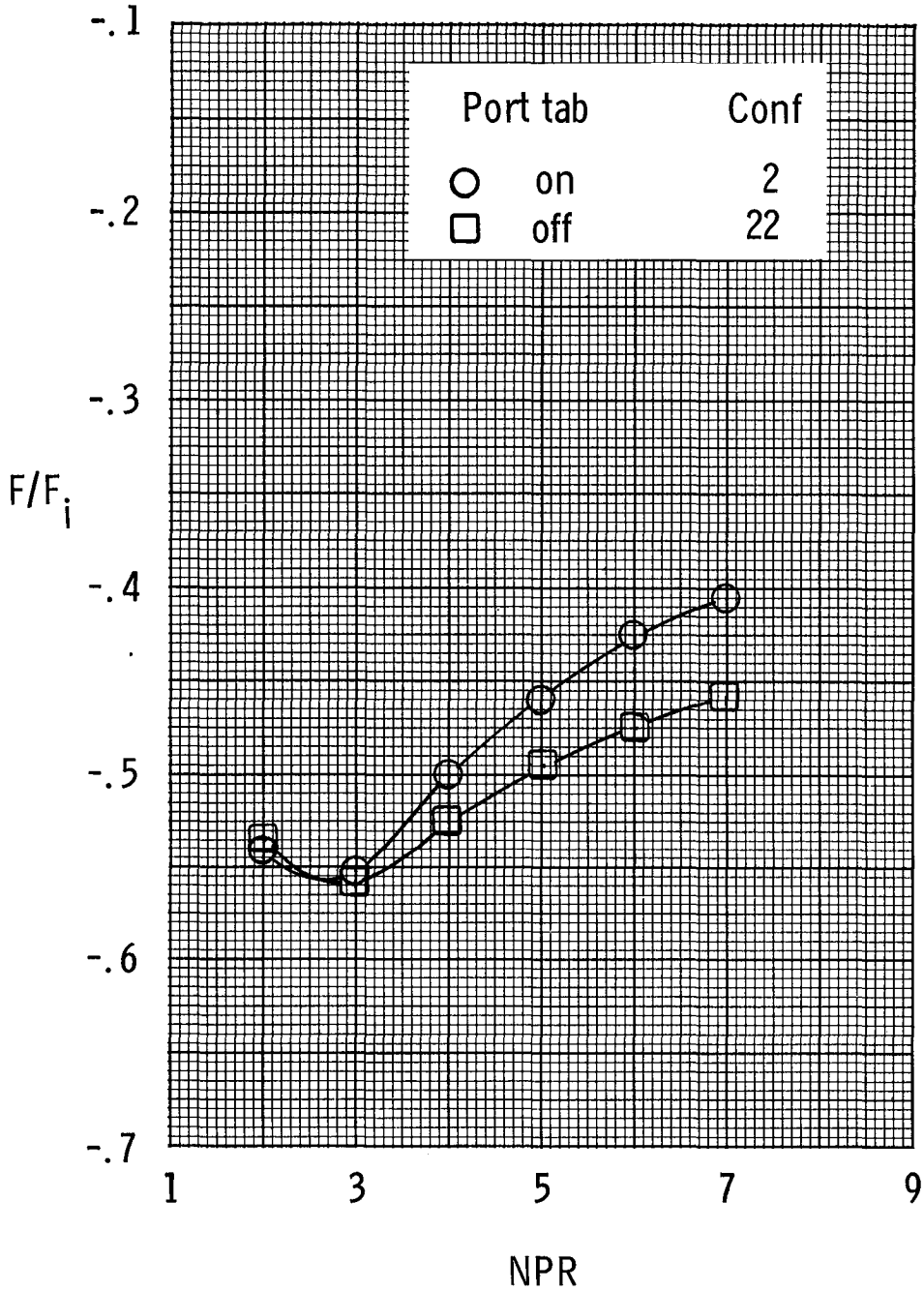

Figure 18. Effect of port tab on thrust ratio. $\theta_t/\theta_b = 130°/130°$; $\psi_t/\psi_b = 60°/60°$; slider door open; $A_{t,\text{main}} = 0.0$ in^2.

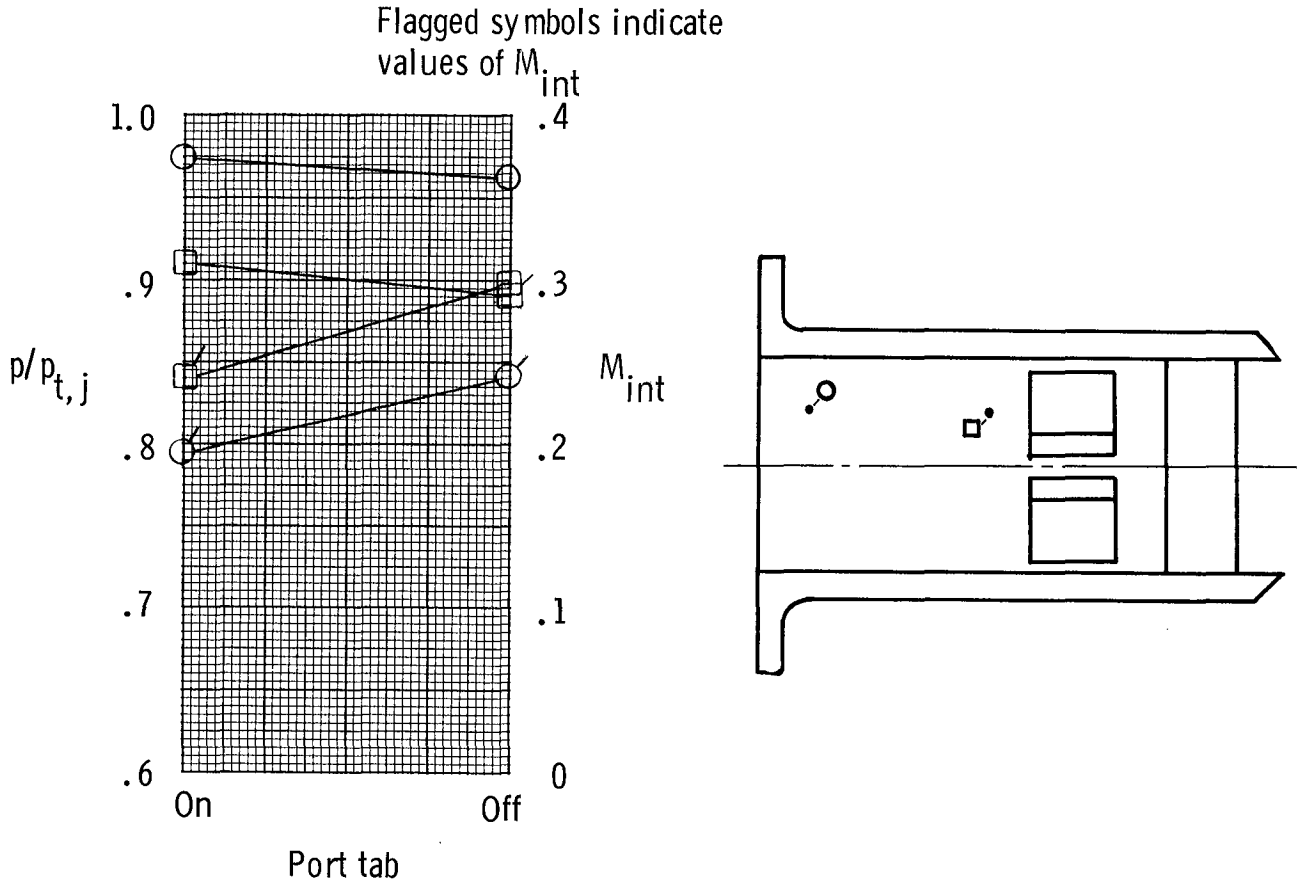

(a) Upper flap pressures and Mach numbers.

Figure 19. Effect of port tab on reverser static-pressure ratio and internal Mach number. $\theta_t/\theta_b = 130°/130°$; $\psi_t/\psi_b = 60°/60°$; slider door open; $A_{t,\text{main}} = 0.0$ in^2; NPR = 3.0.

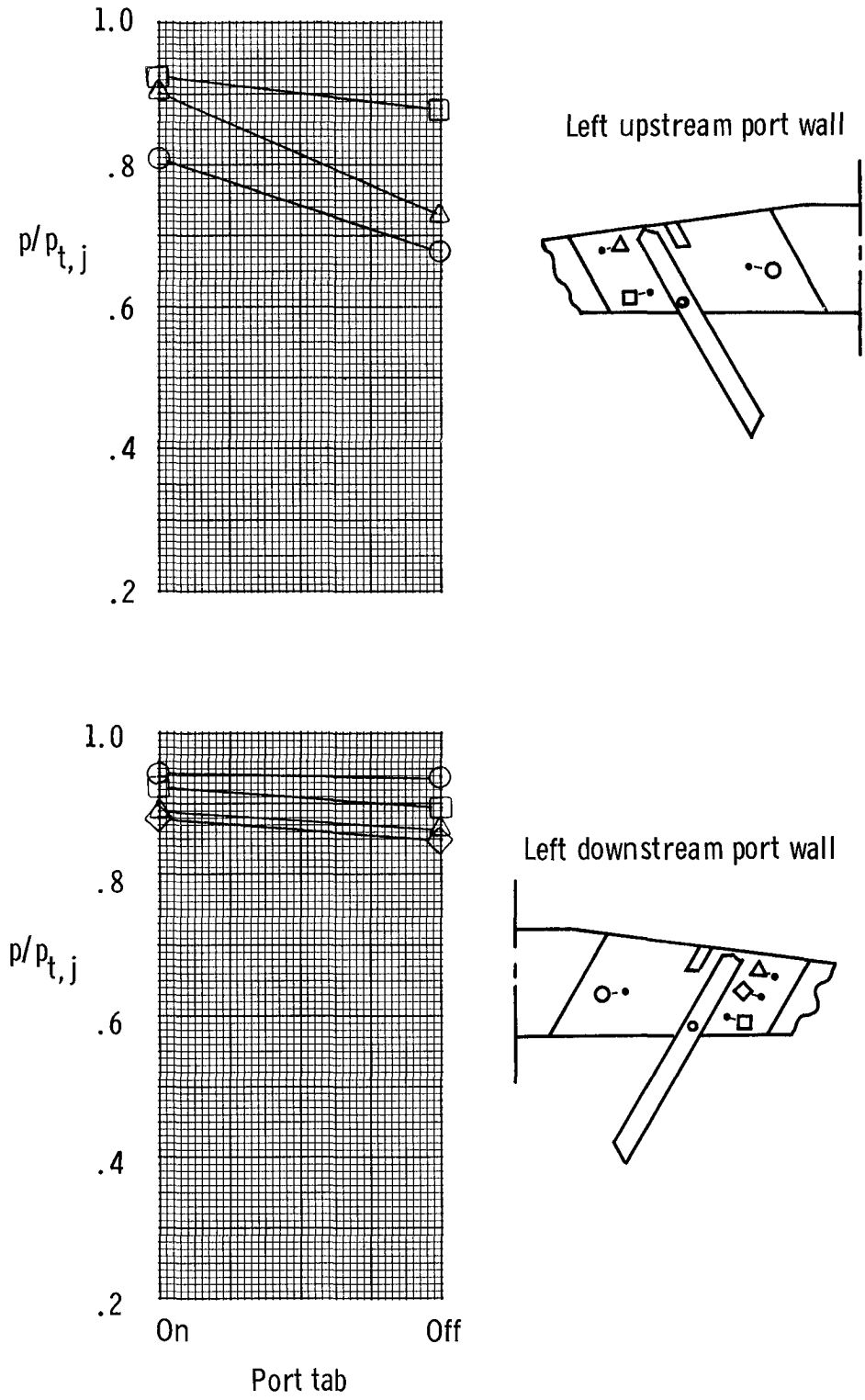

(b) Port pressures.

Figure 19. Concluded.

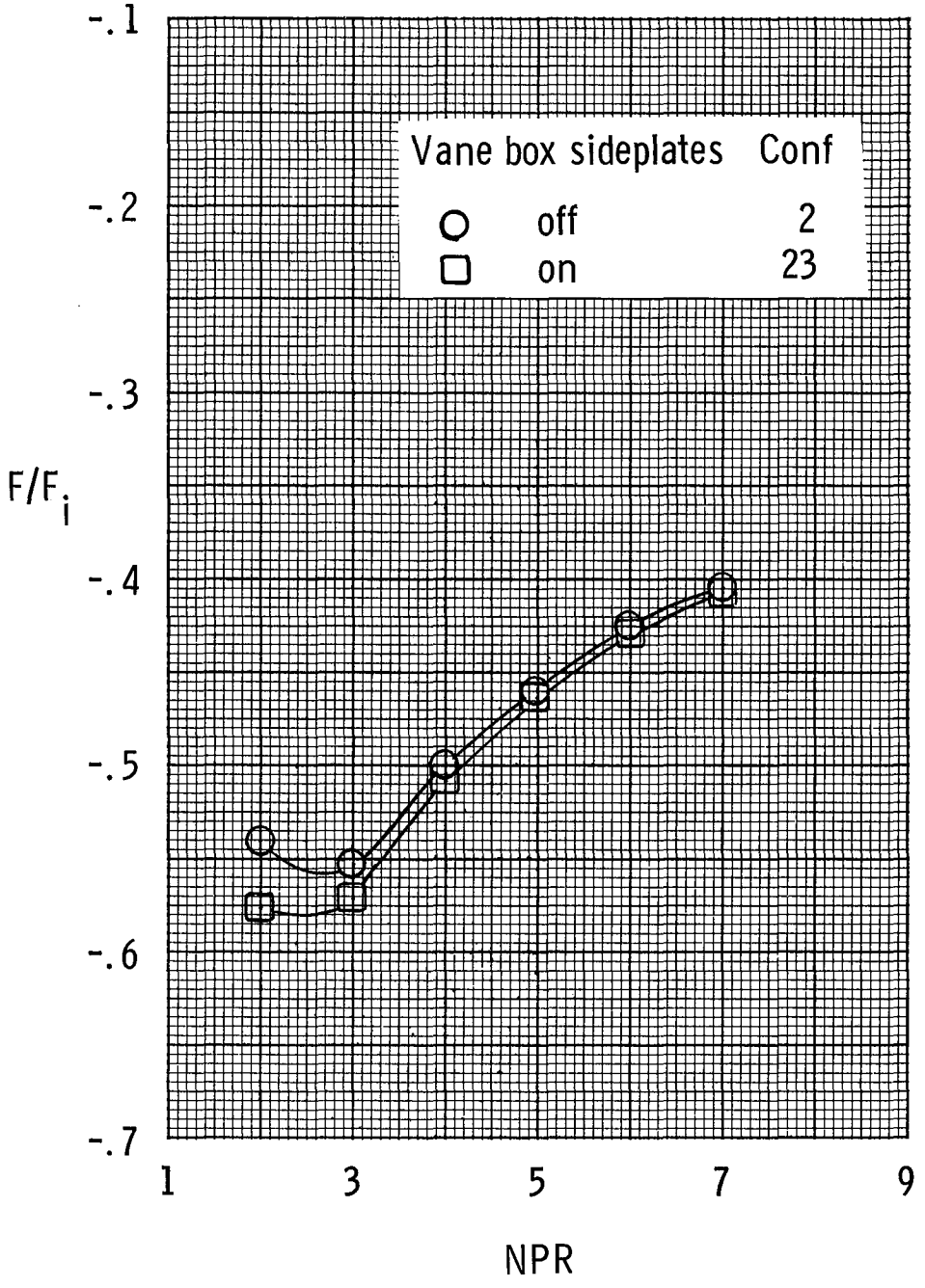

Figure 20. Effect of vane box sideplates on thrust ratio. $\theta_t/\theta_b = 130°/130°$; $\psi_t/\psi_b = 60°/60°$; slider door open; $A_{t,\text{main}} = 0.0$ in^2.

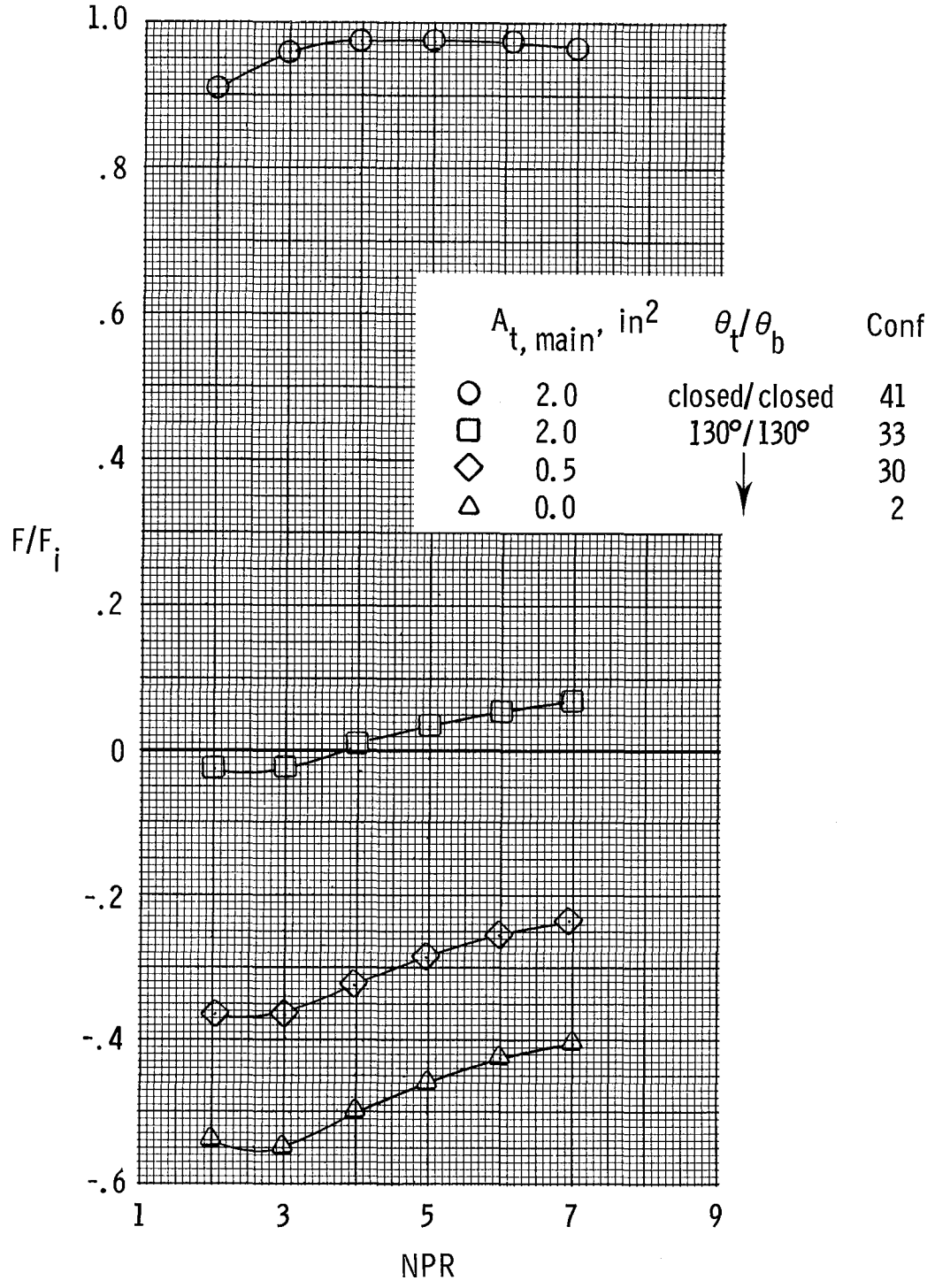

Figure 21. Effect of thrust modulation on thrust ratio. $\psi_t/\psi_b = 60°/60°$; slider door open when thrust reverser was in operation; $\delta_v = 0°$.

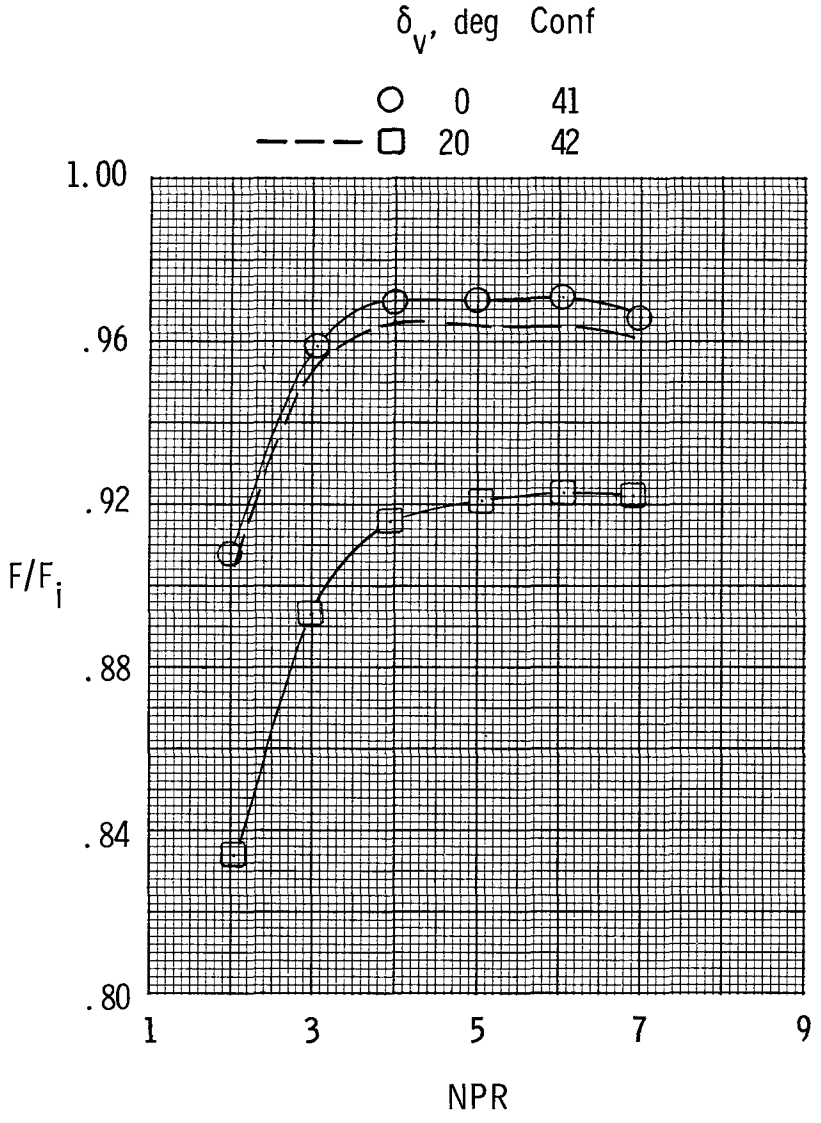

(a) Reverser ports closed.

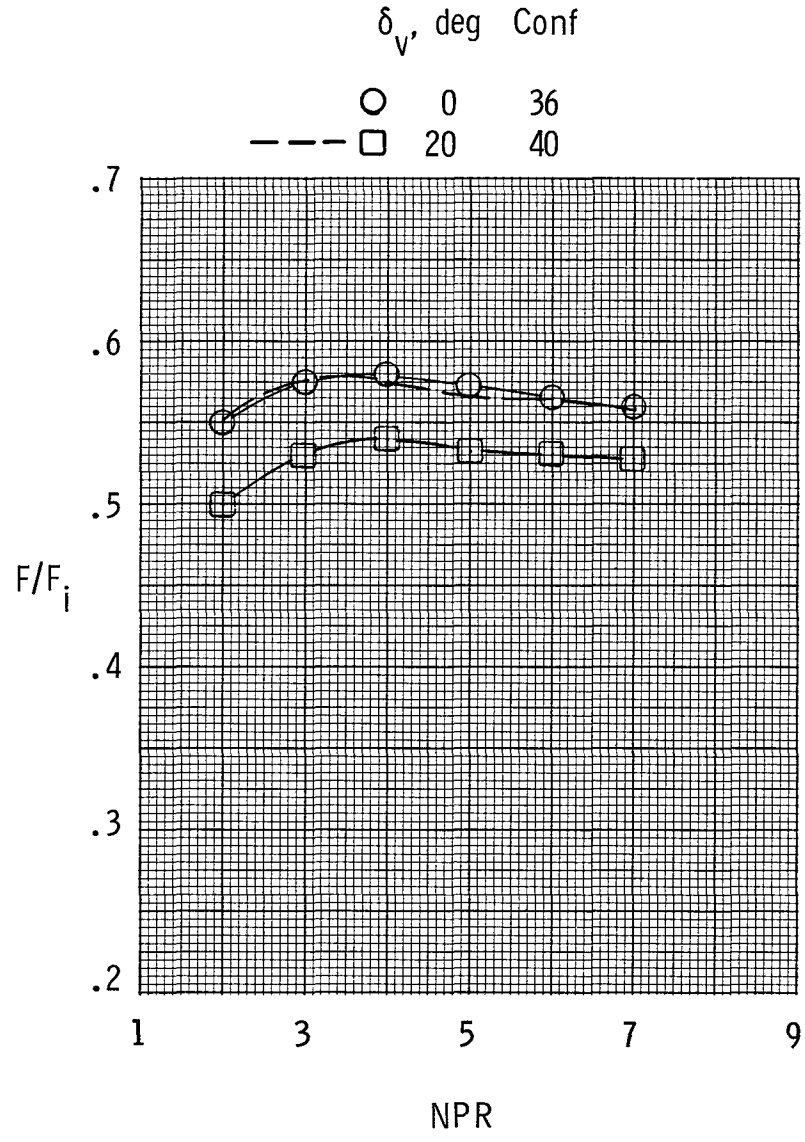

(b) $\psi_t/\psi_b = 10°/10°$.

Figure 22. Effect of main nozzle vector angle on thrust ratio for forward mode and approach configurations. $\theta_t/\theta_b = 130°/130°$; slider door open when reverser was in operation; $A_{t,\text{main}} = 2.0$ in^2. Lines with no symbols indicate resultant thrust ratio F_r/F_i.

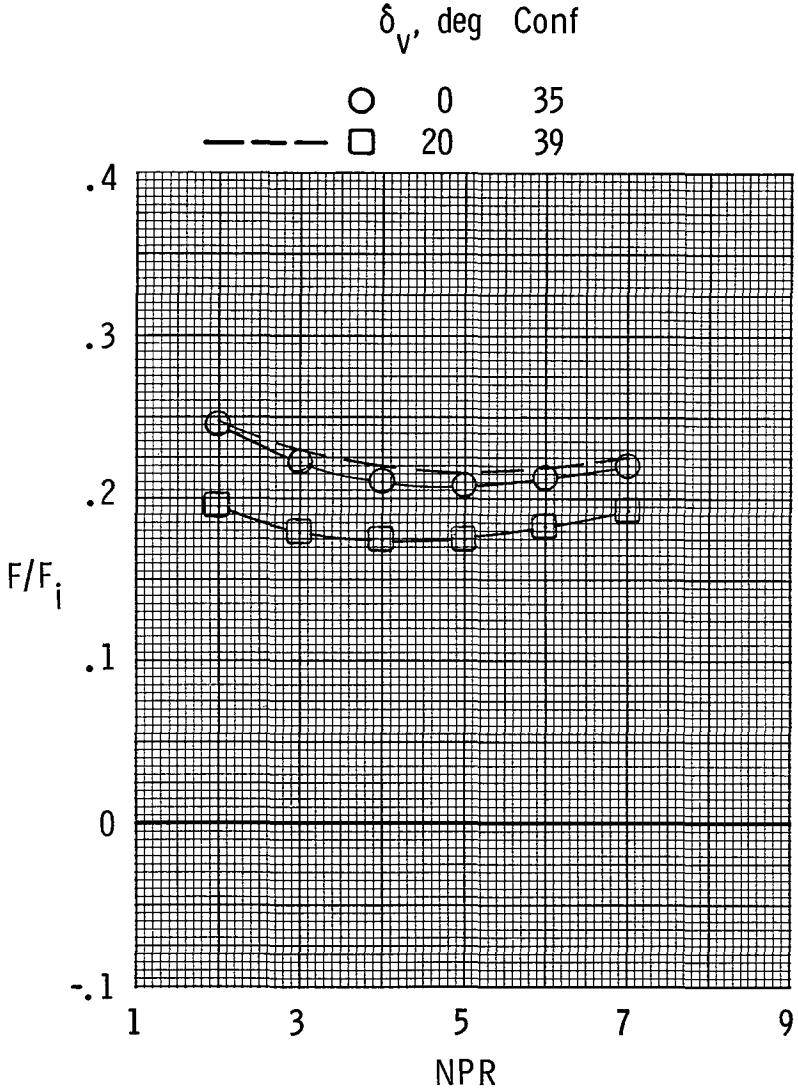

(c) $\psi_t/\psi_b = 20°/20°$.

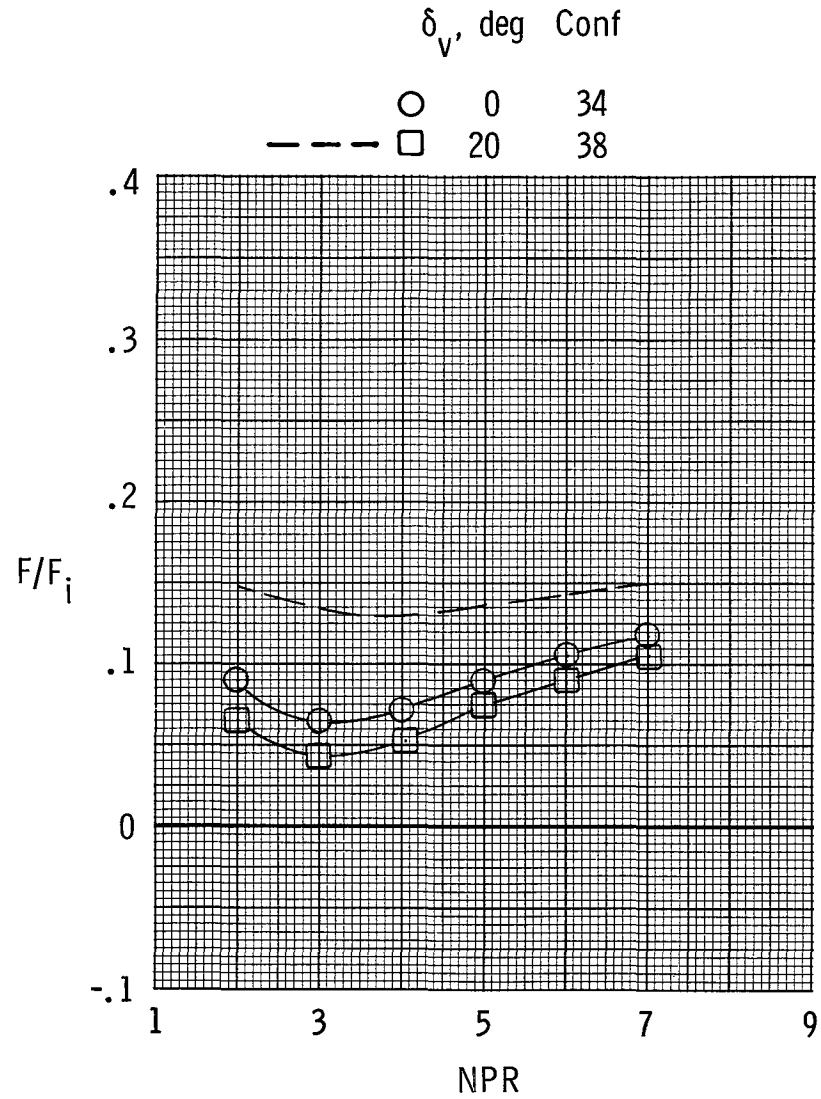

(d) $\psi_t/\psi_b = 30°/30°$.

Figure 22. Concluded.

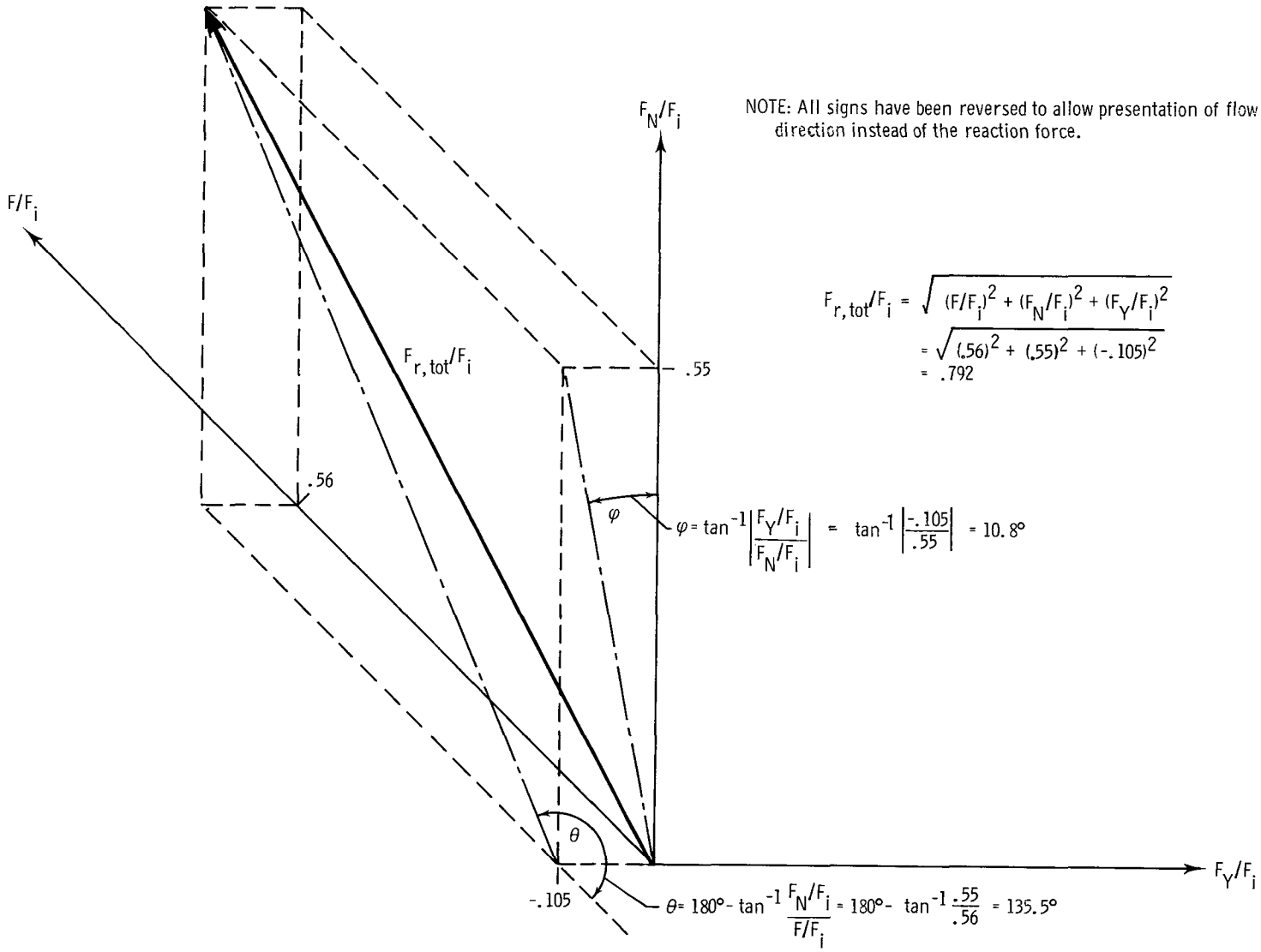

Figure 23. Component breakdown of resultant flow vector for top left-hand port. Conf 2; $\theta_t/\theta_b = 130°/130°$; $\psi_t/\psi_b = 60°/60°$; slider door open; $A_{t,\text{main}} = 0.0$ in^2; NPR = 3.0. Data obtained from splitter plate runs.

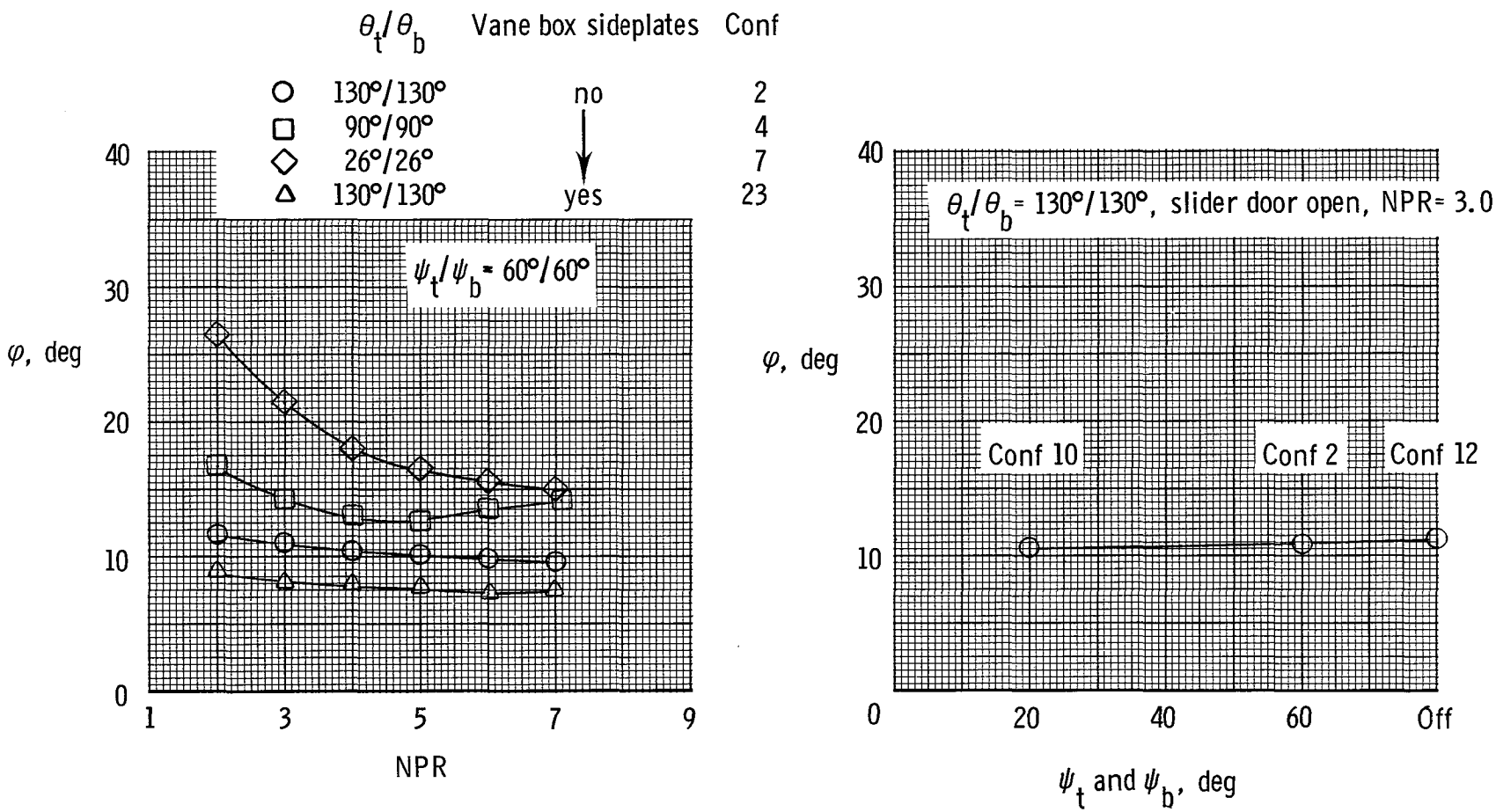

Figure 24. Effect of geometric efflux angle and inner door angle on reverser splay angle. Slider door open.

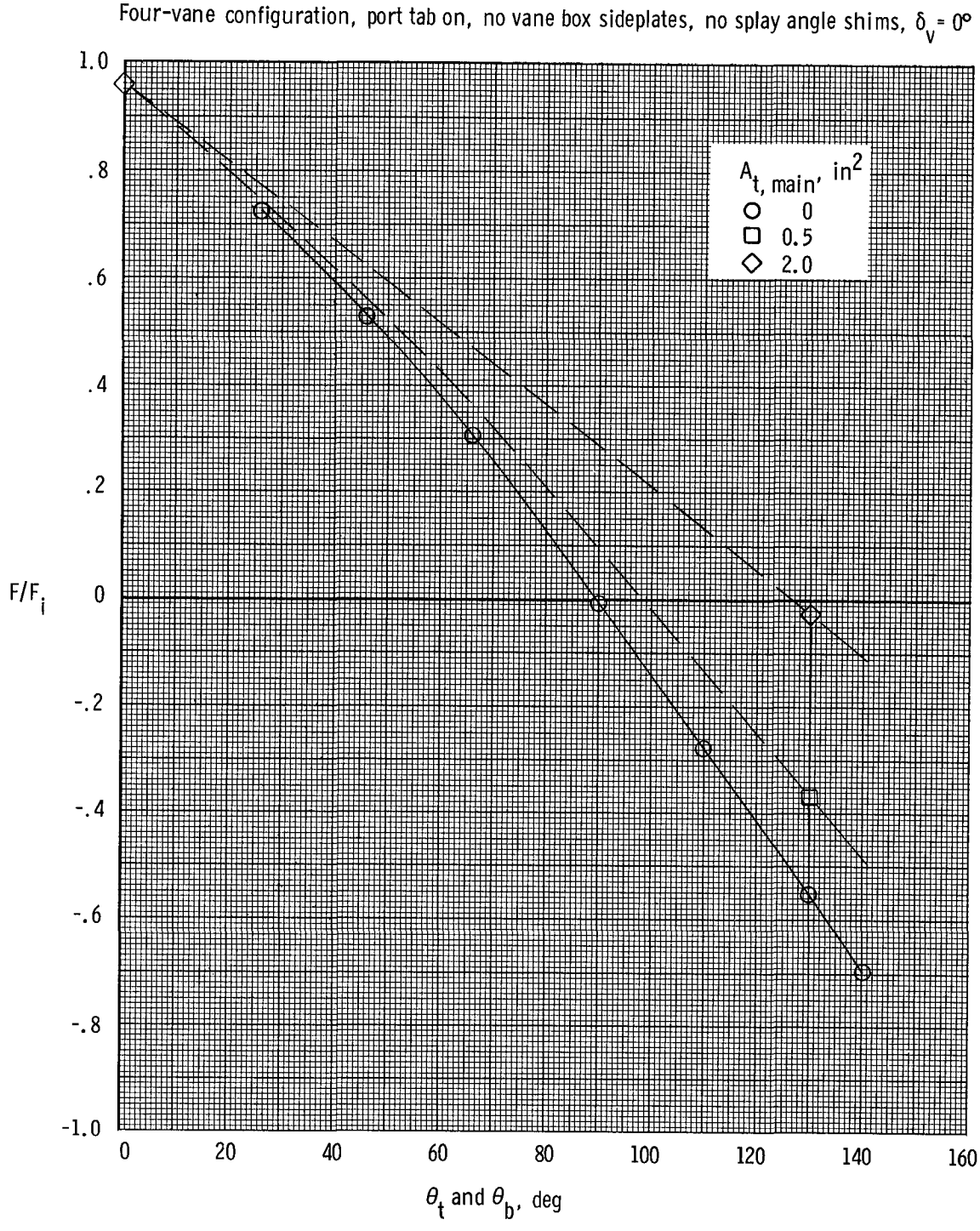

Figure 25. Summary of geometric efflux angle and main nozzle throat area effects on thrust ratio. ψ_t/ψ_b = 60°/60°; slider door open; NPR = 3.0.

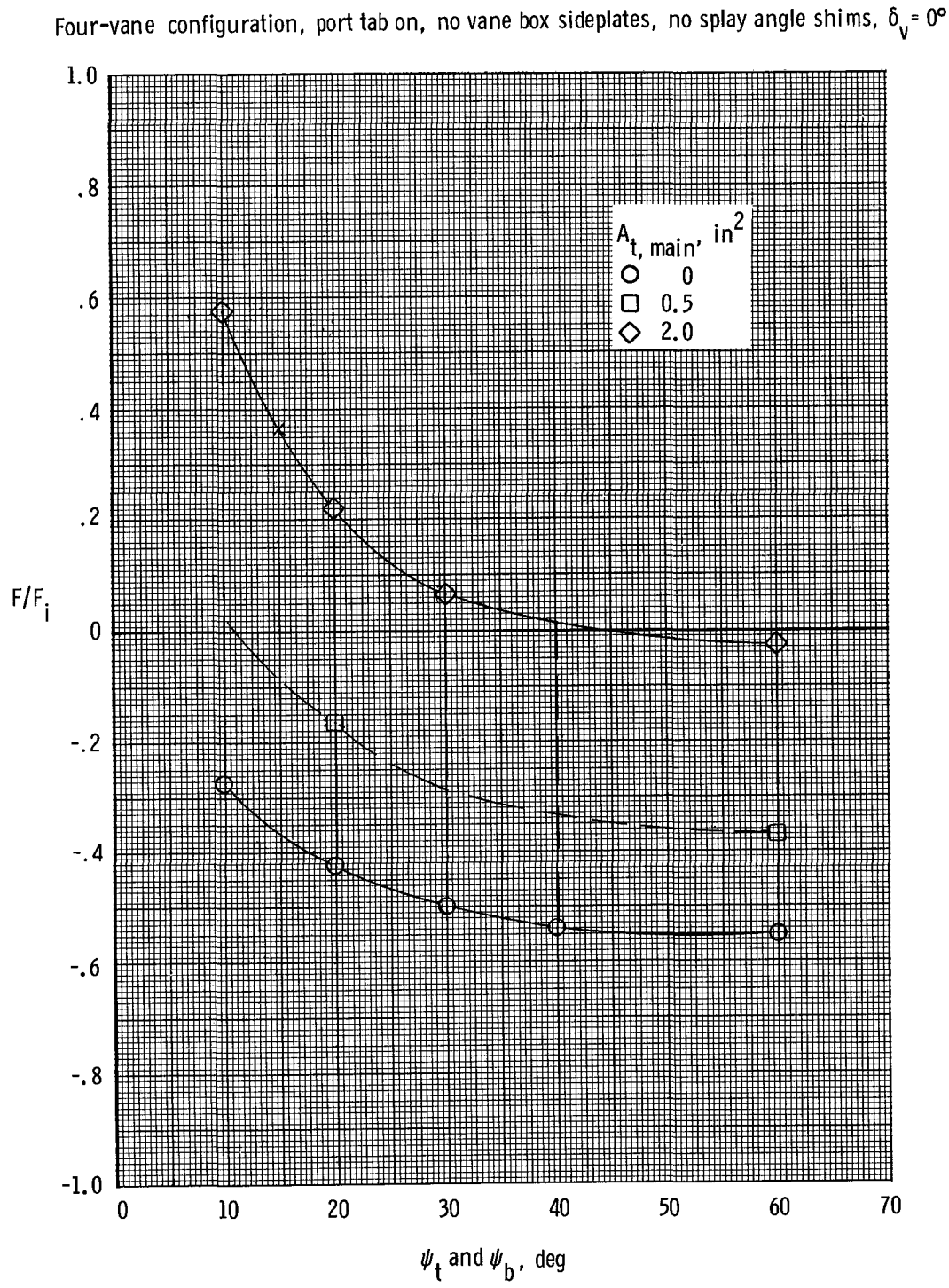

Figure 26. Summary of inner door angle and main nozzle throat area effects on thrust ratio. $\theta_t/\theta_b = 130°/130°$; slider door open; NPR = 3.0.

1. Report No.	2. Government Accession No.	3. Recipient's Catalog No.
NASA TP-2519		

4. Title and Subtitle	5. Report Date
Static Internal Performance of a Single-Engine Nonaxisymmetric-Nozzle Vaned-Thrust-Reverser Design With Thrust Modulation Capabilities	December 1985
	6. Performing Organization Code: 505-40-90-01
7. Author(s): Laurence D. Leavitt and James R. Burley II	8. Performing Organization Report No.: L-15991
9. Performing Organization Name and Address: NASA Langley Research Center, Hampton, VA 23665-5225	10. Work Unit No.
	11. Contract or Grant No.
12. Sponsoring Agency Name and Address: National Aeronautics and Space Administration, Washington, DC 20546-0001	13. Type of Report and Period Covered: Technical Paper
	14. Sponsoring Agency Code

15. Supplementary Notes

16. Abstract

An investigation has been conducted at wind-off conditions in the static-test facility of the Langley 16-Foot Transonic Tunnel. The tests were conducted on a single-engine reverser configuration with partial and full reverse-thrust modulation capabilities. The reverser design had four ports with equal areas. These ports were angled outboard 30° from the vertical to impart a splay angle to the reverser exhaust flow. This splaying of reverser flow was intended to prevent impingement of exhaust flow on empennage surfaces and to help avoid inlet reingestion of exhaust gas when the reverser is integrated into an actual airplane configuration. External vane boxes were located directly over each of the four ports to provide variation of reverser efflux angle from 140° to 26° (measured forward from the horizontal reference axis). The reverser model was tested with both a butterfly-type inner door and an internal slider door to provide area control for each individual port. In addition, main nozzle throat area and vector angle were varied to examine various methods of modulating thrust levels. Other model variables included vane box configuration (four or six vanes per box), orientation of external vane boxes with respect to internal port walls (splay angle shims), and vane box sideplates. Nozzle pressure ratio was varied from 2.0 to approximately 7.0.

17. Key Words (Suggested by Authors(s))	18. Distribution Statement
Nonaxisymmetric nozzles Thrust reversing Internal performance External vanes	Unclassified—Unlimited Subject Category 02

19. Security Classif.(of this report)	20. Security Classif.(of this page)	21. No. of Pages	22. Price
Unclassified	Unclassified	107	A06

For sale by the National Technical Information Service, Springfield, Virginia 22161

NASA-Langley, 1985

National Aeronautics and
Space Administration
Code NIT-4

Washington, D.C.
20546-0001

Official Business
Penalty for Private Use, $300

BULK RATE
POSTAGE & FEES PAID
NASA Washington, DC
Permit No. G-27

POSTMASTER: If Undeliverable (Section 158 Postal Manual) Do Not Return